SEMICONDUCTOR QUANTUM DOTS

BIOCONJUGATION

By

NATALIYA NIKOLAJEVNA MAMEDOVA

Bachelor of Science
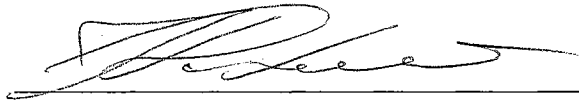Belarussian State University
Minsk, Belarus
1994

Master of Science
Belarussian State University
Minsk, Belarus
1995

Submitted to the Faculty of the
Graduate College of the
Oklahoma State University
in partial fulfillment of
the requirement for
the Degree of
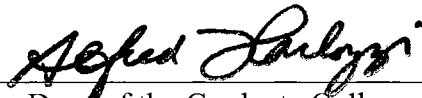DOCTOR OF PHILOSOPHY
December, 2003

SEMICONDUCTOR QUANTUM DOTS

BIOCONJUGATION

Thesis Approved:

_____
Thesis Advisor

_____

Charlotte L. Ownby
_____

_____

_____
Dean of the Graduate College

DEDICATION

Dedicated
To my two precious daughters

ACKNOWLEDGMENTS

Many people have contributed to my goal of obtaining a Ph.D. at Oklahoma State University. To my advisor, Dr. Nicholas Kotov, I express gratitude for collaboration with various research projects and financial assistance through employment at the OSU Department of Chemistry.

I wish to thank the members of my committee, Dr. Neil Purdie, Dr. Ziad El Rassi, Dr. Carey Pope and Dr. Charlotte Ownby for their time, effort and expertise.

I am grateful for Dr. Larry James and the University of Texas Medical Branch and especially Tarl Prow, for their efforts, contributions and results concerning the research data in this dissertation.

I would also like to thank all my group members with whom I have worked over the years, but especially, Ms. Tong Ni, Dr. Dattari Nagesha, Dr. Arif Mamedov, Mr. Todd Crisp and Mr. John Ostrander for their support and friendship.

Most of all, I would like to thank my immediate and extended family for their love and support through what has often been a trying endeavor. Special thanks to my precious girls, Nadya and Victoria, for their love and understanding in completing this strenuous academic process, I dedicate this work to them.

To my parents, thank you for instilling in me the need to finish what I started, no matter what the circumstances.

TABLE OF CONTENTS

LIST OF TABLES

LIST OF FIGURES

Chapter III

Chapter IV

LIST OF SYMBOLS AND ABBREVIATIONS

a	nanocrystal radius
a_{ex}	exciton Bohr radius
a.u.	absorbance units
arb.u.	arbitrary units
BSA	bovine serum albumin
CL	cathodoluminescence
CD	circular dichroism
DI	deionized
d	diameter
EDC	(1-ethyl-3-(3-dimethylaminopropyl) carbodiimide hydrochloride
EL	electroluminescence
ELISA	enzyme-linked immunosorbent assay
e	electron charge
FG	functional coupling group
FRET	Froster resonance energy transfer
FTIR	Fourier Transform Infrared Spectroscopy
G	glutaraldehyde
HPLC	high performance liquid chromatography
I	integrated area of luminescence
IgG	immunoglobulin G

k	semiconductor permittivity
L	one of the dimensions
LED	light-emmiting device
Lys	lysine
M_W	molecular weight
MWCO	molecular weight cutoff
m_{ex}	reduced exciton mass
N_A	Avogadro number
NMR	nuclear magnetic resonance
NP	nanoparticle
OD	optical density
PBS	phosphate buffered saline
PL	photoluminescence
r	radius
QD	quantum dot
SDS	sodium dodecyl sulfate
STR	streptavidin
Sulfo-NHS	N-hydroxysulfosuccinimide sodium salt
TEM	transmission electron microscopy
TGA	thioglycolic acid
TOP	trioctylphosphine
TOPO	trioctylphosphine oxide
Trp	triptophan

Tween 20	polyoxyethylene sorbitan monolaurate
UV	ultraviolet
Vis.	visible
V	reaction volume
V_0	volume of one particle
XPS	X-ray photoelectron spectroscopy
$\hbar$	Plank's constant
ρ	density
v	number of moles
φ	quantum yield
λ	wavelength

CHAPTER I

INTRODUCTION TO QUANTUM DOT BIOCONJUGATES

Introduction and scope of the study

Nanochemistry derives its name from the fact that the nanometer – one billionth of a meter - is its basic measuring unit. In the nanoworld, the width of the average human hair (about 80,000 nm) is huge. One nanometer is roughly the width of five carbon atoms. Metal and semiconductor nanoparticles (NPs) in the 2–6 nm size range are of considerable current interest, not only do to their unique size-dependent properties, but also because of their dimensional similarities with biological macromolecules (e.g. most proteins are about 10 nm wide and a virus is about 100 nm long) [1-4]. These similarities could allow an integration of nanotechnology and biology, leading to major advances in medical diagnostics, targeted therapeutics, molecular biology and cell biology [5].

Recent research by several groups has linked colloidal NPs to bio-molecules such as peptides [6], proteins [7-9], and DNA [10,11]. These nanoparticle bioconjugates are being used for assembling new materials [12,13], for developing homo-geneous bioassays [14-16], and as multicolor fluorescent labels for ultrasensitive detection and imaging [7-11].

NPs possess several valuable qualities that are very attractive for fluorescent tagging: broad excitation spectrum, narrow emission spectrum, precise tunability of their

emission peak, longer fluorescence lifetime than organic fluorophores and negligible photobleaching.

The purpose of this chapter is to explain aspects of the synthesis, optical properties, surface chemistry, and biological applications of semiconductor NPs, also known as quantum dots (QDs), often composed of atoms from groups II-VI or III-V elements in the periodic table. QDs are defined as particles with physical dimensions smaller than the exciton Bohr radius [1-4]. For example, for spherical CdSe particles, this definition applies when the particle diameter is less than ~10 nm. The effect of quantum confinement results in unique optical and electronic properties that are not available in either discrete atoms or in bulk solids. Carrier confinement in all three dimensions results in size dependence of QDs optical properties, including light absorption, photoluminescence (PL), electroluminescence (EL) [17-20] and cathodoluminescence (CL) [9,21]. Additionally, nanocrystal QDs can be chemically manipulated like large molecules.

The combination of tunable electronic energies and chemical flexibility makes QDs ideal building blocks for biological applications. Recent work has demonstrated the dramatic benefits of QDs, including long-term photostability, high brightness, multi-target labeling with several colors, and single-source excitation for all colors of QDs. New avenues of research are being developed using QD conjugates in live cell analysis.

Most reported examples of QD conjugation to biomolecules are based on CdSe/ZnS core-shell colloids prepared in high boiling temperature organic solvents. The scope of this dissertation encompasses the development of novel bioconjugation approaches using different semiconductor materials: cadmium telluride (CdTe) and

core/shell cadmium selenide /cadmium sulfide (CdSe/CdS) quantum dots, synthesized in water, which significantly simplifies the preparation procedure. The challenges to using QDs for biological studies are threefold: (1) designing hydrophilic QDs that are luminescent, with surface chemistry adaptable to varied biological applications; (2) developing versatile techniques for selectively and specifically labeling cells and biomolecules; and (3) demonstrating that bioconjugates of QDs do not interfere with normal physiology. This dissertation addresses these concerns.

Besides this introductory chapter, this dissertation contains three additional chapters with different nanoparticle-biomolecule conjugation approaches. Chapter II describes the conjugation of luminescent CdTe NPs with a simple protein, bovine serum albumin (BSA), reports the structure of protein-NP conjugates, and describes their optical properties. Chapter III further elaborates on the bioconjugation of NPs with proteins as (1) a method for their organization in more complex structures and (2) a pathway to new sensing and imaging technologies. In this chapter, the preparation of bioconjugates from an antigen and an antibody conjugated to NPs of different sizes is described. It is demonstrated that the NP-labeled antigen and antibody form an immunocomplex, which pairs together NPs with red and green luminescence. Chapter IV presents the results of the combination of developed bioconjugation procedures in order to design new NP conjugates for cell targeting that will be photo stable, water soluble and biocompatible. Obtained bioconjugates were applied for cell labeling by our collaborators at University of Texas Medical Branch (Galveston, TX).

Potential of quantum dots in biochemistry

With the completion of the Human Genome Project and the cataloging of all gene sequences, biological and biomedical investigations are now focusing on how the tens or hundreds of thousands of proteins in a single cell function and interact with each other. A promising approach is fluorescence microscopy which has exquisite sensitivity down to the single-molecule level together with high spatial and subcellular resolution [22,23]. Because most cellular functions are accomplished by many proteins working together, a clear need exists to study multiple biological targets simultaneously in the cell. This goal has driven the development of new fluorescent labels that permit multiplexed labeling of cellular targets.

Colloidal semiconductor nanocrystal QDs are luminescent inorganic fluorophores that have the potential to overcome some of the functional limitations encountered by organic dyes in fluorescence labeling applications.

Small organic dyes commonly used for diagnostics applications and in biological imaging [24] have characteristics that limit their effectiveness in these applications.

Problems with organic fluorophores include narrow excitation bands and broad emission spectra, which can make detection of multiple light emitting probes difficult do to spectral overlap and low resistance to chemical degradation and photodegradation [25]. Fluorescent QDs have size-dependent tunable photoluminescence (PL) with broad excitation spectra and narrow emission bandwidths (full width at half maximum of ~30-45 nm) that span the visible spectrum [20,21,26-28], which allows for simultaneous excitation of several particle sizes at a single wavelength. In addition QDs have high photochemical stability, excellent resistance to chemical degradation and

4

photodegradation, and a good fluorescence quantum yield. Luminescence emission from QDs is detected at concentrations comparable to organic dyes by using conventional fluorescence methods, and individual QDs and QD-bioconjugates are easily observable by confocal microscopy [9,29].

History of semiconductor quantum dots

Victorian-era glass-melt recipes for red and orange colors contain, essentially, dilute concentrations of NPs (from zinc and cadmium sulfides and selenides). The nineteen-century chemists created these NPs spontaneously (and unknowingly) during the glass manufacturing process. These glasses were used to create colored windows. However, these richly hued progenitors lacked the fluorescence of the currently used semiconductor QDs.

Modern QD technology traces its origins, in part, to the mid-1970's quest for new answers to meet the worldwide energy crisis that renewed interest for devices capable of an efficient utilization of solar energy. Research in photoelectrochemistry (e.g., solar cell energy conversion) was tapping the semiconductor/liquid interface to exploit the advantageous surface area-to-volume ratio of nanocrystal particles for energy generation. A side product of these works was the exploration of their luminescent properties, and in particular the relationship between nanocrystal size and fluorescence properties [3,30-32].

Seminal development arose in the early 1980's from two laboratories, located far apart: Dr. Louis Brus at Bell Laboratories, and Drs. Alexander Efros and A.I. Ekimov of the Yoffe Institute in St.Peterburg (then Leningrad) in the former Soviet Union. Two Bell

Labs scientists, introduced to this field by Dr. Brus – Dr. Moungi Bawendi and Dr. Paul Alivisatos – moved to MIT and UC Berkeley, respectively, and continued to investigate QD optical properties. Their pioneering work paved the way for the current QDs applications.

Semiconductor QDs provide the opportunity to study the evolution of electronic behavior in a size regime intermediate between the molecular and bulk limits of matter.

Quantum confinement

Quantum confinement arises when one of the dimensions L of the object becomes of the order of the exciton Bohr radius:

$$a_{ex} = (k\hbar^2) / (m_{ex}{}^*e^2)$$

where k is the semiconductor permittivity, m_{ex} is the reduced exciton mass, and e the electron charge (for example, $a_{CuCl} = 7$Å, $a_{GaAs} = 100$Å and $a_{CdSe} = 56$Å).

The first controlled synthesis and systematic studies of nanometer size semiconductor crystals in all three dimensions were performed by Ekimov and Efros [33,34]. They studied quantum dot inclusions that were embedded in an insulating glass matrix. Ekimov's sample was the first to exhibit the quantum-confined blue shift of the first absorption (exciton) peak, varying as a^{-2} (a being the nanocrystals radius) [33]. Solving the effective Hamiltonian for a spherical geometry, Al.L.Efros and A.L.Efros computed the electron and hole energies in such a sphere and found a series of discrete lines, recovering the a^{-2} dependency observed in the experiment [34].

The most useful outcome of quantum confinement for application is the discretization of the energy levels at the edges of conduction and valence bands upon dimensional reduction. Because QDs exhibit discrete structure in their optical and electrical characteristics, they are sometimes referred to as "artificial atoms", even though to a chemist, they appear to be very large and complex molecules [3].

Optical properties and detection

The optical properties of semiconductor nanoclusters arise from interactions between electrons, holes, and their local environments. QDs emit light in a similar manner as a bulk semiconductor light-emitting diode (LED). However, LEDs are electrically activated, whereas QDs are activated by the absorption of a photon of light. A semiconductor QD absorbs a photon when the excitation energy exceeds the bandgap. This absorbed photon of light creates an electron-hole pair. During this process, electrons are promoted from the valence band to the conduction band.

Measurements of UV–visible spectra reveal a large number of energy states in QDs. The lowest excited energy state is shown by the first observable peak, known as the quantum-confinement peak. The created electron-hole pair quickly recombines leading to emission of a lower energy photon. In a semiconductor material, the energy of the emitted photon is determined by quantum confinement (or the size of the QD). Moreover, QDs just a few angstroms different in size emit different wavelengths of light (Figure I-1). This quantum mechanical physics [3,13,26,28,35-38] can be simply summarized: smaller QDs emit blue light, medium sized emit green/yellow light, and larger ones emit red light.
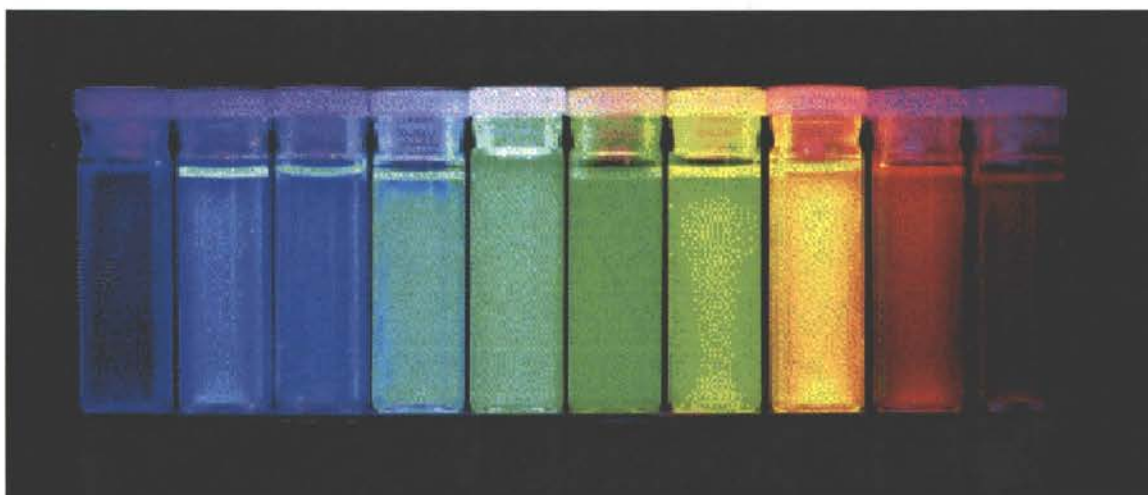
Figure I-1. Ten distinguishable emission colors of ZnS capped CdSe QDs excited with a near-UV lamp. From left to right (blue to red), the emission maxima are located at 443, 473, 481, 500, 518, 543, 565, 587, 610, and 655 nm (Adopted from Ref. [39]).

Excitation at shorter wavelengths is possible because multiple electronic states are present at higher energy levels. In fact, the molar extinction coefficient gradually increases towards shorter wavelengths. This is an important feature for biological applications because it allows simultaneous excitation of multicolor QDs with a single light source.

Light emission arises from the recombination of mobile or trapped charge carriers. The emission from mobile carriers is called excitonic fluorescence and is observed as a sharp peak. The excited-state lifetimes of nanocrystals contain three exponential components. In bulk measurements, the lifetimes are 5 ns, 20–30 ns, and 80–200 ns, with 20–30 ns dominating [40]. These excited-state decay rates are slightly slower than those of organic dyes (1–5 ns), but much faster than those of lanthanide probes (1 s–1 ms). Single-dot measurement further reveals that the excited-state lifetimes are dependent on the emission intensity, but the exact origins of this multi-exponential behavior remain unclear.

Difference between optical properties of semiconductor QDs and typical dyes

The applicability of QDs as luminescent probes is summarized in Table I-1 [41], where their properties are compared with those of traditional dyes. From this table, it is evident that although not yet a panacea, QDs present considerable advantage over conventional organic dyes.

Table I-1. Desirable features of a luminescent probe: comparison of the properties of conventional fluorescent probes and quantum dots.

	Property	Fluorescent probe	Quantum dot probe
1	Broadband excitation	$\mathbf{X}^a$	$\sqrt{}^b$
2	Narrow bandwidth emission	$\mathbf{X}$	$\sqrt{}$
3	Emit light of high intensity	**moderate**	$\sqrt{}$
4	Available in many colors	$\sqrt{}$	$\sqrt{}$
5	Readily attachable to analytes	$\sqrt{}$	**moderate**
6	Resistant to quenching	$\mathbf{X}$	$\sqrt{}$
7	Photochemically stable	$\mathbf{X}$	$\sqrt{}^c$
8	Cheap and readily available	$\sqrt{}$	$\mathbf{X}$

[a] X = "No"

[b] $\sqrt{}$ = "Yes"

[c] Quantum dots are prone to "blinking" [36]

In order to illustrate the information in Table I-1, as an example, the excitation and the emission spectra of a typical dye rhodamine 6G and CdSe QDs are shown in Figure I-2 [39]. The QD emission spectrum is nearly symmetric and much narrower in peak width. Its excitation profile is broad and continuous. The QDs can be efficiently excited at any wavelength shorter than ~530 nm. By contrast, the organic dye rhodamine 6G has a broader and more asymmetric emission peak and is excited in a narrower wavelength range.

Quantum yield (i.e., the number of photons emitted divided by number of photons absorbed) is a critical property of any fluorescent material. With a low quantum yield, the efficiency is very low, and so the signal intensity and sensitivity can be poor.

In comparison to organic dyes such as rhodamine 6G and fluorescein, CdSe nanocrystals show similar or slightly lower quantum yields at room temperature, but the lower quantum yields are compensated by their larger absorption cross-sections and much reduced photobleaching rates. Bawendi and coworkers [26,28] estimated that the molar extinction coefficients of CdSe QDs are about 10^5–10^6 $M^{-1}cm^{-1}$, depending on the particle size and the excitation wavelength. These values are 10–100 times larger than those of organic dyes, but are similar to the absorption cross-sections of phycoerytherin, a multichromophore fluorescent protein. Chan and Nie [7] estimated that single ZnS-capped CdSe QDs are ~20 times brighter and ~100–200 times more stable than single rhodamine 6G molecules.

The quantum yield of most organic dye molecules is reduced, sometimes to zero, upon conjugation to biomolecules. Some QD conjugates have quantum yields up to 80% and are typically unaffected by the attachment to biomolecules.
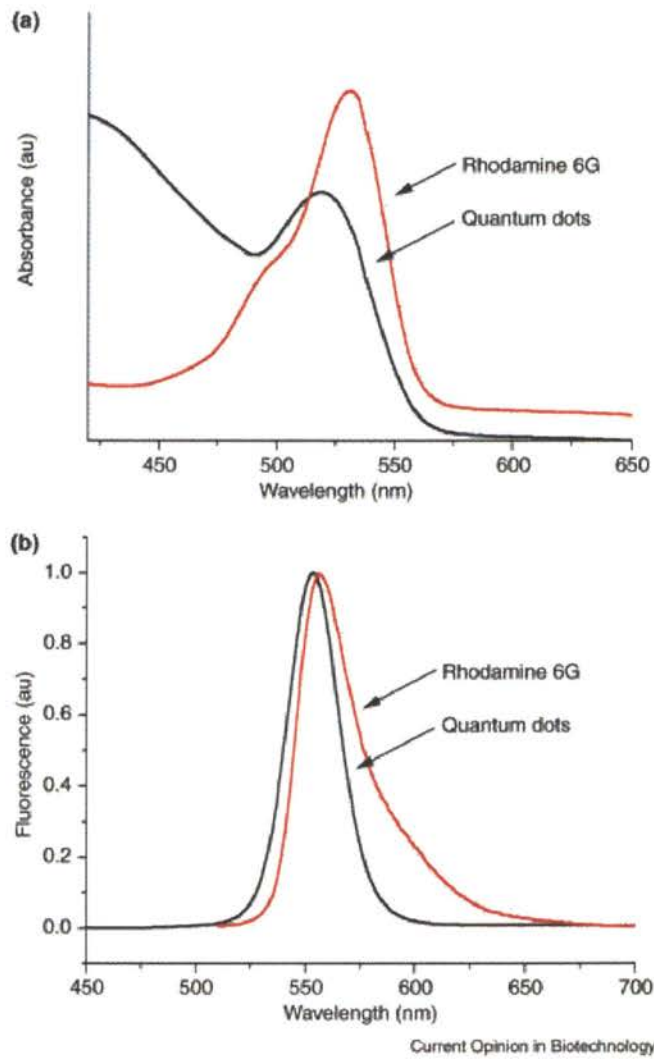
Figure I-2. Comparison of the excitation and the emission profiles between Rhodamine 6G (red) and CdSe QDs (black). (**a**) excitation profile, (**b**) emission profile (Adopted from reference [39]).

12

Epifluorescence microscopy

QDs can be used immediately in exciting epifluorescence microscopes that are equipped with dye-optimized filter sets. The broad absorbance spectrum of the QD allows a unique possibility in lamp-based fluorescent microscopes. The integrated absorbance across a broader excitation band is substantially higher than any single wavelength value. Using a lamp with a short-pass filter allows highly efficient excitation of the QDs with a much larger proportion of the lamp energy utilized. The narrow emission spectra of QDs allow the use of narrower emission filters compared to dye filter sets. The narrow bandpass filters reject more of sample autofluorescence (increasing signal to noise ratio).

The QD emission is very photostable. This makes the QDs very easy to be scanned without concerns of losing the fluorescence image. Quantitative analysis may also be simplified, as photobleaching effects are removed. High photostability also allows the use of long integration times, to improve sensitivity and signal-to-noise ratio.

Confocal microscopy

QD bioconjugates are ideal for confocal microscopy. The broad excitation allows the use of any of several commonly available lasers. QDs allow true multicolor confocal anlysis since all of the QDs can be excited by a single laser source. This removes issues such as accurate laser alignment or excitation chromatic effects. The high photostability exhibited by the QDs is especially valuable for confocal microscopy. When data is being gathered from one image plane, other planes remain illuminated by the laser source. In

the case of organic dyes, out-of-plane images may be unintentionally photobleached, leading to inaccurate measurements. Out-of-plane QDs remain highly luminescent.

In confocal microscopes, a very high power density may be achieved through the use of a highly focused laser. Leaving photobleaching effects aside, the light emitted from an organic dye increases with increasing power density only up to the point of saturation of the dye, according to the "excited state lifetime" of the dye (i.e., the time between absorption of a photon and emission of a photon from a dye molecule). In the excited state, the organic dye is unable to absorb another photon; therefore, saturation occurs at high power densities. The excited state of QDs is approximately 12 ns, compared to around 2 ns for an organic dye.

Blinking, where single QDs change from a "dark" to an "active" state, has been reported [36] and could be expected to reduce the signal from a QD assay.

QDs have been reported to be efficiently excited in a dual- or multi-photon mode [42]. However, the author is not yet aware of any literature results that describe the use of QD conjugates in multi-photon microscopy.

Synthesis of quantum dots

There are two distinct synthetic routes to semiconductor nanostructures: in the first "physical" approach, they are grown by lithographic or molecular beam techniques, and in the second "chemical" approach, they are formed either by particle growth in solid (glass) matrices or by methods of colloidal chemistry.

Typically, the wet-chemical preparation of NPs is carried out in the presence of stabilizing agents (often citrate, phosphanes, or thiols) which bind to the atoms exposed

at the surface of the NPs. This capping leads to a stabilization and prevents uncontrolled growth and aggregation of the NPs. This approach allows production of stable colloids of nanocrystalline particles, which are easily processable and can be handled like ordinary chemical substances.

Colloids of II-VI crystallites were first prepared by arrested precipitation in homogenous solution [43,44]. Before 1993, QDs were mainly prepared in aqueous solution with added stabilizing agents (e.g. thioglycerol or polyphosphate). This procedure yielded low-quality QDs with poor fluorescence efficiencies and large size variations (relative standard deviation [RSD]>15%).

In 1993, Bawendi and coworkers [26] synthesized highly luminescent CdE (E= S, Se, Te) QDs by using high-temperature organometallic procedure via the reaction below:

$$Cd(CH_3)_2 + (C_8H_{17})_3PSe \xrightarrow{\ 300^{\circ}C,\ HDA\text{-}TOPO\text{-}TOP\ } Q-CdSe + \cdots.$$
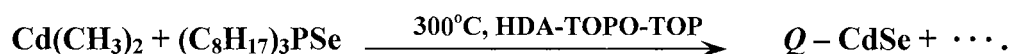
The nanocrystals had nearly perfect crystal structures and narrow size variations ([RSD] <5%), but the fluorescence quantum yields were still relatively low (~ 10%)

A recent excellent contribution in this area is the large-scale synthesis of high-quality QDs. Peng et al. [45] described the synthesis of CdTe, CdSe, and CdS NPs in large quantities using inexpensive starting materials and also developed procedures for controlling the surface structure of QDs and for producing stable QDs with red emissions.

Various II–VI QDs have been prepared in aqueous solutions by the metathesis reaction as shown below: CdS [46], CdSe [47], CdTe [48], $Cd_xHg_{1-x}Te$ [49] and HgTe [50].

$$\text{Cd(ClO}_4)_2 + H_2Te \xrightarrow{\quad 100°C,\ H_2O,\ thiol \quad} Q - CdTe + \cdots.$$
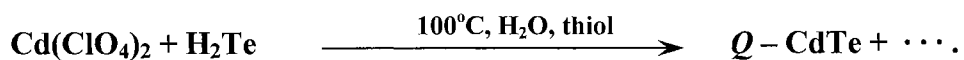
The presence of different thiols (thioethanol, thioglycerol, thioglycolic acid, dithioglycerol, mercaptoethylamine, etc.) as stabilizing agents and capping ligands allows control over the particle size during the synthesis (a size range of 2.0–8.0 nm is generally possible).

The advantages of the aqueous synthesis are low-cost, reproducibility and the simplicity of mass production.

Synthesis of core/shell quantum dots

Some examples of core-shell quantum dot structures reported earlier include CdS on CdSe and CdSe on CdS [51], ZnS grown on CdS [52], ZnS on CdSe and the inverse structure [53], CdS/HgS/CdS quantum dot quantum wells [54], ZnSe overcoated CdSe [55], and SiO_2 on Si [56,57].

Overcoating NPs with higher band gap inorganic materials has been shown to improve the photoluminescence quantum yields by passivating surface nonradiative recombination sites. Particles passivated with inorganic shell structures are more robust than organically passivated dots and have greater tolerance to processing conditions necessary for incorporation into solid state structures.

The deposition of a surface-capping layer such as ZnS or CdS was found to dramatically increase the quantum yields of CdSe NPs up to 40–50% at room temperature [27,28,38]. ZnS has a wider bandgap (energy difference between the valence band and the conduction band) than CdSe, but the Zn—S bond length is similar to that of

Cd—Se. This property allows the epitaxial growth of a thin ZnS layer on the CdSe core. In practice, the $Zn(CH_3)_2/S$ solution is added slowly in small aliquots to a CdSe/tri-n-octylphosphine oxide (TOPO, a high boiling point and coordinating solvent) solution to prevent ZnS nucleation.

Surface chemistry

The complex surface chemistry of nanocrystals has been studied by NMR spectroscopy, Fourier Transform Infrared Spectroscopy (FTIR) and X-ray photoemission spectroscopy (XPS) [58,59]. Morphologically, QDs are not smooth spherical particles, but are faceted with many planes and edges. QDs are generally considered to be negatively charged owing to molecules adsorbed on the surface [60].

Capping quantum dots for biological application

A key requirement for the successful use of QDs in biological applications is aqueous solubility.

Most QDs used for biological applications were generally produced with a capping layer composed of one or more organic ligands such as trioctylphosphine (TOP) or trioctylphosphine oxide (TOPO). These ligands are hydrophobic and thus QDs capped with these coatings are not compatible with aqueous assay conditions.

To make the QDs water soluble, these organophilic surface species are generally exchanged with more-polar species, and both monolayer [7] and multilayer [8] ligand shells have been pursued. Although the monolayer method is reproducible, rapid, and

produces QDs with a regular, well oriented, thin coating, their colloidal stability is poor [61]. In contrast, the multilayer method yields QDs that are stable in vitro [62] , but the coating process is long and the coating is difficult to control. A more serious concern is that both approaches still produce QDs that tend to aggregate and adsorb nonspecifically.

To resolve this problem, researchers have explored two additional coatings. First, the outer ligand shell of the QD has been overcoated with proteins adsorbed through hydrophobic or ionic interactions [9]. Other layers can then be added to allow conjugation with specific biomolecules. Indeed, this method has provided new reagents for fluoroimmunoassays [63]. Second, the outer ligand shell has been overcoated with surfactants or polymers to prevent nonspecific adsorption of biomolecules while still permitting bioconjugation. For example, silica coated QDs have been further modified with small monomers of poly(ethylene glycol) to reduce nonspecific adsorption [64].

Methods for conferring water solubility on semiconductor QDs prepared in hydrophobic environments remains an active topic of research.

Bioconjugation of semiconductor quantum dots

Analogous to the interactions that are abundant in many reaction centers of enzymes between the amino acid side chains and the metal centers, the interaction between organic ligands and the surface of an inorganic NP paves the way for the coupling of biomolecular recognition systems to generate novel materials. Although inorganic NPs can be prepared from various materials by several methods, (as discussed above) the coupling and functionalization with biological components has only been performed with a limited number of chemical methods.

Some examples for QDs bioconjugation are summarized in Table I-2. The general schematic representation of methods to couple inorganic NPs and biomolecules is shown on Figure I-3.

Current bioconjugation methods are schematically illustrated in Figure I-4. There are two general approaches to bioconjugation of QDs. The first approach is linking biomolecules covalently to the capping layer that surrounds each QD using conventional synthetic methodologies. The second approach is attachment of biomolecules to QDs via different non-covalent interactions.

Covalent attachment of biomolecules to capped quantum dots

Reactive functional groups on the surface of QDs can include primary amines, carboxylic acids, alcohols, and thiols. Primary amines react with carboxylic acids, catalyzed with a carbodiimide or sulfo *N*-hydroxysuccinimide ester, to form a stable amide bond [25]. The example of such covalent attachment is illustrated in Figure I-4 (a) where standard carbodiimide-based chemistry was used to couple both transferrin and IgG to mercaptoacetic acid-coated nanocrystals [7].

Table I-2. Coupling of inorganic nanoparticles and biomolecules. *

Nanoparticle	Ligand on the QD surface	Functional group of biomolecule	Biomolecule	Reference
ZnS		HS-Cys	gluthathione	[65]
CdS		HS-Cys	peptides	[66]
CdS	Cd^{2+}, HS-$(CH_2)_2$-OH[a]		DNA	[67,68]
CdSe/ZnS[b]		HS-$(CH_2)_6$-	DNA	[10]
CdSe/ZnS[b]	HS-(CH_2)-$COOH$	H_2N-Lys	immunoglobulin, transferrin	[7]
CdSe/CdS/SiO$_2$[b]	3-aminopropyl-trimethoxysilane	NHS-biotin	streptavidin	[8]
SnO$_2$, TiO$_2$	$HOOC$-$(CH_2)_n$-NH_2	HOOC-Glu	proteins[c]	
CdSe/ZnS[b]	Lipoic acid	H_2N-Lys[a]	leucine zipper fusion proteins	[21]
GaAs, InP	phosphoramide s -NH$_2$	HOOC-Glu	proteins[c]	[69]
CdSe/ZnS	dithiothreitol (DTT)		5'-aminated oligonucleotides, DNA	[11]
CdTe	L-cysteine	H_2N-Lys	BSA	Chapter II and [70]
CdTe	Mercatoacetic acid	H_2N-Lys	BSA, anti-BSA	Chapter III and [71]
CdSe/CdS	L-cysteine	H_2N-Lys	BSA	Chapter IV

(*) - Examples of chemical interactions used for the coupling of nanoparticles with biological macromolecules. [a] Adsorption through Coulombic interactions. [b] Core/shell nanoparticles. [c] Proposed from related studies of nanoparticle binding to analogously modified solid substrates.

Figure I-3. General schematic representation of methods to couple inorganic nanoparticles and biomolecules (FG=functional coupling group). Representative structures of typical linkers are listed beneath (see also Table I-2).

(a) Bifunctional linkage

S-CH$_2$-CO-NH-biomolecule

(b) Hydrophobic attraction

O=P ... HNOC { COOH
         HNOC { CO-NH-biomolecule
                { COOH

(c) Silanization

S ~ Si-O-Si ~ biomolecule

(d) Electrostatic attraction

biomolecule

(e) Nanobeads

-CH$_2$-CO-NH-biomolecule

Current Opinion in Biotechnology

Figure I-4. Schematic illustration of bioconjugation methods. **(a)** Use of a bifunctional ligand such as mercaptoacetic acid for linking QDs to biomolecules [7]. **(b)** TOPO-capped QDs bound to a modified acrylic acid polymer by hydrophobic forces. **(c)** QD solubilization and bioconjugation using a mercaptosilane compound [8]. **(d)** Positively charged biomolecules are linked to negatively charged QDs by electrostatic attraction [9]. **(e)** Incorporation of QDs in microbeads and nanobeads [72].

Another example is covalent attachment of *N*-hydroxysuccinimide ester activated biotin onto the surface of the quantum dots allowing subsequent streptavidin–biomolecule conjugates to be immobilized [8].

In recent development, Arnheim and co-workers describe activating the free hydroxyl groups of bidentate ligand dithiothreitol (DTT) capped CdSe/ZnS quantum dots as carbonyl diimidazole (CDI) derivatives [11]. These CDI-activated quantum dots react readily with 5'-aminated oligonucleotides, simply by mixing and stirring, to form stable carbamate linkages. Pre-activating nanocrystals in this manner ensures that the coupling procedure is trivial and negates any requirement for additional coupling reagents, etc. Moreover, since such modified oligonucleotides are readily available commercially this immobilization technique has generic applicability for the quantum dot labeling of DNA. The methodology is not restricted to 5'-aminated oligonucleotides, in theory any molecule that possesses an appropriate nucleophilic center, such as the amino termini of a peptide or protein, may be labeled with quantum dots in analogous fashion.

Non-covalent attachment of biomolecules to capped quantum dots

Biomolecules may alternatively be attached to quantum dots by the whole spectrum of non-covalent interactions.

In the case of nanoparticles that are stabilized by anionic ligands, the biomolecules are often coupled through noncovalent electrostatic interactions. (Figure I-4 d).

The first example of this kind of attachment was described by Alivisatos and co-workers [8] who labeled cell nuclei with aqueous compatible, silanized CdSe/CdS

23

quantum dots via electrostatic and hydrogen bonding interactions with trimethoxysilylpropyl urea, a component of the silanized cap (Figure I-4 c).

A similar approach has been used by Mattoussi et al. [9] in which engineered positively charged recombinant fusion protein composed of a basic leucine zipper domain fused to a maltose binding protein domain was directly adsorbed onto negatively charged QDs stabilized with lipoic acid (Figure I-3) through electrostatic interactions.

Similarly, the adsorption of DNA molecules to positive or neutral CdS nanoparticles has been studied in detail [67,68,73].

Another approach for linking biomolecules to nanocrystals is to use a thiol-exchange reaction. Here, mercapto-coated QDs (prepared by direct adsorption) are mixed with thiolated biomolecules (such as oligonucleotides or proteins) [10,74]. After overnight incubation at room temperature, a chemical equilibrium is reached between the adsorbed thiols and the free thiols. In this case, immobilization is formally non-covalent since it arises as a result of displacement of some of the capping agents by the thiolated oligonucleotides. Willner et al. describe similar conditions for immobilizing thiolated oligonucleotides onto cystamine / thioethanesulfonate coated CdS quantum dots and estimate that between 20 and 24 oligonucleotides can be immobilized onto each nanoparticle [75].

The above examples demonstrate that some chemical means have already been explored for the physical linkage of inorganic and biological materials. However, there is still a great demand for alternative methods to allow for compensation of typical problems that arise in the biofunctionalization of inorganic nanoparticles. In particular, harsh reaction conditions often lead to the degradation and inactivation of sensitive

biological compounds, and ligand-exchange reactions that occur at the colloid surface often hinder the formation of stable bioconjugates. Moreover, the synthesis of stoichiometrically defined nanoparticle-biomolecule complexes is a great challenge, and is particularly important from a molecular engineering point-of-view to generate well-defined nanoarchitectures.

Some examples of biological application of quantum dots

Bioconjugated QDs have been used in DNA hybridization [10], immunoassay [7], receptor-mediated endocytosis [7], and time-gated fluorescence imaging of tissue sections [40].

Alivisatos et al. and Nie et al. were the first to label biological cells with luminescent semiconductor nanocrystals (QDs) [7,8]. QD binding was achieved through non-specific interactions or through secondary binding to molecular receptors. In one case, nanocrystals were attached to cells through non-specific electrostatic/hydrogen bonding interactions or by using avidin and biotin molecules as intermediaries between the nanocrystal and the cell [8]. In another study, QDs were modified with transferrin protein for non-specific cellular uptake, or attached to immunoglobulin G (IgG) secondary antibodies [7].

An important advantage is that the extremely high photostability of QDs allows real-time monitoring or tracking of intracellular processes over long periods of time (minutes to hours). Another advantage is the ability to use multicolor nanocrystals to simultaneously image multiple targets inside living cells or on the cell surface.

Furthermore, with an inert layer of surface coating, the toxicity of Cd derivatives may be mediated.

QD conjugates have been shown to detect the breast cancer marker Her2 on fixed cells, mouse mammary tumor sections, and on the surface of unfixed live cells [76]. The size of the QDs does not appear to have a significant effect: intracellular targets, including microtubules, actin filaments, nuclei, and mitochondria have been effectively labeled [76].

Also QDs have been injected inside living *Xenopus* embryos [77]. Authors of this paper reported that they were able to inject single cells with quantum dots. By following the QD fluorescence during embryo development, cell lineage could be followed all the way to the tadpole stage.

Endocytic uptake of QDs by cells has been demonstrated [78]. In this study, the cells appeared unaffected by the presence of the QDs over a period of more than a week. Furthermore, the QD fluorescence signal remained detectable throughout this period.

Nanocrystals are also emerging as a new class of fluorescent labels for *in vivo* cellular imaging. QDs bearing co-adsorbed peptides and polyethylene glycol QDs conjugated to lung-targeting peptides were injected into mice and showed accumulation in the lungs [79]. QDs specific for blood vessels of lymphatic vessels in tumors were targeted in a similar manners.

A further application of QDs is the multiplexed optical encoding and high-throughput analysis of genes and proteins, as reported by Nie and coworkers [72]. Polystyrene beads are embedded with multicolor CdSe QDs at various color and intensity combinations. The use of six colors and 10 intensity levels can theoretically encode one

million protein or nucleic acid sequences. Specific capturing molecules such as peptides, proteins, and oligonucleotides are covalently linked to the beads and are encoded by the bead's spectroscopic signature. A single light source is sufficient for reading all the QD-encoded beads. To determine whether an unknown analyte is captured or not, conventional assay methodologies (similar to direct or sandwich immunoassay) can be applied. This so-called `barcoding' technology can be used for gene profiling and high-throughput drug and disease screening.

Conclusions

Published papers demonstrate the successful application of bioconjugated quantum dots for labeling cells and macromolecular constituents of cells.

QDs conjugates exhibit extremely desirable properties for biological imaging. Their photostability makes them easy to use and allows integration of signal to increase sensitivity. Many spectrally narrow QD colors can be created to allow simultaneous analysis of many conjugates. QDs can be excited by the same light source, simplifying the instrumentation. Quantum yield and excitation cross sections are very high giving very bright signals. The large difference between excitation and emission colors reduces autofluorescence and simplifies instrumentation. Immediate improvements can be realized using quantum dots in current immunostaining applications.

In the future, QDs promise to open up new applications in live cell and whole organism imaging. As further colors and conjugates of QDs become widely used, a plethora of additional applications is anticipated.

References

1. Henglein, A. *Chem.Rev.* **1989,** *89*(8), 1861-1873.

2. Schmid, G. *Chem.Rev.* **1992,** *92*(8), 1709-1727.

3. Alivisatos, A. P. *Science* **1996,** *271*(5251), 933-937.

4. Nirmal, M.; Brus, L. *Acc.Chem.Res.* **1999,** *32*(5), 407-414.

5. Niemeyer, C. M. *Angewandte Chemie, International Edition* **2001,** *40*(22), 4128-4158.

6. Whaley, S. R.; English, D. S.; Hu, E. L.; Barbara, P. F.; Belcher, A. M. *Nature* **2000,** *405*(6787), 665-668.

7. Chan, W. C. W.; Nie, S. *Science* **1998,** *281* 2016-2018.

8. Bruchez, M. J.; Moronne, M.; Gin, P.; Weiss, S.; Alivisatos, A. P. *Science* **1998,** *281* 2013-2016.

9. Mattoussi, H.; Mauro, J. M.; Goldman, E. R.; Anderson, G. P.; Sundar, V. C.; Mikulec, F. V.; Bawendi, M. G. *J.Am.Chem.Soc.* **2000,** *122*(49), 12142-12150.

10. Mitchell, G. P.; Mirkin, C. A.; Letsinger, R. L. *J.Am.Chem.Soc.* **1999,** *121*(35), 8122-8123.

11. Pathak, S.; Choi, S. K.; Arnheim, N.; Thompson, M. E. *J.Am.Chem.Soc.* **2001,** *123*(17), 4103-4104.

12. Mirkin, C. A.; Letsinger, R. L.; Mucic, R. C.; Storhoff, J. J. *Nature* **1996,** *382*(6592), 607-609.

13. Alivisatos, A. P.; Johnsson, K. P.; Peng, X. G.; Wilson, T. E.; Loweth, C. J.; Bruchez, M. P.; Schultz, P. G. *Nature* **1996,** *382* 609-611.

14. Elghanian, R.; Storhoff, J. J.; Mucic, R. C.; Letsinger, R. L.; Mirkin, C. A. *Science* **1997,** *277*(5329), 1078-1080.

15. Dubertret, B.; Calame, M.; Libchaber, A. J. *Nature Biotechnology* **2001,** *19*(4), 365-370.

16. Reynolds, R. A., III; Mirkin, C. A.; Letsinger, R. L. *J.Am.Chem.Soc.* **2000,** *122*(15), 3795-3796.

17. Colvin, V. L.; Schlamp, M. C.; Alivisatos, A. P. *Nature* **1994,** *370* 354-357.

18. Dabbousi, B. O.; Bawendi, M. G.; Onitsuka, O.; Rubner, M. F. *Appl.Phys.Lett.* **1995,** *66*(11), 1316-1318.

19. Schlamp, M. C.; Peng, X. G.; Alivisatos, A. P. *J.Appl.Phys.* **1997,** *82* 5837-5842.

20. Mattoussi, H.; Radzilowski, L. H.; Dabbousi, B. O.; Thomas, E. L.; Bawendi, M. G.; Rubner, M. F. *J.Appl.Phys.* **1998,** *83* 7965-7974.

21. Rodriguez-Viejo, J.; Mattoussi, H.; Heine, J. R.; Kuno, M. K.; Michel, J.; Bawendi, M. G.; Jensen, K. F. *J.Appl.Phys.* **2000,** *87*(12), 8526-8534.

22. Kues, T.; Peters, R.; Kubitscheck, U. *Biophysical Journal* **2001,** *80*(6), 2954-2967.

23. Weiss, S. *Science* **1999,** *283*(5408), 1676-1683.

24. Schrock, E.; de Manoir, S.; Veldman, T.; Schoell, B.; Wienberg, J.; Ferguson-Smith, M. A.; Ning, Y.; Ledbetter, D. H.; Bar-Am, I. *Science* **1996,** *273*(5274), 494-497.

25. Hermanson, G. T. *Bioconjugate Techniques;* Academic Press: San Diego, CA, 1996.

26.   Murray, C. B.; Norris, D. J.; Bawendi, M. G. *J.Am.Chem.Soc.* **1993,** *115*(19), 8706-8715.

27.   Hines, M. A.; Guyot-Sionnest, P. *J.Phys.Chem.* **1996,** *100* 468.

28.   Dabbousi, B. O.; Rodriguezviejo, J.; Mikulec, F. V.; Heine, J. R.; Mattoussi, H.; Ober, R.; Jensen, K. F.; Bawendi, M. G. *J.Phys.Chem.B* **1997,** *101* 9463-9475.

29.   Kuno, M.; Fromm, D. P.; Hamann, H. F.; Gallagher, A.; Nesbitt, D. J. *J.Chem.Phys.* **2000,** *112*(7), 3117-3120.

30.   Henglein, A. *J.Phys.Chem.* **1982,** *86*(13), 2291-2293.

31.   Rossetti, R.; Brus, L. *J.Phys.Chem.* **1982,** *86*(23), 4470-4472.

32.   Fojtik, A.; Weller, H.; Koch, U.; Henglein, A. *Berichte der Bunsen-Gesellschaft* **1984,** *88*(10), 969-977.

33.   Ekimov, A. I.; Onushchenko, A. A. *Tr.Vses.Konf.Fiz.Poluprovodn* **1982,** *2*.

34.   Efros, Al. L.; Efros, A. L. *Fizika i Tekhnika Poluprovodnikov* **1982,** *16*(7), 1209-1214.

35.   Du, H.; Chen, C.; Krishnan, R.; Krauss, T. D.; Harbold, J. M.; Wise, F. W.; Thomas, M. G.; Silcox, J. *Nano Letters* **2002,** *2*(11), 1321-1324.

36.   Empedocles, S.; Bawendi, M. *Acc.Chem.Res.* **1999,** *32*(5), 389-396.

37.   Norris, D. J.; Bawendi, M. G. *Phys.Rev.B: Condens.Matter* **1996,** *53*(24), 16338-16346.

38.   Peng, X. G.; Schlamp, M. C.; Kadavanich, A. V.; Alivisatos, A. P. *J.Amer.Chem.Soc.* **1997,** *119* 7019-7029.

39.   Chan Warren, C. W.; Maxwell, D. J.; Gao, X.; Bailey, R. E.; Han, M.; Nie, S. *Current Opinion in Biotechnology* **2002,** *13*(1), 40-46.

40. Dahan, M.; Laurence, T.; Pinaud, F.; Chemla, D. S.; Alivisatos, A. P.; Sauer, M.; Weiss, S. *Optics Letters* **2001,** *26*(11), 825-827.

41. Sutherland, A. J. *Current Opinion in Solid State & Materials Science* **2002,** *6*(4), 365-370.

42. Blanton, S. A.; Hines, M. A.; Schmidt, M. E.; Guyot-Sionnest, P. *Journal of Luminescence* **1996,** *70*(1-6), 253-268.

43. Brus, L. *IEEE J.Quantum Electron.* **1986,** *QE-22*(9), 1909-1914.

44. Brus, L. *J.Phys.Chem.* **1986,** *90*(12), 2555-2560.

45. Peng, Z. A.; Peng, X. *J.Amer.Chem.Soc.* **2001,** *123*(1), 183-184.

46. Vossmeyer, T.; Katsikas, L.; Giersig, M.; Popovic, I. G.; Diesner, K.; Chemseddine, A.; Eychmueller, A.; Weller, H. *J.Phys.Chem.* **1994,** *98*(31), 7665-7673.

47. Rogach, A. L.; Kornowski, A.; Gao, M.; Eychmueller, A.; Weller, H. *J.Phys.Chem.B* **1999,** *103*(16), 3065-3069.

48. Rogach, A. L.; Katsikas, L.; Kornowski, A.; Su, D.; Eychmueller, A.; Weller, H. *Ber.Bunsen-Ges.* **1996,** *100*(11), 1772-1778.

49. Harrison, M. T.; Kershaw, S. V.; Burt, M. G.; Eychmuller, A.; Weller, H.; Rogach, A. L. *Mater.Sci.Eng., B* **2000,** *B69-70* 355-360.

50. Rogach, A.; Kershaw, S.; Burt, M.; Harrison, M.; Kornowski, A.; Eychmuller, A.; Weller, H. *Advanced Materials* **1999,** *11* (7), 552-555.

51. Tian, Y.; Newton, T.; Kotov, N. A.; Guldi, D. M.; Fendler, J. H. *J.Phys.Chem.* **1996,** *100*(21), 8927-8939.

52. Youn, H. C.; Baral, S.; Fendler, J. H. *J.Phys.Chem.* **1988,** *92*(22), 6320-6327.

53. Kortan, A. R.; Hull, R.; Opila, R. L.; Bawendi, M. G.; Steigerwald, M. L.; Carroll, P. J.; Brus, L. E. *J.Amer.Chem.Soc* **1990,** *112*(4), 1327-1332.

54. Mews, A.; Eychmueller, A.; Giersig, M.; Schooss, D.; Weller, H. *J.Phys.Chem.* **1994,** *98*(3), 934-941.

55. Danek, M.; Jensen, K. F.; Murray, C. B.; Bawendi, M. G. *Chem.Mater.* **1996,** *8*(1), 173-180.

56. Wilson, W. L.; Szajowski, P. F.; Brus, L. E. *Science* **1993,** *262*(5137), 1242-1244.

57. Littau, K. A.; Szajowski, P. J.; Muller, A. J.; Kortan, A. R.; Brus, L. E. *J.Phys.Chem.* **1993,** *97*(6), 1224-1230.

58. Becerra, L. R.; Murray, C. B.; Griffin, R. G.; Bawendi, M. G. *J.Chem.Phys.* **1994,** *100*(4), 3297-3300.

59. Katari, J. E. B.; Colvin, V. L.; Alivisatos, A. P. *J.Phys.Chem.* **1994,** *98*(15), 4109-4117.

60. O'Neil, M.; Marohn, J.; McLendon, G. *J.Phys.Chem.* **1990,** *94*(10), 4356-4363.

61. Aldana, J.; Wang, Y. A.; Peng, X. *J.Am.Chem.Soc.* *123*(36), 8844-8850.

62. Gerion, D.; Pinaud, F.; Williams, S. C.; Parak, W. J.; Zanchet, D.; Weiss, S.; Alivisatos, A. P. *J.Phys.Chem. B* **2001,** *105* (37), 8861-8871.

63. Goldman, E. R.; Anderson, G. P.; Tran, P. T.; Mattoussi, H.; Charles, P. T.; Mauro, J. M. *Analytical Chemistry* **2002,** *74*(4), 841-847.

64. Gerion, D.; Parak, W. J.; Williams, S. C.; Zanchet, D.; Micheel, C. M.; Alivisatos, A. P. *J.Am.Chem.Soc.* **2002,** *124*(24), 7070-7074.

65. Bae, W.; Abdullah, R.; Henderson, D.; Mehra, R. K. *Biochem.Biophys.Res.Comm.* *237*(1), 16-23.

66. Dameron, C. T.; Reese, R. N.; Mehra, R. K.; Kortan, A. R.; Carroll, P. J.; Steigerwald, M. L.; Brus, L. E.; Winge, D. R. *Nature* **1989**, *338*(6216), 596-597.

67. Mahtab, R.; Harden, H. H.; Murphy, C. J. *J.Am.Chem.Soc.* **2000**, *122*(1), 14-17.

68. Mahtab, R.; Rogers, J. P.; Murphy, C. J. *J.Am.Chem.Soc.* **1995**, *117*(35), 9099-9100.

69. Chopra, S. K.; Martin, J. C. *Heteroatom Chemistry* **1991**, *2*(1), 71-79.

70. Mamedova, N. N.; Kotov, N. A.; Rogach, A. L.; Studer, J. *Nano Letters* **2001**, *1*(6), 281-286.

71. Wang, S.; Mamedova, N.; Kotov, N. A.; Chen, W.; Studer, J. *Nano Letters* **2002**, *2*(8), 817-822.

72. Han, M.; Gao, X.; Su, J. Z.; Nie, S. *Nature Biotechnology* **2001**, *19*(7), 631-635.

73. Mahtab, R.; Rogers, J. P.; Singleton, C. P.; Murphy, C. J. *J.Am.Chem.Soc.* **1996**, *118*(30), 7028-7032.

74. Willard, D. M.; Carillo, L. L.; Jung, J.; van Orden, A. *Nano Letters* **2001**, *1*(10), 581.

75. Willner, I.; Patolsky, F.; Wasserman, J. *Angewandte Chemie, International Edition* **2001**, *40*(10), 1861-1864.

76. Wu, X.; Liu, H.; Liu, J.; Haley, K. N.; Treadway, J. A.; Larson, J. P.; Ge, N.; Peale, F.; Bruchez, M. P. *Nature Biotechnology* **2003**, *21*(1), 41-46.

77. Dubertret, B.; Skourides, P.; Norris, D. J.; Noireaux, V.; Brivanlou, A. H.; Libchaber, A. *Science* **2002**, *298*(5599), 1759-1762.

78. Jaiswal, J. K.; Mattoussi, H.; Mauro, J. M.; Simon, S. M. *Nature Biotechnology* **2003**, *21*(1), 47-51.

79.   Akerman, M. E.; Chan, W. C. W.; Laakkonen, P.; Bhatia, S. N.; Ruoslahti, E.

Proceedings of the National Academy of Sciences of the United States of America

2002, *99*(20), 12617-12621.

CHAPTER II

ALBUMIN-CdTe NANOPARTICLE BIOCONJUGATES: PREPARATION,

STRUCTURE, AND INTERUNIT ENERGY TRANSFER

WITH ANTENNA EFFECT[1]

Introduction

Fluorescence semiconductor nanoparticles (NPs) properties and applications stand among the most exciting research fields in chemistry, physics and biology.

High quality nanocrystals of different II-VI semiconductor materials are currently available. One beneficial property of cadmium telluride CdTe NPs is the very stable luminescence that covers almost the whole visible spectral range depending on the particle size. CdTe NPs provide very high photoluminescence quantum efficiencies. The quantum efficiency value of 65% at room temperature has been reported for organometallically prepared CdTe NPs [1,2]. Unfortunately, potential applications of these NPs are limited due to instability of their photoluminescence in air. However, since the appearance of the first report on the aqueous synthesis of mercaptoethanol- and thioglycerol-capped CdTe NPs in 1996 [3], sufficient progress has been made in the preparation and the design of the surface properties of thiol-capped CdTe nanoparticles,

---

[1] *The content of this Chapter has been published in Nano Letters, 2001, 1(6), p.281-286.*

35

as well as in their characterization [4,5]. These NPs have been used in numerous applications. Worth mentioning is the utilization of luminescent thiol-capped CdTe QDs in light-emitting devices (LEDs) [6-8], photonic [9-12] and core-shell structures [12-14]. Recent investigations have shown the attractive properties of this material for light energy conversion [15]. Summarizing the experimental data available today, thiol-capped CdTe nanoparticles synthesized in aqueous solution represent a relatively stable highly luminescent core-shell QD system with a naturally sulfur-capped surface (CdS shell) created by mercapto-groups covalently attached to the surface cadmium atoms that make them very attractive for fluorescent tagging.

Although some of the photophysical properties of NP are not fully understood and are still actively investigated, researchers have begun developing bioconjugation schemes and applying such probes to biological assays.

This chapter is concerned with the conjugation of luminescent CdTe NPs with a simple protein, bovine serum albumin (BSA). The purpose of this chapter is three-fold: (1) to present a simple method of protein-NP conjugation utilizing amino acid-coated NP and discuss its limitations, (2) to report on the structure of protein-NP conjugates, and (3) to describe their optical properties.

As a convenient model for the fundamental studies of protein - NP conjugates BSA was chosen as one of the most studied proteins, whose structure and properties are known to the smallest details. Since albumin is a typical plasma protein, albumin-coated NPs are important for the study of their interactions with live blood cells and the immune response of the organism to their intravenous administration. Also, despite low biospecificity, BSA has a strong affinity to a variety of organic molecules binding to

different sites, which makes possible utilization of BSA-decorated NPs in a variety of supramolecular assemblies. For the conjugate preparation, glutaraldehyde (G) was used as a linker applicable to the majority of proteins.

Experimental procedures

Instrumentation

A Hewlet-Packard HP-8453 diode array spectrophotometer was used to collect optical absorption spectra at room temperature using 1-cm quartz cuvettes.

Photoluminescence experiments were recorded at room temperature in 1 cm × 1 cm quartz cuvettes on FluoroMax-3 and Fluorolog-3 spectrofluorometers from Jobin Yvon / Spex, Horiba group (Edison, NJ) with use of front face or right angle collection with 5 nm slits.

Circular dichoism (CD) spectra were recorded on a JASCO J-500A spectropolarimeter using a JASCO cell of 0.10 cm path length.

Native and SDS-PAGE gel electrophoresis were performed on the Mini-PROTEAN 3 electrophoresis cell (Bio-Rad, Hercules, CA) using precast gels.

Reagents and materials

All chemicals and biochemicals used in this work were of analytical grade or of highest purity available and were obtained from commercial sources. Cadmium perchlorate hydrate, 2-mercaptoethanol, L-cysteine, glutaraldehyde (25% aqueous solution), powder of phosphate buffered saline (PBS), pH 7.4 and bovine serum albumin

were purchased from Sigma - Aldrich Co. (St. Louis, MO, USA). Sodium hydroxide, glycine and tris(hydroxymethyl)aminomethane (Tris-base) were purchased from EM Science (Gibbstown, NJ, USA). Glycerin, ethylene glycol, sodium dodecyl sulfate (SDS) and (tris(hydroxymethyl)aminomethane hydrochloride (Tris-HCl) were obtained from Fisher Scientific (Fair Lawn, NJ, USA). Aluminum telluride was from Cerac Inc. (Milwaukee, WI, USA). Bromophenol blue was obtained from Eastman Kodak Co. (Rochester, NY, USA). Sulfuric acid was purchased from Pharmco (Brookfield, CT, USA). Rhodamine B was obtained from Fluka (Milwaukee, WI, USA).

Bio-Safe colloidal Coomassie Blue G-250 stain, precast 4-20% linear gradient Tris-HCl gel plates used for native and SDS-PAGE electrophoresis, Kaleidoscope and SDS-PAGE prestained standards were purchased from Bio-Rad (Hercules, CA, USA). Spectra/Por dialysis membranes with molecular weight cutoff (MWCO) = 50,000 were from Spectrum Laboratories, Inc. (Rancho Dominguez, CA, USA).

Deionized water (Barnstead) with 18.2 MΩ/cm was used for all experiments.

Synthesis of cadmium telluride (CdTe) nanoparticles

L-cysteine-stabilized CdTe NPs were synthesized according to the standard technique of arrested precipitation in aqueous solution reported previously [3,16]. The typical experimental setup is pictured on Figure II-1.

$$Cd(ClO_4)_2 + H_2Te \xrightarrow[\text{NaOH}]{100^\circ C,\ H_2O} Q\text{-CdTe} + \ldots$$
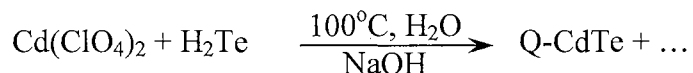
Figure II-1. Schematic presentation of the synthesis of thiol-capped CdTe QDs. First stage: formation of CdTe precursors by introducing H_2Te gas. Second stage: formation and growth of CdTe nanoparticles promoted by reflux (Adopted from ref. [17]).

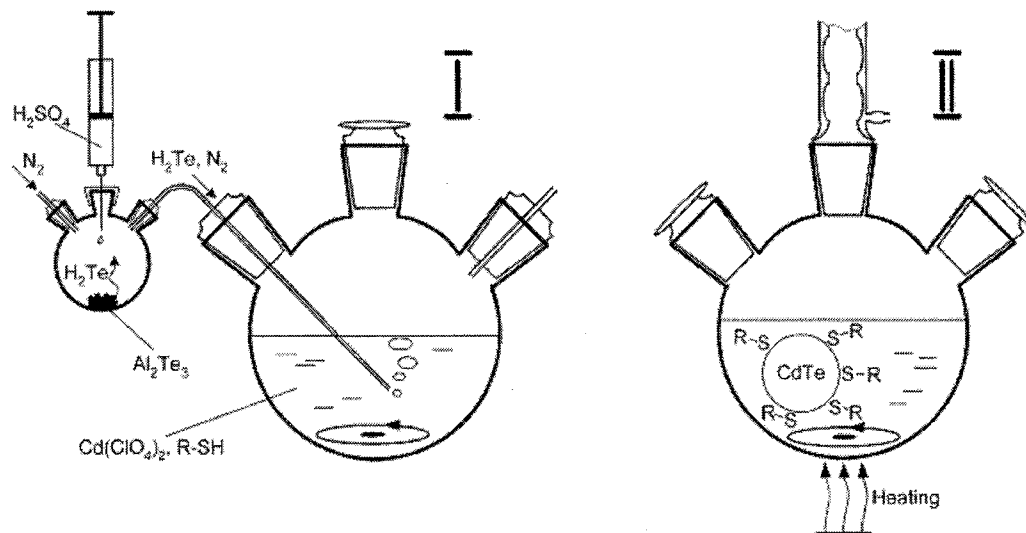Since L-cysteine is a hydrophilic stabilizer this method overrides the stages of silica coating and/or stabilizer exchange, which makes it simpler than the previously reported procedures of protein-NP composites [18,19]. At the same time, it is important to point out, that the protective encapsulation of NPs is necessary for prevention of their slow decomposition and nonspecific luminescence quenching.

Briefly, in a typical synthesis as shown in Figure II-1 0.7741 g (2.35 mmol) of $Cd(ClO_4)_2 \cdot H_2O$ was dissolved in 125 mL of water, and 5.7 mmol of the thiol stabilizer (0.6906g of L-cysteine) was added under stirring, followed by adjusting the pH to 11.2-11.8 by drop wise addition of 1 M solution of NaOH. Occasionally, the solution remained slightly turbid at this stage because of the incomplete solubility of Cd-thiolate complexes, but this did not influence the further synthesis. The solution was placed in a three-necked flask fitted with a septum and valves and was deaerated by N_2 bubbling for ~30 min. Under stirring, H_2Te gas (generated by the reaction of 0.2 g (0.46 mmol) of Al_2Te_3 lumps with 15-20 mL of 0.5 M H_2SO_4 under N_2 atmosphere) was passed through the solution together with a slow nitrogen flow for ~20 min. The molar ratio of $Cd^{2+}:Te^{2-}:L$-cysteine was 1:0.47:2.43. CdTe precursors were formed at this stage accompanied by a change of the solution color from transparent to yellow.

The CdTe precursors showed an absorption spectrum unstructured in the visible spectral region with a tail extending to 650-700 nm, and no luminescence. The precursors were converted to CdTe nanoparticles by refluxing the reaction mixture at 100 °C under open-air conditions with condenser attached (Figure II-1). A clearly resolved absorption maximum of the first electronic transition of CdTe QDs appeared at ~420 nm in 5-10 min after beginning of reflux corresponding to the smallest CdTe NPs (<2 nm size) which

40

shifted to longer wavelengths as the particles grew in the course of heating. Green (luminescence maximum at ~510-520 nm) band-edge emission appeared in 10-15 min after beginning of reflux when the CdTe NPs reached the size of ~2 nm. The size of the CdTe QDs growth further was controlled by the duration of reflux and could easily be monitored by absorption and PL spectra.

The same tendency was observed for the growth of CdSe NPs stabilized with thio acids or thioalcohols [20].

Determination of final concentration of CdTe nanoparticles

Molecular weight (M_W) of the NPs is calculated according to the formula:

$$M_W = \rho * N_A * V_0$$

where N_A is the Avogadro number, $\rho = 6.20$ g/cm^3 is the density of cadmium telluride[21], and V_0 is the volume of one particle, that can be calculated, assuming spherical particle shape, according to the formula:

$$V_0 = 4/3 \pi r^3 = (\pi d^3)/6$$

where r is the radius, d is the diameter of the particle.

Size of the particles was estimated to be ~ 2 nm by TEM (transmission electron microscopy). Thus, the volume of one particle V_0 will be:

$$V_0 = (3.14*(2.0*10^{-9})^3)/6 \text{ m}^3 = 4.19 *10^{-27} \text{ m}^3 = 4.19 *10^{-21} \text{ cm}^3$$

Hence:

$$M_W \text{(NPs)} = 6.20 \text{ g/cm}^3 * 6.02*10^{23} \text{ 1/mol} * 4.19 *10^{-21} \text{ cm}^3 =$$

$$= 15626.29 \text{ g/mol} \approx 15600 \text{ g/mol}$$

The reaction equation:

$$Cd(ClO_4)_2 + H_2Te + 2NaOH = CdTe + 2NaClO_4 + H_2O$$

The quantities of $Cd(ClO_4)_2$ and H_2Te were 2.35 mmol and 1.1 mmol respectively, hence, the number of moles (v) of CdTe NPs will be:

$$v(NPs) = (1.1mmol * M_W(CdTe))/M_W(NPs)$$

$$v(NPs) = (1.1mmol * 240 \text{ g/mol}) /15626.29 \text{ g/mol} = 1.69 * 10^{-5} \text{ mol}$$

Since the reaction volume V was 125 mL, the molarity of the NPs solution (M) will be:

$$M = v(NPs)/V = 1.69 * 10^{-5} \text{ mol}/ 0.125 \text{ L} =$$

$$= 1.35 * 10^{-4} \text{ mol/L} = \textbf{0.135 mmol/L.}$$

So that, the final concentration of CdTe NP was estimated to be 0.135 mM.

Quantum yield determination

The quantum yields of NPs luminescence (φ_{NP}) were determined by using Rhodamine B as a standard. The choice of the standard was based on the principle that the emission maxima of both the standard and unknown were comparable. Rhodamine B, in ethylene glycol, has an emission maximum at $\lambda_{max} = 580nm$, and its quantum yield (φ_S) integrated over the emission peak was taken as 1.0. Optical density of the NP dispersion in water (OD_{NP}) and that of the standard (OD_S) at the excitation wavelength (350nm) were adjusted to be within 0.05 absorbance units within each other. The overall optical density of both solutions did not exceed 0.1 AU. The quantum yield was calculated by the formula:

$$\varphi_{NP} = \varphi_S * (I_{NP}/I_S) * (OD_S/OD_{NP})$$

where, I_{NP} and I_S are the integrated areas of luminescence for NPs and standard respectively.

Conjugation procedure

The CdTe nanoparticles of ca. 2.0 nm size of the semiconductor core with band-edge emission at 520 nm (quantum efficiency 15% at room temperature) were used for conjugation.

A one-step G linkage conjugation procedure (Figure II-2) was used, previously shown to work well for the protein-protein conjugation [22-24] and for the preparation of self-assembled monolayers [25-27].

One aldehyde group of glutaraldehyde (G) ($O=CH-(CH_2)_3-HC=O$) forms a Schiff base linkage with the L-cysteine amino group on the surface of nanoparticles (NPs), while the other side forms an identical bond with predominantly lysine moieties on albumin (BSA).

In a typical preparation of the BSA-G-CdTe conjugate, 4 mL of obtained aqueous CdTe NPs solution was mixed with 0.150 mL of glutaraldehyde (25% in water) and 0.625 mL of a 40 mg/mL solution of BSA in a pH 7.4 phosphate buffer, and 0.225 mL of phosphate-buffered saline (PBS, 0.01 M phosphate buffered saline, pH = 7.4, of the composition 0.138 M NaCl-0.0027 M KCl) was added. Final concentrations were as follows: [NP] = 0.11 mM, [G] = 0.0752 M, [BSA] = 5 mg/mL = 0.07 mM, which corresponds to molar ratios NP:G:BSA $1.5:10^3:1$. After the mixture was incubated for 1hr at 60 °C, it was dialyzed (48 hrs, using Spectra/Por dialysis membranes with MWCO = 50,000) against the PBS and placed in a refrigerator at 4 °C for storage. No subsequent
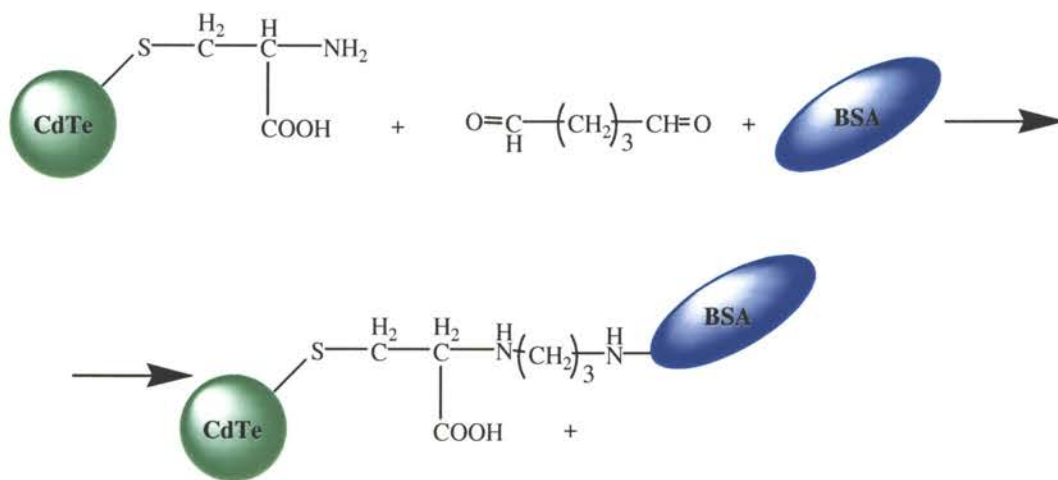
43

Figure II-2. Conjugation nanoparticles with albumin using glutaraldehyde.

treatment with sodium borohydride (NaBH$_4$) or sodium cyanoborohydride (NaCNBH$_3$) was used because the excess of L-cysteine present in the mixture as a mild reducing agent converted the initially forming Schiff base into the secondary amine bond.

The selection of proper conditions and reagent ratios resulted in a minimal formation of oligomers that is often mentioned as one of the disadvantages of glutaraldehyde coupling.

Gel electrophoresis

The cigar-shaped ellipsoidal molecules of BSA with hydrodynamic dimensions of 40 Å (short axis) by 140 Å (long axis) are often used in gel electrophoresis assay as a molecular weight standard (M_W 67 kDa) [28]. Thus, the products of BSA-G-CdTe conjugation could be conveniently analyzed by this technique.

Native and SDS-PAGE gel electrophoresis were conducted for analysis of conjugates. Precast 4-20% linear gradient Tris-HCl gel plates were used. Gel electrophoresis was run for 1.5 hrs at 82 V, 25 mA. A 10 μL aliquot of the sample was mixed with 2 μL of the sample buffer, and the appropriate amount (2-10 μL) of the mixture was injected into the gel plate to obtain well-resolved spots of desirable dimensions.

Sample buffer for SDS-PAGE contained 50% glycerol, 25% 2-mercaptoethanol, 10% SDS, 0.1 bromophenol blue, and Tris-HCl pH 6.8. SDS electrophoresis running buffer was made from 6.06 g of Tris base, 28.5 g of glycine, and 1.0 g of SDS dissolved in 1 L of water.

The sample buffer for native state gel electrophoresis was prepared from 15.5 mL of 1 M Tris-HCl pH 6.8, 2.5 mL of a 1% solution of bromophenol blue, 7 mL of water, and 25 mL of glycerol. The electrophoresis running buffer was made by dissolving 3.0 g of Tris base and 14.4 g of glycine in water and adjusting the volume to 1 L at pH 8.3.

Luminescence in gel plates

A 0.5 × 0.5 cm piece was cut out from the gel plate after separation of the conjugation products. The piece of gel was attached to a glass slide and placed in the sample compartment of a Fluorolog 3 instrument. The luminescence spectrum was obtained at the excitation wavelength of 360 nm.

Circular dichroism

BSA sample was dissolved in 0.01 M PBS buffer. A sample of CdTe, cysteine-stabilized nanoparticles, and the conjugate sample were at pH 7.4. The initial solutions were diluted to approximately 1 mg/mL concentration of BSA immediately before the spectra were taken.

Results and discussion

Native and SDS gel electrophoresis

In all samples, free CdTe NPs (M_w ~ 16 kDa, as estimated for a 2 nm CdTe core covered with a monolayer of L-cysteine), compact and highly negatively charged,

traveled far ahead of BSA and were typically found at the lower edge of the gel plate with other components traveling with the electrophoretic front. The bands of BSA were always positioned in the middle of the gel plate and could be clearly identified by the comparison with the standard protein ladder (Figure II-3). CdTe NPs used were strongly luminescent with a quantum yield of 15-20%, while that for BSA under the best conditions was about 3%. Hence, the emission intensity of SDS-PAGE electrophoresis spots was used for the optimization of conjugation conditions. The yield of BSA-G-CdTe conjugate gradually increased with the increasing temperature of the reaction (Figure II-3 a, wells 3-6). The yield reached the maximum at approximately 50 °C for 1 hr reaction time, as indicated by the strongest luminescence of the BSA band (Figure II-3 a well 6). For longer times and higher temperatures, the yield of BSA-G-CdTe decreased due to oligomerization reactions (Figure II-3 a, wells 7-9). Unfolding of BSA occurs above 65 °C and is quite reversible unless extreme pH conditions are used [28].

More detailed information about the products of the conjugation reaction could be obtained from native gel electrophoresis data. Contrary to SDS-PAGE, the denaturation of the protein caused by the addition of SDS does not occur in this technique and the protein retains its original charge, which makes it more informative.

When BSA was mixed with NPs without coupling agent (Figure II-3 b, wells 4 and 5), the luminescence of the BSA band was very weak regardless the time of exposure, while all NPs were run off the gel plate. Importantly, this demonstrated that there is very little, if any, nonspecific binding of NPs to BSA. The BSA bands in wells 4

47
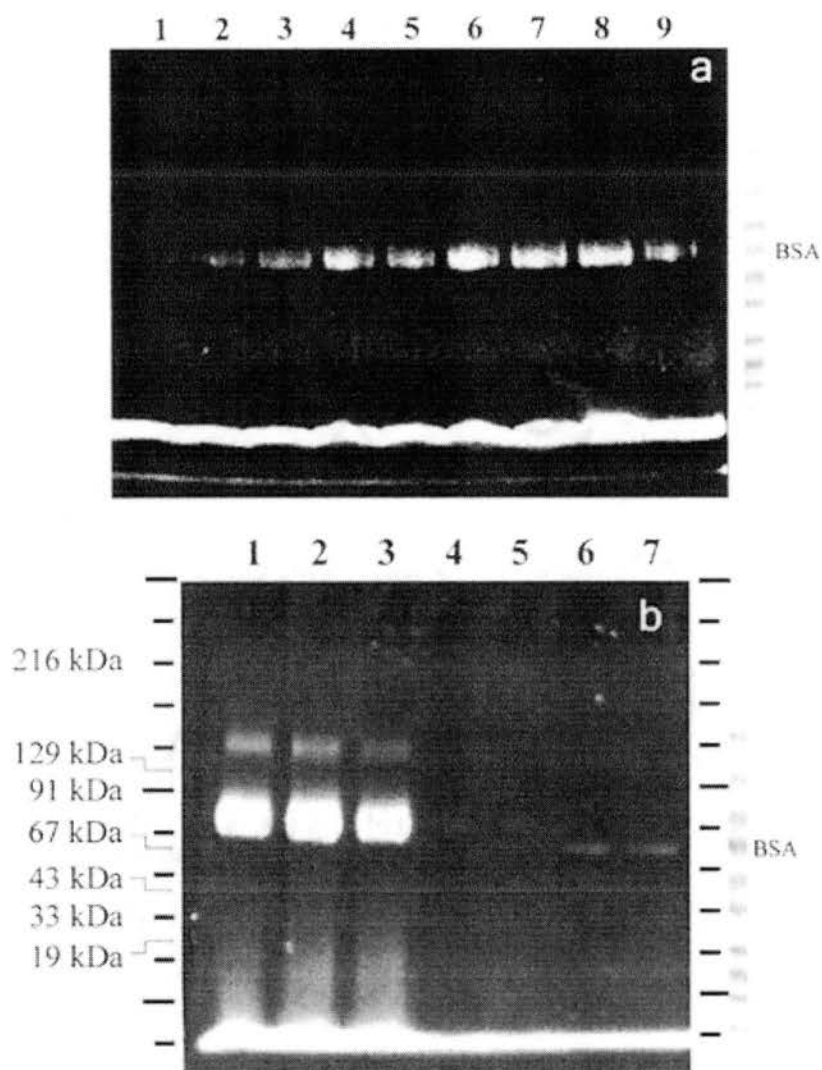
Figure II-3. Luminescence images of SDS PAGE and native gel electrophoresis assays of BSA-G-CdTe conjugates. a) SDS PAGE assay. Wells: (1) CdTe; (2) BSA; (3) CdTe + BSA (no G); (4) CdTe + G + BSA heated at 25 °C 1 hr; (5) CdTe + G + BSA heated at 40 °C for 1 hr; (6) CdTe + G + BSA heated at 50 °C for 1 hr; (7) CdTe + G + BSA heated at 60 °C for 1 hr; (8) CdTe + G + BSA heated at 60 °C for 1.5 hrs; (9) CdTe + G + BSA heated at 60 °C for 2 hrs. The standard protein prestained ladder with spot marked BSA was run on the same gel plate. (b) The native gel electrophoresis assay. Wells: (1-3) (all the same) CdTe + G + BSA heated at 50 °C for 1 hr; (4-5) CdTe + BSA (no G); (6-7) BSA. The molecular weight scale on the left was graduated by the positions of reference proteins in the standard protein ladder given on the right with BSA spot marked.

48

and 5 were slightly shifted to higher molecular weights as compared to pure BSA in NP-free buffer (Figure II-3b, wells 6 and 7). This occurred due to the complexation of Cd^{2+} ions present in colloidal solution of CdTe by metal-binding sites for which BSA is well-known [28,29]. The net charge per one BSA molecule is -19 at pH 7.4 [28]. The addition of Cd^{2+} reduced the negative charge of BSA and resulted in lowering its electrophoretic mobility. As expected, this shift disappeared when the protein was denatured by sodium dodecyl sulfate in the SDS-PAGE electrophoresis experiment (Figure II-3 a). Cd^{2+} ions may be present in solution both due to incomplete removal by the dialysis as well as due to slow decomposition of the NPs caused by the exposure to light and oxygen. Regardless of the origin, for any biomedical applications of NPs, it is important to minimize the presence of heavy metals because of their cytotoxicity.

Two new strong luminescent bands appeared after addition of G and incubating the reaction mixture at 50 °C for 1 hr (Figure II-3 b, wells 1-3). By using the standard protein ladder as a reference, the molecular weights of the conjugation products were determined to be 82 and 150 kDa. As it was demonstrated later, the use of M_W from gel plates has to be done very cautiously because the mass addition of NPs, which are compact and highly charged, may not follow the dependence of the SDS-PAGE shifts calibrated for proteins. The position of the band at 82 kDa matched the sum of masses of BSA (67 kDa) and NP (16 kDa), and therefore, should be attributed to 1:1 BSA:CdTe conjugate (~83 kDa), although the coincidence may be fortuitous. At the same time, the mobility of the conjugate has not significantly changed in respect to the BSA-CdTe mixture (Figure II-3 b, wells 4 and 5). It may be suggested that the added weight and high negative charge associated with the formation of the BSA-G-CdTe diad partially

49

compensate each other. The band at 150 kDa should be attributed to a 2:1 BSA-CdTe conjugate with an estimated mass of 152 kDa. Unlike the case of NP-DNA conjugates [30], the attachment of a greater number of BSA units to CdTe did not occur, most likely due to the steric hindrances related to the difficulty with the accommodation of bulky protein units around relatively small NPs (2 nm).

The electrophoresis experiment has been performed in a variety of conditions and no further separation of the luminescence bands has been noticed. Although no direct evidence indicates the formation of conjugates with two or more CdTe attached to one albumin unit, the possibility of their formation should also be considered and may contribute to broadening the 1:1 conjugate band. Importantly, virtually no byproducts, such as (BSA-G-NP)$_n$ oligomers, were present in solution, as could be seen by the absence of luminescent bands for masses above 150 kDa, which was one of the goals of the optimization of reaction conditions.

Luminescence in gel plates

To confirm the binding of CdTe to BSA, the luminescence spectrum of the 82 kDa band in the native gel electrophoresis was obtained. The spot on the gel plate corresponding to this band had noticeably yellow coloration indicative of CdTe NPs.

The luminescence spectrum of the gel piece showed a characteristic band-edge emission peak of CdTe red-shifted by ~25 nm from its original position in the NP solution (Figure II-4).

A series of additional experiments showed that this shift was caused by the growth of NP due to the reaction with G (Figure II-4, trace 3). Heating at 50 °C did not
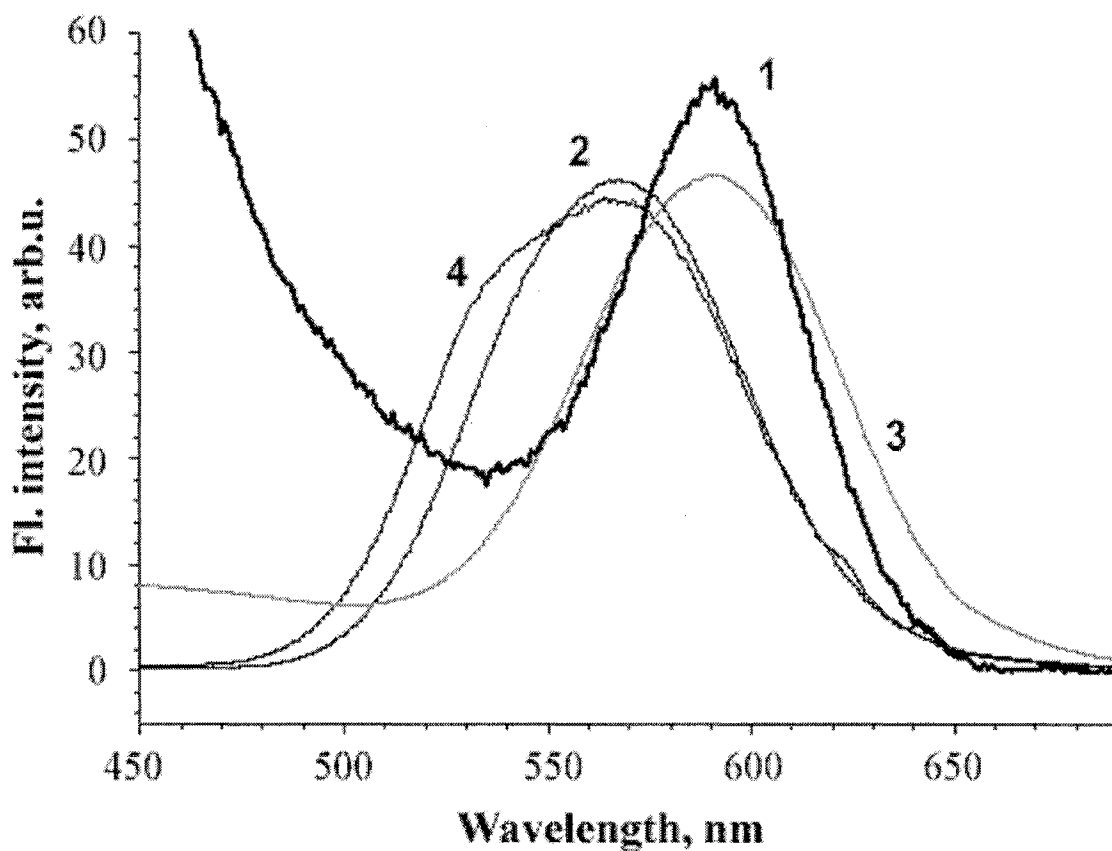
Figure II-4. Comparison of photoluminescence emission spectrum of band cut out from the native state electrophoresis gel plate to the corresponding spectra of NPs in solution. Luminescence spectra of (1) 82 kDa band cut out from the native state electrophoresis gel plate, (2) CdTe as synthesized, (3) CdTe + G (no BSA) heated at 50°C for1 hr, and (4) CdTe (no BSA, no G) heated at 50 °C for1 hr. Excitation wavelength λ_{ex} = 360 nm.

51

result in the luminescence spectral shift (Figure II-4, trace 4). The quantum yield of NP excitonic emission for 360 nm excitation did not change appreciably after the reaction with G or BSA and decreased by 1-3% during heating without conjugation.

Circular dichroism

Circular dichroism spectra of BSA and BSA-G-CdTe are represented on Figure II-5.

Circular dichroism spectra indicate a small disturbance of the BSA conformation observed as a curve shift in 210-214 nm range as expected when highly charged species, such as NPs, are conjugated to protein molecules. Also, the circular dichroism spectra coincided well with each other and with reported BSA data [31]. This shows that the tertiary structure of BSA remains mostly intact that is essential for the preparation of protein-based assemblies of NPs.

Luminescence and adsorption spectra

Luminescence spectra are shown on Figure II-6. Excitation wavelength λ_{ex} was 290 nm. The concentration of NPs and their optical density at 290 nm were kept the same for all the experiments.

In aqueous solution, free BSA emitted at 340 nm (Figure II-6, trace 1). This emission peak originated from the luminescence of two aromatic tryptophan moieties present in BSA amino acid sequence: Trp134 and Trp 214 [28]. Simple addition of nonbound CdTe NPs reduced the maximum intensity of the 340 nm BSA luminescence
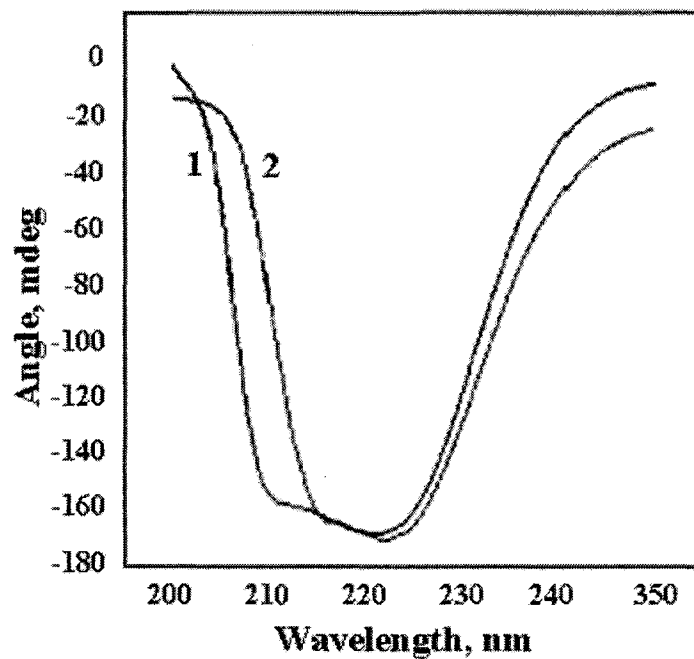
Figure II-5. Circular dichroism spectra of BSA before (1) and after (2) the conjugation to CdTe NP.
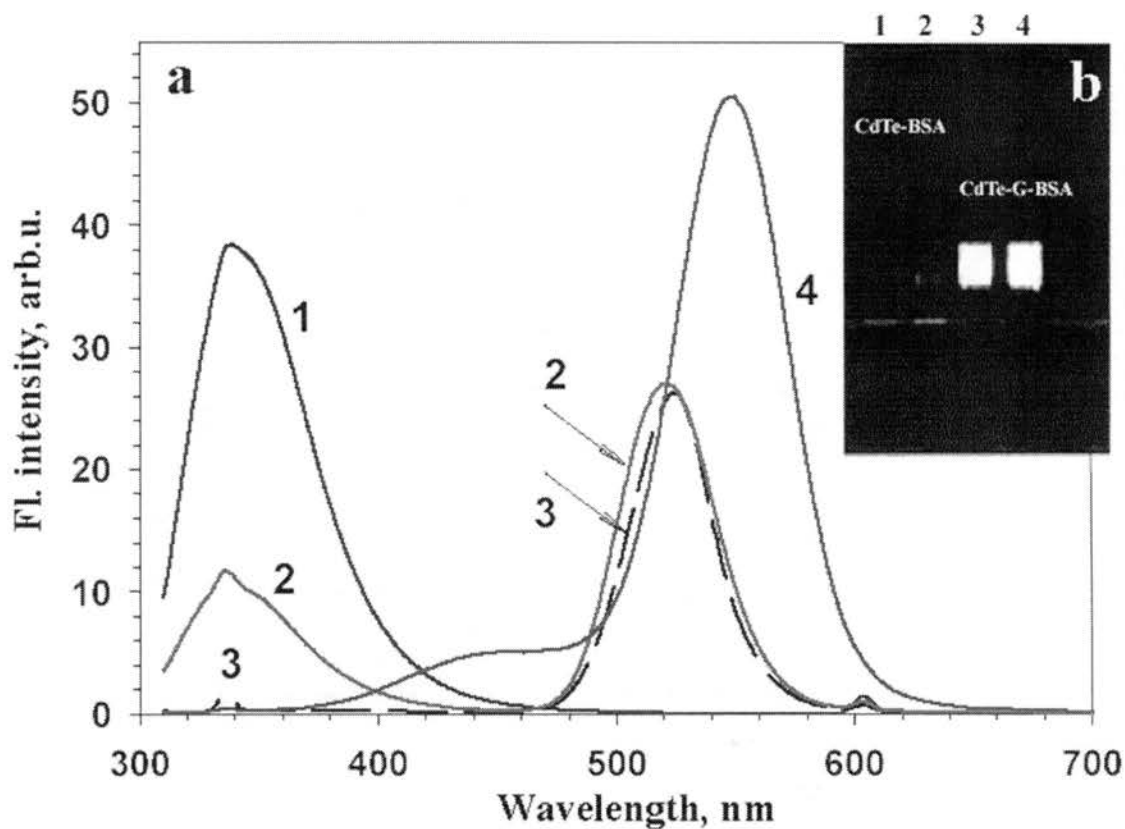
Figure II-6. Photoluminescence emission spectra of BSA, NPs, their mixture and BSA-G-CdTe conjugate. (a) Luminescence spectra of (1) BSA, (2) BSA + CdTe (no G), (3) CdTe heated at 50 °C for 3 hrs (no G, no BSA), (4) CdTe + G heated at 50 °C for 1 hr, and (5) BSA + CdTe + G heated at 50 °C for 1 hr. (b) Gel electrophoresis of BSA + CdTe (wells 1 and 2) and BSA-G-CdTe conjugate (wells 3 and 4) carried out in 18% Tris-HCl Gel (Bio-Rad, 18% resolving gel, 4% stacking gel) for 45 min to resolve the band of the NP and to avoid gel edge effects.

band by ca. 2.5 times, while the NP luminescence did not significantly change (Figure II-6, trace 2). This can be understood as a response to, among other factors, the change in pH and presence of Cd^{2+} ions, which alters the presentation of Trp moieties to water and the efficiency of quenching their luminescence by ambient oxygen.

Interestingly, the produced BSA-G-NP conjugates demonstrated effective interaction between the excited states of the biological and the inorganic parts. This effect should be attributed to the spatial closeness of BSA and NP in the tightly bound covalent supramolecule.

The emission intensity of both biological and inorganic components changed dramatically in the BSA-G-CdTe conjugates. The luminescence of BSA was quenched completely, while the excitonic peak of CdTe increased ca. 2-fold in amplitude and 2.8-fold in the area under the curve (Figure II-6, trace 5). All the spectra were taken for 290 nm excitation, where both BSA and NP absorb light. Since there was no major change in the quantum yield for long wavelength excitation, such a strong increase in luminescence efficiency of NPs is quite remarkable. The strong increase of the luminescence after the conjugation can also be seen in the gel-electrophoresis taken for the short running times (Figure II-6 b). The bands of the conjugates not yet separated are noticeably brighter (Figure II-6 b wells 3 and 4) than the band of unconjugated NP (Figure II-6 b wells 1 and 2). In addition, in this image, one can also see that the relative amount of unconjugated NP for BSA-G-CdTe is negligible.

The luminescence enhancement effect can be associated with the concentration of adsorbed energy collected by NP from protein unit(s) through the resonance energy transfer [32] analogous to the classical Förster energy transfer [33]. The excitation energy

transfer from protein to the excitonic state of NP can be confirmed by the excitation spectrum of BSA-G-CdTe conjugates registered in the emission band of CdTe (Figure II-7). The excitation peak of the BSA-G-CdTe conjugate at 280 nm (Figure II-7 a, trace 1) coincided very well with UV-vis absorption peak of BSA (Figure II-7 b, trace 1).

Concomitantly, there was no similar band in the excitation spectrum of CdTe reacted with G (Figure II-7 a, trace 2) or in their UV-vis absorption spectrum (Figure II-7 b, trace 2). This data indicates that the quanta of light absorbed by BSA are emitted by the CdTe. For conjugates bearing two BSA units, the NP collects the light from four Trp moieties. Similar antenna effects had been observed for some metal complexes and polymers [34-40]. However, to the best of the author's knowledge, this is the first observation of such phenomena for NPs.

Conclusions

Protein-NP conjugates were made by using glutaraldehyde as a cross-linking agent in conjunction with L-cysteine-capping of CdTe NPs. This procedure is expected to be applicable to other proteins with exposed Lys moieties primarily targeted by G. While simplifying the protein-NP conjugation procedure, it also shows the necessity of a protective encapsulation of NP to prevent particle growth and photoinduced decomposition.

An important find was that the coupling process yields preferably BSA-NP 1:1 diads with some amount of 2:1 aggregates. These and other analogous products can be used as building blocks in more complex protein-based NP supramolecules.

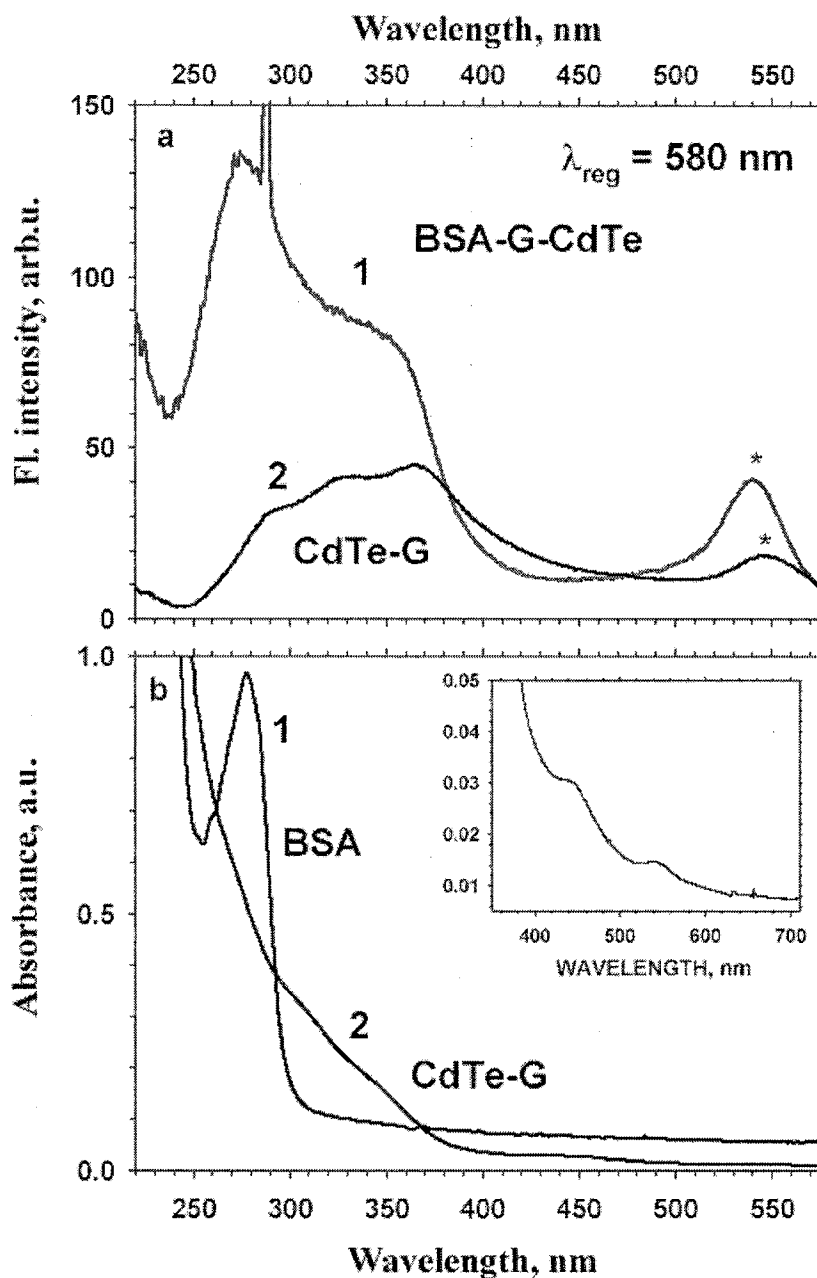**Figure II-7.** Photoluminescence excitation and UV-vis absorption spectra of BSA-G-CdTe conjugate (1) and CdTe heated with G at 50 °C 1 hr (2). (a) Excitation spectra. Registration wavelength λ_{reg} = 580 nm. Peaks marked with a star correspond to the excitonic transition in CdTe NPs. (b) UV-vis absorption spectra. The inset shows the UV-vis absorption spectrum of BSA-G-CdTe conjugate in the visible region of the spectrum.

One of the interesting aspects of this work is the demonstration of the efficient excitation energy transfer between the protein units and core levels of NPs. This can be considered as a communication link between the biological and inorganic components of the conjugate. The significance of this observation is the demonstration of a possible integration of protein-based self-assembly and information exchange functionalities for protein-NP conjugates that can be used in NP-based molecular electronic circuits and bioinformatics.

References

1. Mikulec, F. V.; Bawendi, M. G.; Kim, S. WO 2001007689, **2000**, pp. 39.

2. Talapin, D. V.; Haubold, S.; Rogach, A. L.; Kornowski, A.; Haase, M.; Weller, H. *J.Phys.Chem. B* **2001**, *105*(12), 2260-2263.

3. Rogach, A. L.; Katsikas, L.; Kornowski, A.; Su, D.; Eychmueller, A.; Weller, H. *Ber.Bunsen-Ges.* **1996**, *100*(11), 1772-1778.

4. Rockenberger, J.; Troger, L.; Rogach, A. L.; Tischer, M.; Grundmann, M.; Eychmuller, A.; Weller, H. *J.Chem.Phys.* **1998**, *108*(18), 7807-7815.

5. Kapitonov, A. M.; Stupak, A. P.; Gaponenko, S. V.; Petrov, E. P.; Rogach, A. L.; Eychmueller, A. *J.Phys.Chem. B* **1999**, *103*(46), 10109-10113.

6. Gao, M.; Lesser, C.; Kirstein, S.; Mohwald, H.; Rogach, A. L.; Weller, H. *J.Appl.Phys.* **2000**, *87*(5), 2297-2302.

7. Gaponik, N. P.; Talapin, D. V.; Rogach, A. L. *Phys.Chem.Chem.Phys.* **1999**, *1*(8), 1787-1789.

8. Gaponik, N. P.; Talapin, D. V.; Rogach, A. L.; Eychmuller, A. *J.Mater.Chem.* **2000**, *10*(9), 2163-2166.

9. Gaponenko, S. V.; Bogomolov, V. N.; Kapitonov, A. M.; Prokofiev, A. V.; Eichmuller, A.; Rogach, A. L. *Pis'ma v Zhurnal Eksperimental'noi i Teoreticheskoi Fiziki* **1998**, *68*(1-2), 131-135.

10. Gaponenko, S. V.; Bogomolov, V. N.; Petrov, E. P.; Kapitonov, A. M.; Yarotsky, D. A.; Kalosha, I. I.; Eychmueller, A. A.; Rogach, A. L.; McGilp, J.; Woggon, U.; Gindele, F. *Journal of Lightwave Technology* **1999**, *17*(11), 2128-2137.

11. Rogach, A. L.; Kotov, N. A.; Koktysh, D. S.; Ostrander, J. W.; Ragoisha, G. A. *Chem.Mater.* **2000**, *12*(9), 2721-2726.

12. Rogach, A.; Susha, A.; Caruso, F.; Sukhorukov, G.; Kornowski, A.; Kershaw, S.; Mohwald, H.; Eychmuller, A.; Weller, H. *Advanced Materials* **2000**, *12*(5), 333-337.

13. Radtchenko, I. L.; Sukhorukov, G. B.; Gaponik, N.; Kornowski, A.; Rogach, A. L.; Mohwald, H. *Advanced Materials* **2001**, *13*(22), 1684-1687.

14. Susha, A. S.; Caruso, F.; Rogach, A. L.; Sukhorukov, G. B.; Kornowski, A.; Mohwald, H.; Giersig, M.; Eychmuller, A.; Weller, H. *Colloids and Surfaces, A: Physicochemical and Engineering Aspects* **2000**, *163*(1), 39-44.

15. Talapin, D. V.; Poznyak, S. K.; Gaponik, N. P.; Rogach, A. L.; Eychmuller, A. *Physica E: Low-Dimensional Systems & Nanostructures* **2002**, *14*(1-2), 237-241.

16. Rogach, A. L.; Katsikas, L.; Kornowski, A.; Su, D.; Eychmuller, A.; Weller, H. *Ber.Bunsen-Ges.* **1997**, *101*(11), 1668-1670.

17. Gaponik, N.; Talapin, D. V.; Rogach, A. L.; Hoppe, K.; Shevchenko, E. V.; Kornowski, A.; Eychmueller, A.; Weller, H. *J.Phys.Chem. B* **2002**, *106*(29), 7177-7185.

18. Bruchez, M. J.; Moronne, M.; Gin, P.; Weiss, S.; Alivisatos, A. P. *Science* **1998**, *281* 2013-2016.

19. Chan, W. C. W.; Nie, S. *Science* **1998**, *281* 2016-2018.

20. Rogach, A. L.; Kornowski, A.; Gao, M.; Eychmueller, A.; Weller, H. *J.Phys.Chem. B* **1999**, *103*(16), 3065-3069.

21. Dean, J. A. *Lange's Handbook of Chemistry, Fourteenth Edition;* 1992.

22. Aslam, M.; Dent, A. *Bioconjugation-Protein Coupling Techniques for the Biomedical Sciences;* Grove's Dictionaries, Inc.: New York, NY, 1998.

23. Hermanson, G. T. *Bioconjugate Techniques;* Academic Press: San Diego, CA, 1996.

24. Wong, S. S. *Chemistry of Protein Conjugation and Cross-Linking;* CRC Press: Boca Raton, Fl, 1991.

25. Kajiya, Y.; Okamoto, T.; Yoneyama, H. *Chem.Lett.* **1993,** 2107.

26. Ruan, C.; Yang, F.; Lei, C.; Deng, J. *Anal.Chem.* **1998,** *70* 1721.

27. Katz, E.; Schlereth, D. D.; Schmidt, H.-L.; Olsthoorn, A. J. J. *J.Electroanal.Chem.* **1994,** *368* 165.

28. Peters, T., Jr. *All About Albumin. Biochemistry, Genetics, and Medical Applications;* Academic Press: San Diego, 1995.

29. Sadler, P. J.; Viles, J. H. *Inorg.Chem.* **1996,** *35* 4490-4496.

30. Zanchet, D.; Micheel, C. M.; Parak, W. J.; Gerion, D.; Alivisatos, A. P. *NanoLetters* **2001,** *1*(1), 32-35.

31. Reed, R. G.; Feldhoff, R. C.; Clute, O. L.; Peters, T., Jr. *Biochemistry* **1975,** *14*(21), 4578-4583.

32. Kagan, C. R.; Murray, C. B.; Bawendi, M. G. *Phys.Rev.B: Condens.Matter* **1996,** *54*(12), 8633-8643.

33. Förster, T. *Z. Naturforsch.* **1949,** *4a* 321.

34. Nowakowska, M.; Foyle, V. P.; Guillet, J. E. *J.Am.Chem.Soc.* **1993,** *115*(14), 5975-5981.

35. Piguet, C.; Buenzli, J. C.; Bernardinelli, G.; Hopfgartner, G.; Williams, A. F. *J.Am.Chem.Soc.* **1993,** *115*(18), 8197-8206.

36. Jullien, L.; Canceill, J.; Valeur, B.; Bardez, E.; Lefevre, J. P.; Lehn, J. M.; Marchi-Artzner, V.; Pansu, R. *J.Am.Chem.Soc.* **1996,** *118*(23), 5432-5442.

37. Kumar, C. V.; Williams, Z. J.; Turner, R. S. *J.Phys.Chem.A* **1998,** *102*(28), 5562-5568.

38. Nowakowska, M.; Storsberg, J.; Zapotoczny, S.; Guillet, J. E. *New J.Chem.* **1999,** *23*(6), 617-623.

39. Bignozzi, C. A.; Argazzi, R.; Kleverlaan, C. J. *Chem.Soc.Rev.* **2000,** *29*(2), 87-96.

40. Kuroda, Y.; Sugou, K.; Sasaki, K. *J.Am.Chem.Soc.* **2000,** *122* (32), 7833-7834.

CHAPTER III

ANTIGEN/ANTIBODY IMMUNOCOMPLEX FROM

CdTe NANOPARTICLE BIOCONJUGATES[1]

Introduction

Recognition at the molecular level is a fundamental characteristic of biochemical phenomena such as enzyme catalysis, antibody-antigen interaction, transport, and the replication of biological molecules.

Antigen-antibody interactions have been studied extensively from various standpoints including immunology, biochemistry, and structural biology [1]. An antigen is any molecular species that can be recognized by an animal organism as being foreign to itself and which; therefore, triggers the defensive mechanism known as the immune response [1,2]. In natural circumstances such antigens are proteins or lipopolysaccharides at the surfaces of viruses, bacteria, and microfungi, or at the surfaces of cells and in solution in blood or tissues of other species. An antibody is a molecule produced by animals in response to the antigen and which binds to the antigen specifically. In mammals, two distinct types of molecules are involved in the recognition of antigens. These proteins are called immunoglobulins, which are present in the serum and tissue

---

fluids, and the antigen receptors on the surface of specialized blood cell-the T-lymphocytes.

The interaction between antibody and antigen is characterized by relatively high affinity and specificity, making this type of reaction a prime candidate for use as an analytical tool.

The purpose of this chapter is the bioconjugation of NPs with proteins as (1) a method for their organization in more complex structures and (2) a pathway to new sensing and imaging technologies. In this chapter, the preparation of bioconjugates from an antigen and an antibody conjugated to NPs of different sizes is described. It is demonstrated that the NP-labeled antigen and antibody form an immunocomplex, which pairs together NPs with red and green luminescence. In light of programmed assembly of nanostructures [3,4] with nanocolloids as building blocks, the similarity of sizes of NPs and proteins limits the overall number of affinity ligands around one semiconductor core to a few protein units leading to low-valent quantum dots. Such bioconjugates with manageable level of complexity can be used as elements of spatially and/or topologically organized NP superstructures.

A practical aspect of this work is related to highly sensitive and specific detection by immunoluminescence of various biological and nonbiological analytes of military and civilian importance. The excited-state dipole-dipole coupling between NPs of different sizes has been observed in the constructed immunocomplex, that results in the excitation energy transfer from NPs of smaller diameters to those with larger diameters, (i.e., Förster resonance energy transfer (FRET)). The detection limits of analytical processes

based on FRET can be as low as 10 ppt with a linear dynamic range from 0.1 to 1000 ppb [5,6].

A biological component of the conjugates provides highly selective binding to cell components [7-13]. The stability of nanoparticles under UV and visible light makes possible not only high-contrast multiplexed imaging, [7,14] but also a long-term monitoring of the environment for biological warfare agents or natural pathogenic organisms such as cholera and *Escherichia coli* that represent a critical problem for countries with limited water treatment capabilities. This can be accomplished by taking advantage of the competitive inhibition of FRET in antigen-antibody immunocomplexes demonstrated in this chapter.

A model antibody-antigen system bovine serum albumin (BSA) and corresponding antibody (anti-BSA) were chosen. The choice was based on availability of the detailed structural information for BSA and its ability to form different molecular complexes [15].

Experimental procedures

Instrumentation

Optical absorption spectra were obtained on a Hewlett-Packard 8453 diode array spectrophotometer using 1-cm quartz cuvettes.

Fluorolog 3 and Fluoromax 2 from JY SPEX were used to register the luminescence spectra. The right angle registration mode with no intermediate filters was utilized in all the measurements. All FRET experiments were carried out after

centrifugation of the solutions to remove all particles aggregated due to oxidation and coagulation.

Circular dichroism (CD) spectra were recorded for solutions in 0.01 M PBS buffer at pH 7.4 on a JASCO J-500A spectropolarimeter using a JASCO cell of 0.10 cm path length. The initial solutions were diluted to approximately 1 mg/mL concentration immediately before the spectra were taken.

Native and SDS-PAGE gel electrophoresis were performed on the Mini-PROTEAN 3 electrophoresis cell (Bio-Rad, Hercules, CA) using 4-20% precast Tris-HCl gels.

Gel permeation HPLC experiments were carried out on a HP-1090-II instrument equipped with Jordi GPC 500A, 300 mm × 7.8 mm column. Deionized 18 MΩ water was used as an eluent with a flow rate of 1 mL/min. The optical adsorption signal was monitored at 254 nm by a diode array detector.

Materials and reagents

All chemicals and biochemicals were from commercial sources and were used without further purification. In addition to the materials described in Chapter II, the following chemicals were used. Thioglycolic acid, anti-BSA and 1-ethyl-3(3-dimethylaminopropyl) carbodiimide hydrochloride (EDC) were purchased from Sigma - Aldrich Co. (St. Louis, MO, USA). Antibody (IgG fraction of anti-Albumin [bovine serum] [rabbit]) and peroxidase-conjugated rabbit α-bovine immunoglobulin IgG were obtained from Rockland (Gilbertsville, PA). *N*-hydroxysulfo-succinimide (sulfo-NHS) and Rhodamine B were from Fluka (Milwaukee, WI, USA). Sodium carbonate, sodium

chloride and potassium phosphate, monobasic were purchased from Spectrum Quality Products, Inc. (New Brunswick, NJ). Sodium bicarbonate, sodium phosphate, dibasic and potassium chloride were obtained from EM Science (Gibbstown, NJ, USA). Tween 20 (polyoxyethylenesorbitan monolaurate, water ≤ 3%) and OPD tablets were purchased from Acros Organics (Fair Lawn, NJ). Linbro/Titertek 96-well E.I.A. microtitration plates for ELISA were obtained from ICN Biomedicals Inc. (Horsham, PA).

Bio-Safe colloidal Coomassie Blue G-250 stain, precast 4-20% linear gradient Tris-HCl gel plates used for native and SDS-PAGE electrophoresis, Kaleidoscope and SDS-PAGE prestained standards were purchased from Bio-Rad (Hercules, CA, USA). Spectra/Por dialysis membranes with MWCO = 12 000-14 000 were from Spectrum Laboratories, Inc. (Rancho Dominguez, CA, USA).

Deionized water (Barnstead) with 18.2 MΩ/cm was used for all experiments.

Synthesis of cadmium telluride nanoparticles

The details of the synthesis are described in the previous chapter (Chapter II-synthesis). The only difference is that thioglycolic acid was used as the stabilizer for cadmium telluride NPs.

Mainly, two different NP dispersions were utilized. One with a luminescence peak at 553-555 nm and the other one with the peak at 610-611 nm shifting slightly depending on the experimental conditions.

Conjugation to albumin and anti-albumin

NP-conjugated BSA and anti-BSA IgG were prepared by the sulfo-NHS (*N*-hydroxysulfo-succinimide) and EDC (1-ethyl-3(3-dimethylaminopropyl) carbodiimide hydrochloride) reaction (Figure III-1) [16-18].

The carboxylic acid group of thioglycolic acid stabilized NP forms amide bond with the primary amine groups of the protein. NHS-conjugated proteins have shown the highest bioactivity among other conjugates as established by several comparative studies [19-21], that resulted in the departure from the previously used glutaraldehyde conjugation procedure (Chapter II).

Quantum yield determination

The quantum yield of NP luminescence was determined by using Rhodamine B in ethylene glycol (λ_{max} = 580 nm, quantum yield 1) as a standard as described in chapter II. Optical density of bioconjugates in water and the standard samples of 340 nm, where the proteins do not adsorb, were adjusted to be within 0.05 absorbance units with each other. The overall optical density of both solutions did not exceed 0.10.

Detection of NP-BSA antibody by ELISA procedure

This experiment followed the standard procedure described elsewhere [2]. In brief, each well in a 96-well plate (Costar #9018 or Corning #25801EIA/RIA polystyrene) was coated with 100 µl of a 5% BSA solution (e.g., 100 µl of 5 mg/ml BSA
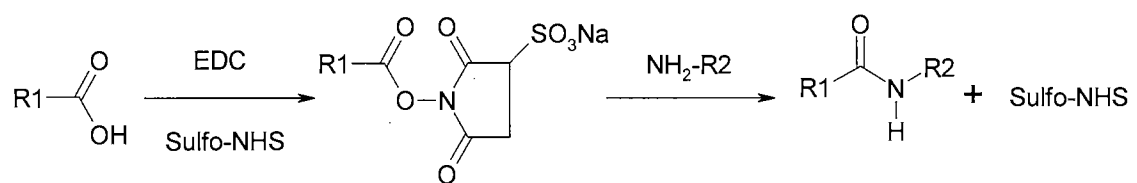
Figure III-1. EDC/Sulfo-NHS conjugation reaction.

in 10 ml coating buffer). Coating buffer was prepared by dissolving 0.78 g Na_2CO_3 and 1.46 g $NaHCO_3$ in 500 ml of H_2O with adjusting pH to 9.6. The plate was covered and rocked for at least 2 hours (preferably overnight) in an incubator at 37°C. After that it was washed 3 times with PBS-Tween 20 buffer in vacuum-apparatus and then patted dry. PBS-0.5% Tween 20 buffer was prepared by dissolving 8.0 g NaCl, 0.2 g KH_2PO_4, 2.9 g $Na_2HPO_4.12H_2O$, 0.2 g KCl, and 0.5 ml Tween 20 (polyoxyethylene sorbitan monolaurate) in 1000 L of deionized H_2O with adjusting pH to 7.2 – 7.4. Test antibody (NP-α-BSA) was diluted in PBS-Tween 20 buffer (normally, one would dilute 25 μl of 1 mg/ml antibody in 10 ml PBS-Tween 20 buffer to give a 1:400 dilution, but also one can serially dilute 1:100, 1:200, 1:400 etc.). Then 100 μl of prepared solution was added to each well and the plate was incubated covered on rocker for 1.5 hours at 37 °C. After that, it was washed 3 times with PBS-Tween 20 buffer and patted dry. Next, peroxidase-conjugated rabbit α-bovine IgG was diluted 400 times in PBS-Tween 20 buffer. This solution was also added in amount 100μl in each well and the plate was incubated as before. Then, it was washed 6 times as before and patted dry. Color substrate was prepared (OPD – 1 tablet + 20 ml deionized H_2O + 15 μl H_2O_2) and added 100 μl/well. The absorption was recorded in a micro plate reader at 450nm. Controls were set up on the same plate.

Results and discussion

Development of the optimal conditions for conjugation

Different conjugation conditions (*i.e.* time, temperature, and concentrations) were tested and the products were examined by native state electrophoresis and SDS-PAGE.

The results corresponding to various reaction times at pH = 6.7 for conjugation reaction of NPs and antibody are presented in Figure III-2. NP-IgG (anti-BSA) has increased mobility do to the high negative charge of NPs. The reaction was finished within 4 hours, since the band position of 3 hours (well 2) and 4 hours (well 1) were about the same. At pH below 7, the excess NPs in the solution were quenched after the reaction, while NPs at pH 7.4 remained active (well 9). However, those NPs conjugated with proteins were stable and kept luminescence at pH 6.7. The bright luminescence on the top of well 1-4 is attributed to oligomers of conjugates forming multiple binding sites on the NP and IgG.

The procedure of the reaction time optimization exemplifies the typical process for adjusting other parameters such as concentration of EDC. An insufficient amount of EDC will result in incomplete conjugation, while the excess of EDC will cause extensive cross-linking and aggregation. The ratio of NP to IgG is also a very significant factor that requires optimization; deviations from its optimum can also lead to predominant formation of oligomers.

The results corresponding to conjugation reaction of NPs and anti-BSA with different EDC and CdTe concentrations at pH 7.0 are presented in Figure III-3. The gel electrophoresis procedure was identical to that described above.
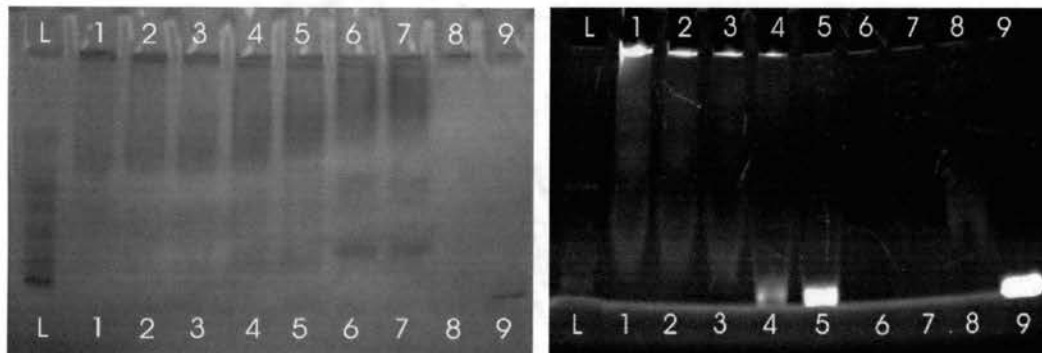
71

Figure III-2. Native state gel electrophoresis of CdTe NPs and NP-IgG (anti-BSA, Sigma) with different reaction times at pH 6.7. Left panel: stained by Coomassie Blue. Right panel: luminescence image before staining (excitation 360 nm). Wells: L) Standard protein ladder; 1) 4 hrs; 2) 3 hrs; 3) 2 hrs; 4) 1 hrs); 5) 30 mins; 6) no NP, 4 hrs; 7) IgG, 4 hrs; 8) no IgG, 4 hrs; 9) NP, pH 7.4, 4hrs. (The antibody purchased from Sigma was a polyclonal IgG fraction and showed multiple protein bands. The data in this chapter refer to anti-BSA from Rockland).
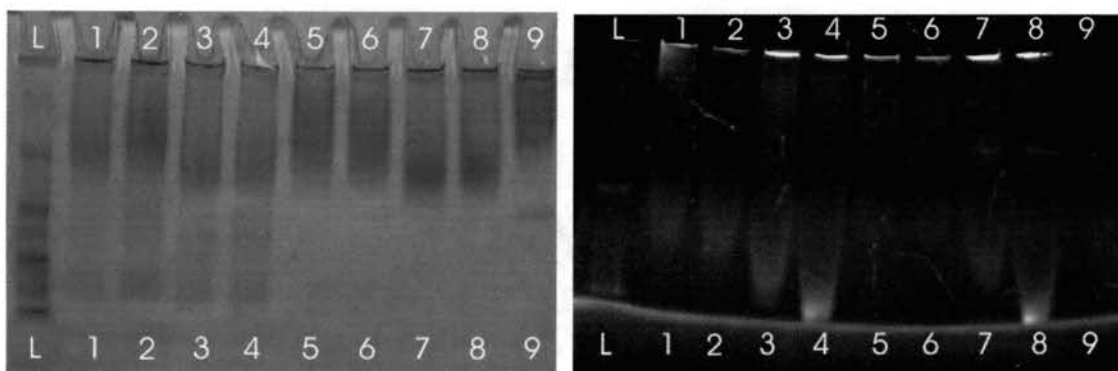
Figure III-3. Native state gel electrophoresis of CdTe and anti-BSA IgG conjugates with different EDC and CdTe concentrations at pH 7.0. Left panel: stained by Coomassie Blue. Right panel: luminescence image (excitation 360 nm). Samples in wells 1-4 has anti-BSA IgG from Sigma, 5-8 has anti-BSA IgG from Rockland; samples in wells 2, 4, 6, 8 has 0.025 M EDC, while samples in well 1, 2, 5, 7 used 0.05 M EDC; samples in well 1, 2, 5, 6 contain 0.025 M NP, while samples in well 3, 4, 7, 8 contain 0.05 M NP; well 9 contains IgG from Rockland only. L) Standard protein ladder.

Considering the data in Figure III-3, it is necessary to point out that IgG from Rockland has higher purity as indicated by much fewer low molecular weight bands than the one from Sigma. Therefore, the data reported here refer to Rockland anti-BSA IgG. BSA samples from different commercial sources were also compared by native gel electrophoresis. Within the resolution of this technique, all commercial sources revealed approximately the same band structure.

The following is the optimal protocol developed in the course of this study. A reaction mixture containing 0.05 mM CdTe NP, 1.5~2.5 mg/mL antigen or antibody, 5 mM NHS, 0.05 M EDC in pH 7.0 PBS buffer was prepared and kept at room temperature for 2-4 hrs, then stored at 4 °C overnight. This allowed the unreacted EDC to hydrolyze and lose its activity. Next, a small amount of precipitate was formed that probably consisted of unconjugated NPs that are known to agglomerate and become non-emissive at fairly low pH. The precipitate (if any) was removed by centrifugation. The stock, ready-to-use solution of the product was stored at 4 °C. Optionally, it can be dialyzed using dialysis membrane with molecular weight cut off (MWCO) 12 000-14 000, in pH 7.4 PBS buffer; however, the remaining small molecules in non-dialyzed solution did not affect the immunocomplex formation as could be seen from ELISA and target-specific FRET.

The luminescence intensity does not decrease after storing the samples at 4 °C for over a month.

Evidence of conjugate formation

Native and SDS-PAGE gel electrophoresis

The native electrophoresis results (Figure III-4, left panel) showed that both NP-conjugated BSA (Figure III-4 well 2) and anti-BSA IgG (Figure III-4 well 4) bands became more mobile in the electric field than the unlabeled biospecific ligands (Figure III-4 well 1 and 3). The BSA monomer band shifted from the relative marker of 65 kDa to 47 kDa, evidence that the high negative charge of the NPs and their compactness overcame the increase of their mass do to labeling. It is important to emphasize, that in the native electrophoresis, the position of the band is not linearly proportional to the molecular weight, do to the different charge status of each sample.

On the gel electrophoresis plate the commercial BSA showed two other bands at 100 kDa and 150 kDa corresponding to BSA-BSA dimer and globulins, respectively. This observation agrees with the specifications of Sigma. These compounds had minor influence on the biospecific reactions discussed below. Both of these bands shifted synchronously with BSA monomer to smaller masses after the NP conjugation. By mixing NPs with BSA and IgG without adding coupling reagents (EDC and NHS), no evidence of nonspecific binding was observed in native state gels.

The mobility of the proteins in SDS-PAGE electrophoresis (Figure III-4, center panel), was determined by the mass/charge ratio of denatured protein chains carrying sodium dodecyl sulfate (SDS), that imparts a negative charge to them. Interestingly, the band positions of NP-labeled and unlabeled proteins virtually coincided at the 65 kDa marker (Figure III-4, center panel). Similarly to the native gel results, the increase of
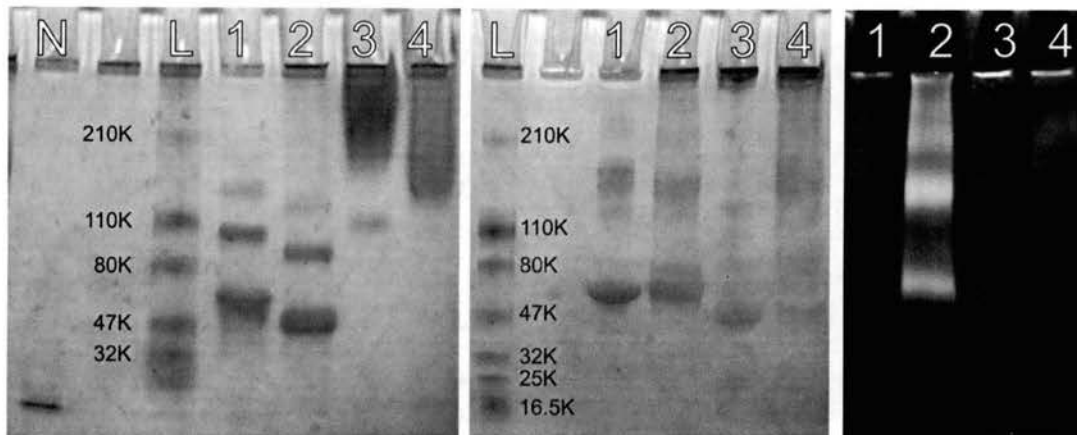
Figure III-4. Native and SDS-PAGE electrophoresis of CdTe bioconjugates. Left panel: native, stained by Coomassie Blue. Center panel: SDS-PAGE, stained by Coomassie Blue. Right panel: SDS-PAGE, luminescence image (excitation 360 nm). Wells: (1) BSA; (2) red-emitting NP-BSA; (3) anti-BSA IgG; (4) green-emitting NP-IgG; (N) Free CdTe NPs; (L) standard protein ladder. Molecular weights are marked on the side in kiloDaltons (kDa).

mass do to the addition of NPs to the protein was compensated by the increase of the overall charge density of the conjugate. Unlike NP-BSA, the SDS-PAGE band of NP-IgG conjugate remained at 150 kDa, while the free IgG were mostly broken apart into small molecular weight fragments because of the SDS plus heat action prior to electrophoretic separation (Figure III-4, center panel, wells 3 and 4).

Considering SDS-PAGE data, it is important to stress two points.

(1) Estimates of molecular masses on the basis of gel electrophoresis results can give erroneous results for bioconjugates from highly charged NPs. Different experimental techniques must be used for this purpose.

(2) Bioconjugation to NP may increase the stability of antibodies. A brief heat treatment 150 sec at 96 °C was used for the preparation of SDS-PAGE samples. The relative intensity of the SDS-PAGE bands indicated that the conjugated antibodies were more resilient to this temperature than the unlabeled ones. The unlabeled antibodies (Figure III-4 well 3) were mostly broken apart by SDS and heat into small fragments, showing as a band at 40-50 kDa. The NP-IgG conjugates band had significantly lower intensity - the antibody remains mostly intact. The latter effect was reproduced in several controlled experiments.

It is important to note that little nonspecific binding of NP and BSA should be expected after the SDS-induced denaturation of the protein, and only covalent binding could make them move through the gel matrix together.

Luminescence of the gel plates

The evidence supporting covalent conjugation of CdTe to BSA and IgG was found from the luminescence analysis of the gel plates. The bands of NP conjugates displayed strong luminescence, while the free proteins did not show any detectable signal in the luminescence image (Figure III-4, right panel). Using procedures described in Chapter II, the gel pieces cut out of the gel plates in the area of the conjugate bands revealed the luminescence spectra with the peaks identical to the original NPs, that is 553-555 nm and 610-611 nm for NP-IgG and NP-BSA, respectively.

Chromatography

The formation of NP bioconjugates was also confirmed by HPLC size exclusion chromatography (Figure III-5). The original BSA revealed three HPLC peaks congruent to the three bands seen in gel electrophoresis (Figure III-4). Since the species with higher molecular weight are eluted in shorter retention times, the observed HPLC peaks at retention times 7.8, 6.8, and 5.4 min should be attributed to BSA monomer, BSA dimer, and globulins, respectively. After the conjugation to CdTe, the same three peaks could be seen at 6.5, 5.3, and 4.2 min, all being shifted to higher molecular weight, as expected for the attachment of NPs to proteins. Considering that the approximate molecular weight of 5.0 nm red-emitting CdTe attached to BSA is 240 kDa (specific density of CdTe is 6.2 g/cm^3), the HPLC peak shift for monomeric BSA shows that not more than one NP is attached to this protein.
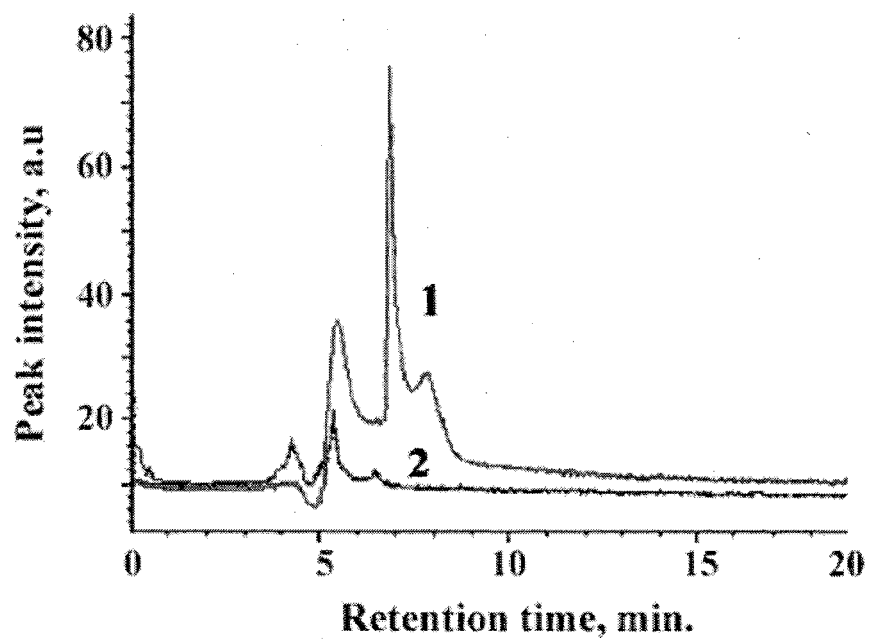
Figure III-5. HPLC chromatograms for (1) BSA and (2) NP-BSA

Similar behavior was observed for the bioconjugates of IgG. The HPLC peak attributed to free IgG was observed at 6.7 min, while shifting to 6.1 min after the conjugation to green-emitting NPs of ca. 2.5 nm in diameter. The molecular mass of these quantum dots was estimated to be 30 kDa, and; therefore, the HPLC molecular weight shift corresponds to the attachment of about one semiconductor particle per IgG as well.

It is necessary to emphasize that the estimates of NP-protein composition of the conjugates should be taken with caution because the mechanism of retention of NPs and polymers/proteins in gel permeation media can be quite different, and; therefore, introduce an error.

No free BSA or large oligomeric NP-BSA agglomerates with gradually increasing molecular masses were detected in elution curves (Figure III-5). In addition to such oligomers, the luminescent bands seen at the starting line in gel electrophoresis could be possibly originated from aggregates produced by accumulation on dust particles rather than multiple chemical cross-linking because of BSA tendency to adsorb on many surfaces [15].

Biological activity of the conjugates

Circular dichroism

Circular dichroism (CD) spectra of BSA and NP-BSA conjugate were very similar to each other (Figure III-6, left panel), which indicates a small disturbance of the
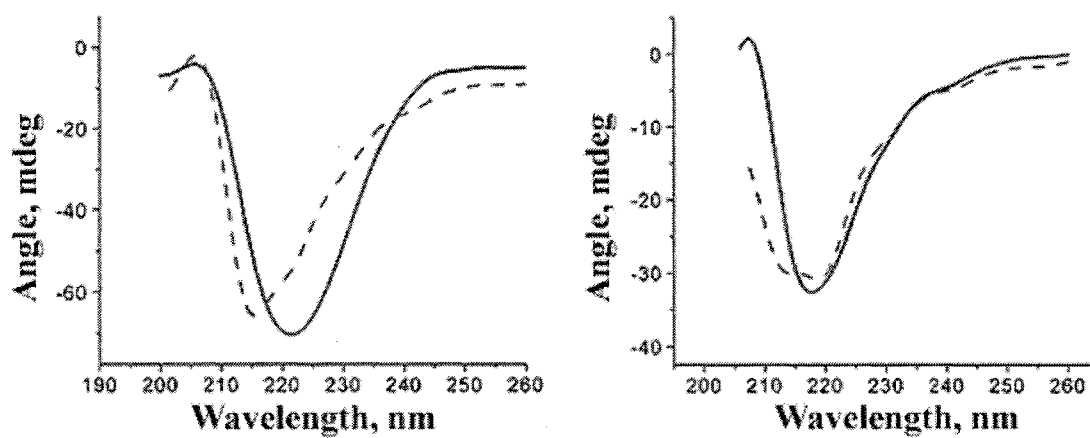
Figure III-6. CD spectra of BSA (left panel) and anti-BSA IgG (right panel) before (solid line) and after (dashed line) the conjugation to CdTe NPs.

BSA conformation manifested as a shift of CD spectral minimum from 222 to 215 nm [22]. Even greater resemblance of CD spectra was observed for anti-BSA and NP-anti-BSA pair (Figure III-6, right panel). These data show that the tertiary structure of both proteins remains mostly intact after the conjugation.

ELISA

The binding affinity of the conjugated anti-BSA IgG was examined by the standard ELISA technique and the results are shown in Figure III-7. Peroxidase-conjugated rabbit α-bovine IgG was used to label the anti-BSA IgG bound to BSA for colorized binding count. The absorbance at 450 nm represents the binding activity of the antigen/antibody pair. The concentrations of IgG under 1 μg/ml respond linearly, and data above 1 μg/ml is saturated (Figure III-7). The binding affinity of NP-IgG was determined to be 25~50% that of unlabeled IgG. Its reduction is believed to originate from partial blocking of binding sites by (1) NP positioned close to the N terminal of the IgG and (2) other bioconjugates in their dynamic aggregates.

The binding activity of NP-BSA was determined with the same ELISA experiments against free polyclonal anti-BSA IgG (results in Figure III-7). No losses of binding activity to the antibody in NP-BSA were detected.
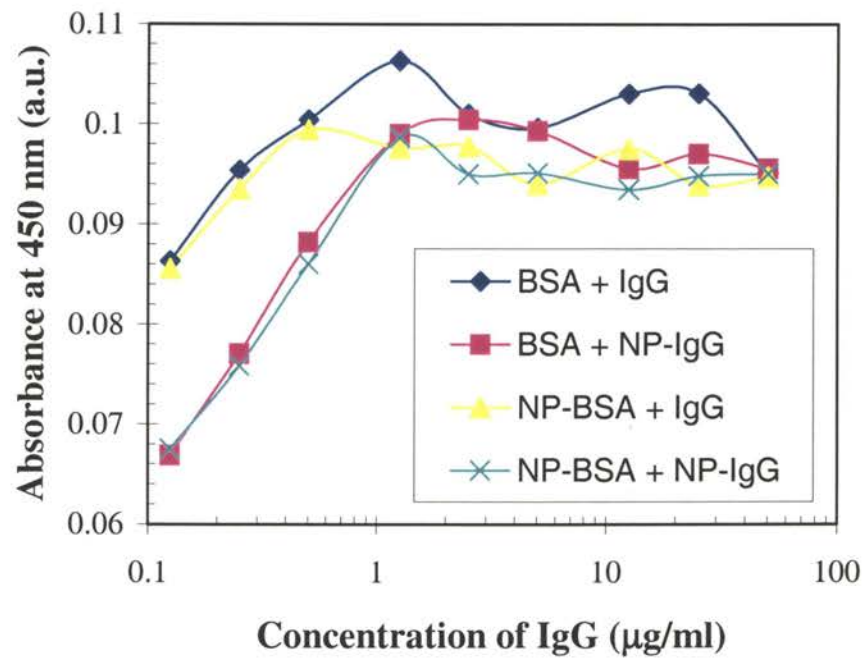
Figure III-7. ELISA results.

Photoluminescence experiments

Formation of the immunocomplex

Figure III-8 represents the fluorescence spectra of the NP-BSA and NP-anti-BSA IgG conjugates in solution. The emission peaks are at the same position as in free NPs.

The BSA and antibody have no absorption at 340~350 nm and do not fluoresce under 340~350 nm excitation. The molar extinction coefficient of free NPs and the conjugates at 340 nm is 3×10^8.

The quantum yield of green-emitting (λ_{max} = 555 nm) NP was determined ~24%, and red-emitting (λ_{max} = 610 nm) NP was ~29%. The quantum yield of green-emitting NP conjugated to IgG was ~6%, and the quantum yield of red-emitting NP conjugated to BSA was about ~5%. The decrease of the quantum yield should be attributed to the effect of low pH required for the EDC/NHS coupling reaction, well known to decrease the luminescence of NP stabilized by thiols [23].

Significantly higher quantum yields were observed for bioconjugation reactions with glutaraldehyde and cysteine-stabilized CdTe, which can be carried out at high pH (Chapter II) [24].

FRET-resonance energy transfer

When NP-IgG (anti-BSA) with green luminescence is combined with NP-labeled BSA with red luminescence, the NP-IgG/BSA-NP immunocomplex should form (Figure III-9).
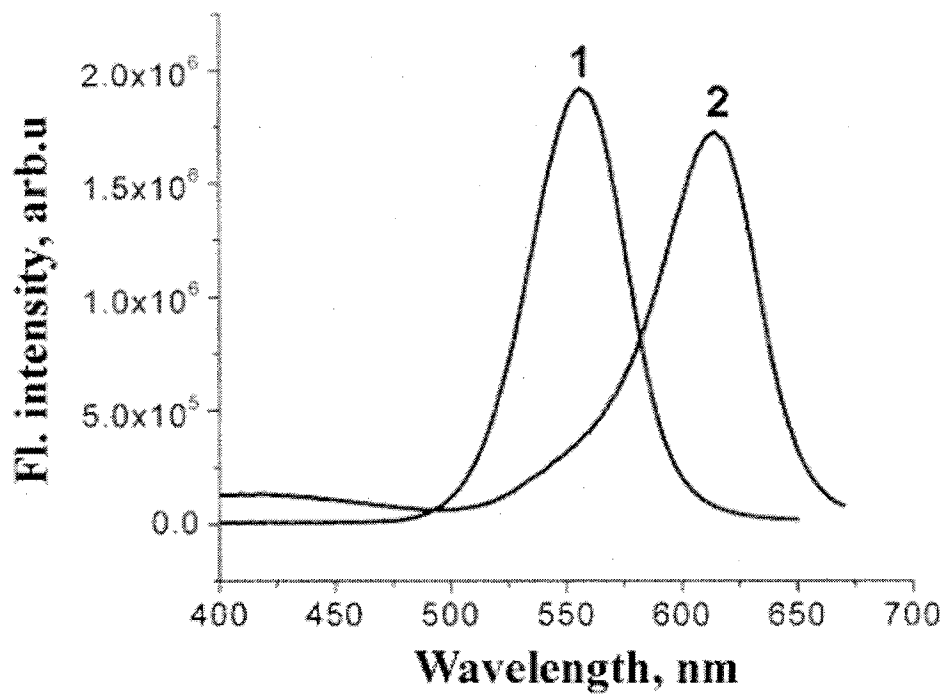
Figure III-8. Fluorescence spectra of (1) NP-labeled anti-BSA IgG with green emission

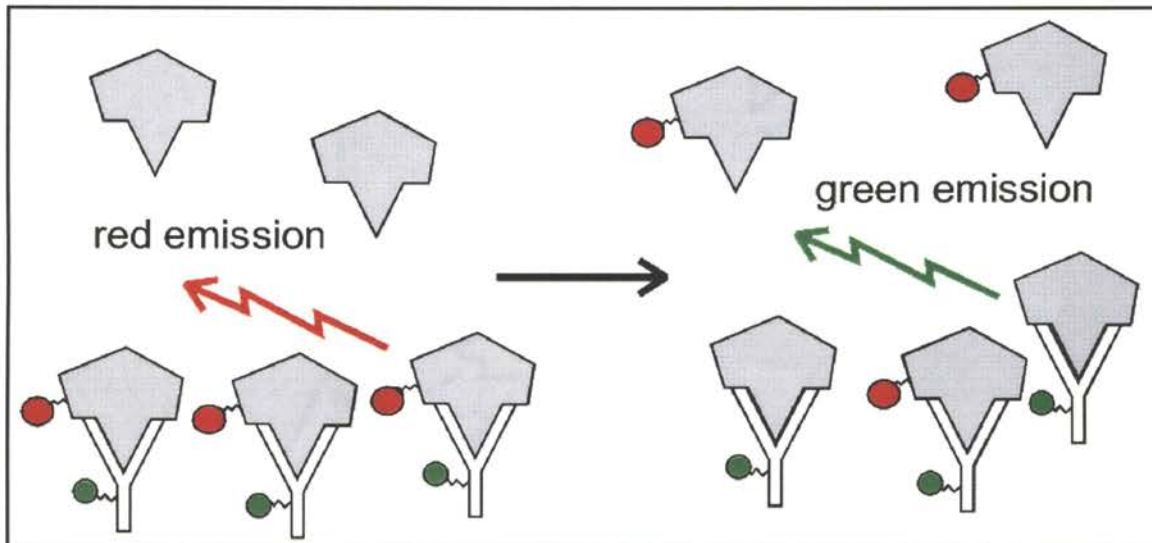and (2) NP-labeled BSA with red emission. Excitation wavelength is 340 nm.

Figure III-9. Schema of an immunocomplex formation from NP-labeled antigen and antibody.

As expected, a significant enhancement of the NP-BSA's red emission at 611 nm and the corresponding quenching of the green emission of NP-IgG at 555 nm were observed after the self-assembly of the labeled biospecific ligands in the immunocomplex (Figure III-10). Concentrations: NP-BSA, 5×10^{-7} M; NP-IgG, 5×10^{-7}M; BSA 2×10^{-6} M. The mutual affinity of the antigen and antibody brought the NPs close enough together to allow the resonance dipole-dipole coupling required for FRET to occur. Thus, the energy of the excitonic state in the green-emitting NP was transferred to the similar state of the red-emitting NP with lower exciton energy. FRET efficiency was particularly high for green/red NP pairs because of the strong overlap of their emission and absorption spectra. Importantly, when unlabeled BSA was added to the immunocomplex, it competitively bound to NP-IgG, thereby replacing it in the immunocomplex with NP-BSA and inhibiting the FRET process. As such, the green emission peak of NP-IgG at 555 nm could be observed again, while the red emission peak at 611 nm showed decreased intensity. Following this approach, we were able to detect as low as 10^{-8} M BSA with 5×10^{-9} M NP-BSA and NP-IgG. Unlike ELISA, the described detection process does not require the multiple binding and washing steps.
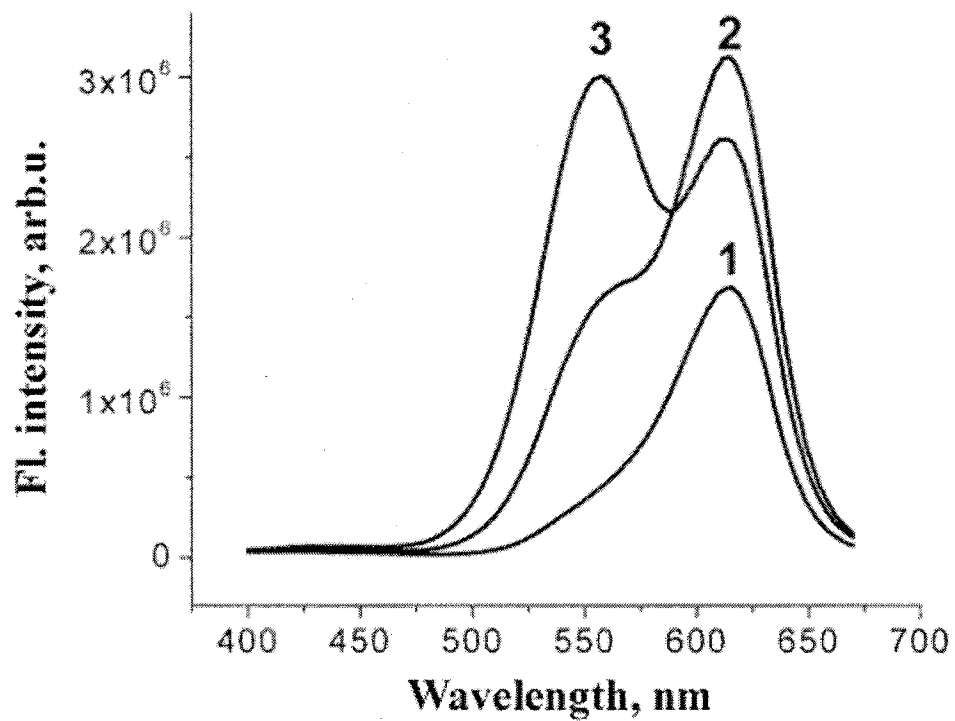
Figure III-10. Effect of competitive BSA binding on FRET of the immunocomplex: (1) NP-BSA; (2) NP-BSA + NP-IgG; (3) BSA + NP-BSA + NP-IgG.

Kinetics in immunocomplex

The kinetics of the competitive replacement of one of the biological ligands in the immunocomplex is presented in Figure III-11. Fluorescence emission spectra recorded at different times after mixing 10^{-7} M NP-BSA with 10^{-7} M NP-IgG (Figure III-11, left panel). The intensity of the peak at 553 nm decreases with time while the intensity of the peak at 611 nm increases.

The efficiency of FRET is estimated as the intensity ratio of the red-emission peak at 611 nm and green-emission peak at 553 nm. Concentrations: NP-BSA, 10^{-7} M; NP-IgG, 10^{-7} M; BSA, 5×10^{-7} M; egg albumin, 10^{-6} M. FRET efficiency decreased and the green luminescence became brighter as can be seen by the lower I_{611}/I_{553} ratio (Figure III-11, right panel, circles). It takes several hours for the reaction to come to completion, that is typical for competitive replacement of noncovalently bound ligands with strong affinity to each other. High concentration of egg albumin, that does not bind to anti-BSA IgG, showed no influence on FRET between NP-IgG and NP-BSA (Figure III-11, right panel, triangles). The time dependence of the immunocomplex luminescence remained virtually unchanged as compared to NP-BSA + NP-IgG immunoreaction. This fact demonstrates the high biospecificity of the prepared conjugates and virtually absent interference from the noncomplimentary proteins.
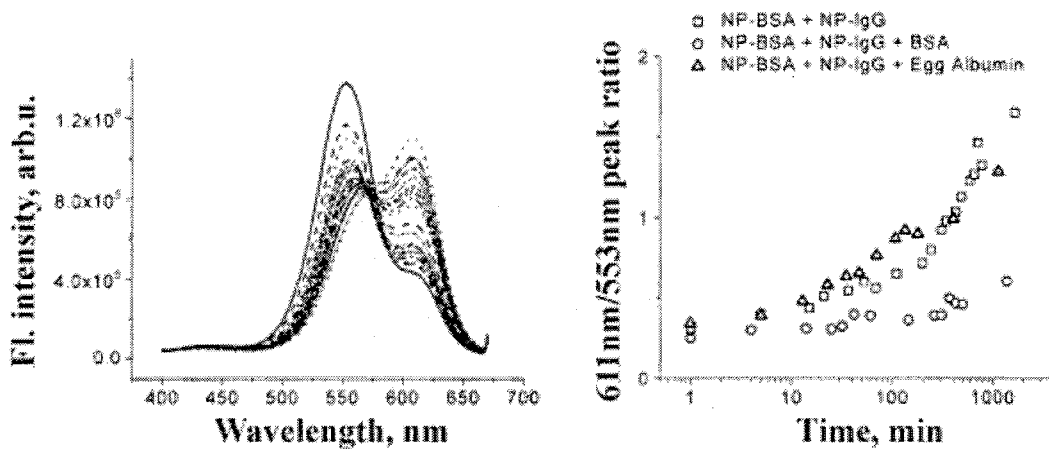
Figure III-11. Left panel: fluorescence emission spectra recorded at different times after mixing NP-BSA with NP-IgG. Right panel: kinetics of the immunocomplex formation as derived from FRET efficiency. NP-BSA + NP-IgG (squares), NP-BSA + NP-IgG + BSA (circles), NP-BSA + NP-IgG + egg albumin (triangles).

Summary

Bioconjugates with complementary antigen and antibody have been prepared from thiol-stabilized green- and red-emitting CdTe NPs.

They retain substantial bioactivity and can form the corresponding immunocomplex and pair NPs with different emission properties in a supramolecular assembly. The molecular weight estimates indicate that such a supramolecule combines one NPs of each color.

Quenching of the green-emitting NPs and the enhancement of the luminescence of the red-emitting quantum dots signify the presence of FRET in the immunocomplex. The exceptional specificity of immunocomplex reactions affords unique possibilities for creating organized assemblies of nanoparticles and other nanocolloids. After synthetic optimization, such as enhancement of the luminescence quantum yield of the bioconjugates, the FRET effect can be taken advantage of in protein sensing and in hybrid photoelectronic devices.

Acknowledgements

References

1. Delves, P. J. *Antibody Applications: Essential Techniques;* 1995.

2. Walker, J. M. *The Protein Protocols Handbook, Second Edition;* 2002.

3. Mann, S.; Shenton, W.; Li, M.; Connolly, S.; Fitzmaurice, D. *Advanced Materials* **2000,** *12*(2), 147-150.

4. Alivisatos, A. P. *Science* **1996,** *271*(5251), 933-937.

5. Charles, P. T.; Kusterbeck, A. W. *Biosensors & Bioelectronics* **1999,** *14*(4), 387-396.

6. Bart, J. C.; Judd, L. L.; Kusterbeck, A. W. *Sensors and Actuators, B: Chemical* **1997,** *B39*(1-3), 411-418.

7. Chan, W. C. W.; Nie, S. *Science* **1998,** *281* 2016-2018.

8. Taylor, J. R.; Fang, M. M.; Nie, S. *Anal.Chem.* **2000,** *72*(9), 1979-1986.

9. Bawendi, M. G.; Mikulec, F. V.; Sundar, V. C. WO 0017642, **1999,** pp. 71.

10. Weiss, S.; Bruchez, M.; Alivisatos, P. US 6207392, **1999,** pp. 28.

11. Sondi, I.; Siiman, O.; Koester, S.; Matievich *Langmuir* **2000,** *16* 3107-3118.

12. Taton, T. A.; Mucic, R. C.; Mirkin, C. A.; Letsinger, R. L. *J.Am.Chem.Soc.* **2000,** *122*(26), 6305-6306.

13. Mirkin, C. A. *Inorganic Chemistry* **2000,** *39*(11), 2258-2272.

14. Bruchez, M. J.; Moronne, M.; Gin, P.; Weiss, S.; Alivisatos, A. P. *Science* **1998,** *281* 2013-2016.

15. Peters, T., Jr. *All About Albumin. Biochemistry, Genetics, and Medical Applications;* Academic Press: San Diego, 1995.

16. Bragg, P. D.; Hou, C. *Archives of Biochemistry and Biophysics* **1975,** *167*(1), 311-321.

17. Lomant, A. J.; Fairbanks, G. *Journal of Molecular Biology* **1976,** *104*(1), 243-261.

18. Staros, J. V. *Biochemistry* **1982,** *21*(17), 3950-3955.

19. Halliday, M. I.; Wisdom, G. B. *Biochemical Society Transactions* **1986,** *14*(2), 473-474.

20. Imagawa, M.; Yoshitake, S.; Hamaguchi, Y.; Ishikawa, E.; Niitsu, Y.; Urushizaki, I.; Knazawa, R.; Tachibana, S.; Nakazawa, N.; Ogawa, H. *J.Appl.Biochem.* **1982,** *4*(1), 41-57.

21. Kishida, Y.; Olsen, B. R.; Berg, R. A.; Prockop, D. J. *Journal of Cell Biology* **1975,** *64*(2), 331-339.

22. Willard, D. M.; Carillo, L. L.; Jung, J.; van Orden, A. *Nano Letters* **2001,** *1*(9), 469-474.

23. Kapitonov, A. M.; Stupak, A. P.; Gaponenko, S. V.; Petrov, E. P.; Rogach, A. L.; Eychmueller, A. *J.Phys.Chem. B* **1999,** *103* (46), 10109-10113.

24. Mamedova, N. N.; Kotov, N. A.; Rogach, A. L.; Studer, J. *Nano Letters* **2001,** *1*(6), 281-286.

CHAPTER IV

CELL LABELING WITH NANOPARTICLE BIOCONJUGATES

Introduction

Nanostructured materials have a great impact on biological research. An exciting application of fluorescent semiconductor nanoparticles is their use in long-term labeling, imaging and tracking of cells.

Recent literature reports indicate that researchers are successfully tackling the problems of biostability and functionalization that plagued earlier quantum-dot bioconjugates [1] and these particles are now available to label a variety of specific cellular targets [2-4].

Preparing QDs with associated avidin (streptavidin) allows conjugation of QDs with any biotin containing antibody, protein, DNA, or synthetic polymer. QD resistance to photobleaching, their ability to be excited at many wavelengths, and their narrow emission wavelengths combined with the ready availability of a wide range of biotinylated chemicals, biomolecules, and antibodies make avidin conjugated QDs useful for additional bioanalytical applications.

The purpose of the research described in this chapter was to design nanoparticle bioconjugates for cell labeling that are photo stable, water soluble and biocompatible. For this purpose CdTe-Adivin bioconjugates, and (CdSe)CdS-BSA-Streptavidin were

synthesized and analyzed. They have been applied by our collaborators at University of Texas Medical Branch (Galveston, TX) for cell labeling.

Unfortunately, it is difficult to design nanostructured materials to interact specifically with cell surfaces. For example, merely attaching peptides to nanoscale materials does not completely dictate their interactions with cellular membrane receptors; other properties, such as general biocompatibility, solubility and nonspecific interactions with cell membranes, have to be correctly engineered as well [5].

These nanoparticle-streptavidin (STR) (or adivin) bioconjugates were further conjugated with antibodies anti-CD95 and anti- CD81 in order to target specific cells. CD95 is a receptor that is expressed just after irradiation. The idea was to deliver nanoparticles to those cells that express CD95 on their surface, because these cells are likely to have been damaged by irradiation (for example by irradiation during deep space missions).

Hepatitis C virus is a difficult virus to study since no cell culture models currently exist. One of the suggested targets of this virus is CD81. Therefore, conjugates of NPs-anti CD81 will target the same cell population that HCV does. This will allow treating and pretreating any cell that would likely be infected by HCV.

Experimental procedures

Instrumentation

Emission and excitation spectra were measured on FluoroMax-3 (Jobin Yvon, Inc.) spectrofluorometer.

UV-visible spectra were recorded with Hewlett-Packard HP8453 diode array spectrophotometer.

Native and SDS-PAGE gel electrophoresis were performed on the Mini-PROTEAN 3 electrophoresis cell (Bio-Rad, Hercules, CA) using precast gels.

Materials and reagents

The chemicals were used as received from the manufacturers. Cadmium perchlorate hydrate, N,N-dimethylselenourea, thioacetamide, L-cysteine, bovine serum albumin (BSA), streptavidin (STR) , glutaraldehyde (25 % in water), (1-ethyl-3-(3-dimethylaminopropyl) carbodiimide hydrochloride (EDC), adivin and PBS buffer (phosphate buffered saline powder) were purchased from Sigma - Aldrich Co. (St. Louis, MO, USA). N-hydroxysulfosuccinimide sodium salt (sulfo-NHS) and rhodamine B were obtained from Fluka (Milwaukee, WI, USA). Sodium citrate and sodium hydroxide were from Spectrum Quality Products, Inc. (New Brunswick, NJ).

Bio-Safe colloidal Coomassie Blue G-250 stain, precast 4-20% linear gradient Tris-HCl gel plates used for native and SDS-PAGE electrophoresis, Kaleidoscope and SDS-PAGE prestained standards were purchased from Bio-Rad (Hercules, CA, USA). Spectra/Por dialysis membranes with MWCO = 2,000 and 50,000 were from Spectrum Laboratories, Inc. (Rancho Dominguez, CA, USA).

Deionized ultrapure water (Barnstead) with 18.2 MΩ/cm was used for all experiments.

Synthesis of core-shell CdSe/CdS nanoparticles capped with sodium citrate

These nanoparticles were synthesized according to the procedure described previously [6]. Briefly, 0.05 g of sodium citrate and 2mL of 4×10^{-2} M cadmium perchlorate were added to 45mL of water and pH was adjusted to 9.0 by 0.1 M sodium hydroxide. The solution was bubbled with nitrogen for 10 min. Then 2mL of 1×10^{-2} M N,N-dimethylselenourea was added and the mixture was heated in a conventional 700W (Sharp) microwave oven for 55 sec. The molar ratio Cd:Se used in this recipe was 4:1.

The obtained CdSe nanoparticles were used as the initial material for the preparation of core-shell CdSe/CdS NPs according to the following recipe. To a prepared volume of CdSe nanoparticle 0.5 mL of 4×10^{-2} M solution of thioacetamide (thioacetamide was used as a sulfur source) was added in a quantity that the molar ratio of S_{added} : $Se_{initial}$ was 1:1. The mixture was heated in the sealed round-bottom flask in a silicon oil bath at 70-80°C for up to 24 hrs.

Calculation of the molecular weight and concentration of CdSe/CdS nanoparticles

Molecular weight (MW) of CdSe/CdS nanoparticles is calculated according to the formula:

$$MW = \rho * N_A * V_0$$

where N_A is the Avogadro number, ρ = 5.81 g/cm^3 is the density of cadmium selenide [7], and V_0 is the volume of one particle that can be calculated, assuming spherical particle shape, according to the formula:

$$V_0 = 4/3\pi r^3 = (\pi d^3)/6$$

where r is the radius, d is the diameter of the particle.

Size of the particles was estimated to be $\sim$ 4 nm by TEM (transmission electron microscopy). Thus, the volume of one particle V_0 will be:

$$V_0 = (3.14*(4.0*10^{-9})^3)/6 \text{ m}^3 = 3.35 *10^{-26} \text{ m}^3 = 3.35 *10^{-20} \text{ cm}^3$$

Hence,

$$MW \text{ (NP)} = 5.81 \text{ g/cm}^3 * 6.02*10^{23} \text{ 1/mol} * 3.35 *10^{-20} \text{ cm}^3$$

$$= 117,170.27 \text{ g/mol} \approx \textbf{117,000 g/mol}$$

The molarity of NP solution was calculated based on the fact that ratio $Cd^{2+}:Se^{2-}:S^{2-}$ is equal 4:1:1 (excess of Cd^{2+}) and:

a) Amount of Se^{2-} in 50 ml of reaction mixture:

$$v \text{ (Se}^{2-}) = 0.002 \text{ L}*0.01M = 2*10^{-5} \text{ mol}$$

Since molarity: $M = v(Se^{2-})/ V$, then:

$$M = 2*10^{-5} \text{ mol}/0.050 \text{ L} = 4*10^{-4} M$$

Hence, molarity of CdSe (molecular form) = $4*10^{-4} M$

b) Number of CdSe molecules in one nanoparticle: = MW (NP)/MW (CdSe).

Then number of CdSe molecules in one nanoparticle is equal:

$$117,170.27 \text{ g/mol} / (112.4 + 79) = \textbf{612 molecules}$$

c) Finally, **molarity of NP solution** is equal:

$$4*10^{-4}\, M / 612 = \textbf{6.5} * \textbf{10}^{-7}\, \textbf{\textit{M}} = \textbf{0.65 } \boldsymbol{\mu}\textbf{mol/L}$$

And **number of nanoparticles in 1 ml of solution** is equal to:

$$M * V * N_A = 6.02*10^{23} \text{ 1/mol} * 6.5 * 10^{-7} \text{ mol/L} * 0.001 \text{ L} = \textbf{3.913}*\textbf{10}^{\textbf{14}}.$$

Photoactivation of CdSe/CdS nanoparticles

Freshly made CdSe/CdS nanoparticles dispersions were exposed to ambient light for several days (intensity 0.12 mW) in order to enhance their luminescence efficiency.

Changing the stabilizer from citrate to L-cysteine

The solution of L-cysteine was added to the prepared core-shell CdSe/CdS NPs in the amount that the molar ratio of citrate: cysteine = 10:1. The mixture was heated at 50°C for 1hr, and then it was dialyzed against 3.33×10^{-4} M solution of L-cysteine (pH=7.4) for 48 hrs (SpectraPor™ dialysis membranes with MWCO=2000).

Conjugation of nanoparticles to bovine serum albumin

Obtained core-shell CdSe/CdS nanoparticles capped with L-cysteine were conjugated to BSA according to one step protocol developed previously (Chapter II). In a typical preparation of the BSA-G-CdSe/CdS conjugate, 1 mL of prepared aqueous CdSe/CdS was mixed with 2 μL of glutaraldehyde (25% in water = 2.5 M) and 0.25 mL of a 0.5 mg/mL solution of BSA in a pH 7.4 phosphate buffer. After the mixture was incubated for 1 hr at 50 °C, it was dialyzed (48 hrs, using Spectra/Por dialysis membranes with MWCO = 50,000) against the PBS and placed in the refrigerator at 4 °C for storage. No subsequent treatment with $NaCNBH_3$ was used because the excess of L-cysteine present in the mixture as a mild reducing agent converted the initially forming Schiff base into the secondary amine bond.

Final concentrations were estimated as [BSA] 0.1mg/mL, or M (BSA) =1.5 μmol/L, and M (NP) = 0.52 μmol/L, that corresponds to molar ratio NP: BSA = 1:3.

Also, CdTe-G-BSA conjugates prepared previously (Chapter II) were used for subsequent conjugations.

Conjugation of NP-BSA to streptavidin/avidin

The conjugates NP-BSA-STR or NP-BSA-Adivin were prepared using both conjugation protocols developed during this study (1) through the G linkage (secondary amine bond - see details in chapter II and above) and (2) using zero-linkage agents : N-sulfo-NHS, with EDC (see details in Chapter III).

The glutaraldehyde linkage protocol: To the conjugated NP-BSA, the solution of streptavidin (or adivin) was added to final concentration of streptavidin 0.1mg/mL. After addition of 5μL glutaraldehyde (25% in water) to the mixture, it was incubated for 1 hr at 50°C.

Zero-linkage conjugation protocol: The water-soluble carbodiimide EDC was used to form active ester functional groups with carboxylate groups using the water-soluble compound sulfo-NHS. The advantage of adding sulfo-NHS to EDC reactions is to increase the stability of the active intermediate, which ultimately reacts with the attacking amine. EDC reacts with a carboxylate group to form an active ester (O-acylisourea) leaving group. Forming a sulfo-NHS ester intermediate from the reaction of the hydroxyl group on sulfo-NHS with the active-ester complex extends the half-life of the activated carboxylate to hours. Since the concentration of added sulfo-NHS is much greater than the concentration of the target molecule, the reaction preferentially proceeds through the longer-lived intermediate; however, the final product of this two-step reaction is identical to that obtained using EDC alone: the activated carboxylate reacts with an amine to give a stable amide linkage (Figure IV-1).

The conjugation in this step followed the modified two-step protocol [8] given below. The variation in the pH of activation from the original one-step protocol (pH 7.4) provides greater stability for the active ester intermediate. At pH 6 the amines on the conjugated molecule will be protonated and; therefore, be less reactive toward the sulfo-NHS esters that form. In addition, the hydrolysis rate of the esters is dramatically slower than at acid pH. Thus, the active species live a reasonable time frame without significant
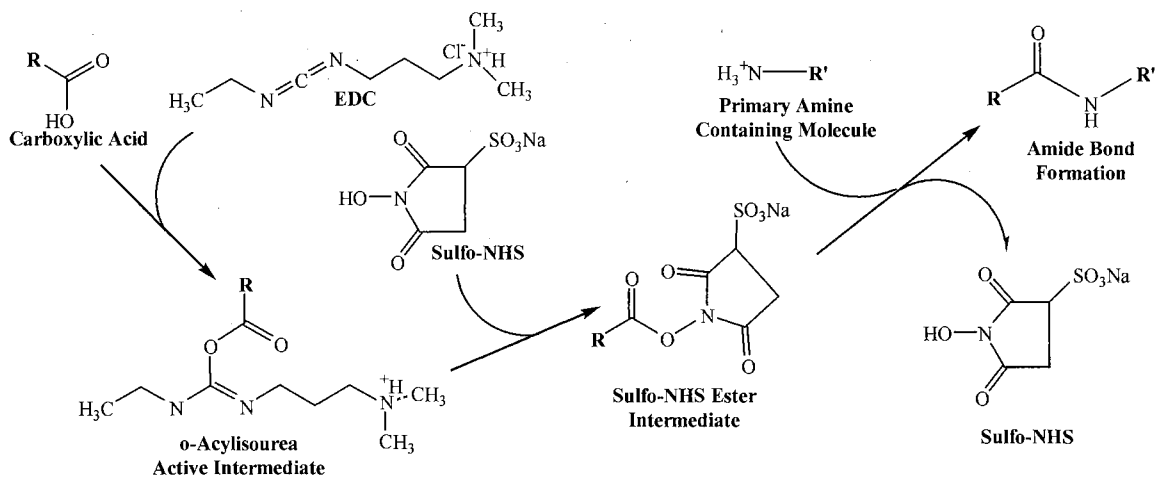
101

Figure IV-1. EDC/Sulfo-NHS conjugation reaction

loss in conjugation potential. To quench the unreacted EDC, usually 2-mercaptoethanol is added to form a stable complex with the remaining carbodiimide, according to [9]. In this case, the small amount of stabilizing agent (L-cysteine) present in the solution of NP-BSA conjugates acts as a quencher.

Briefly, to the solution of streptavidin a quantity of EDC and sulfo-NHS was added to obtain final concentrations of 10 mM EDC and 5 mM sulfo-NHS. The solution was mixed and reacted for 15 min at room temperature. This activated streptavidin was added directly to NP-BSA solution for conjugation. The NP-BSA solution has pH 7.4. This brings the pH of the coupling medium above pH 7 to initiate the active ester reaction. The mixture was left to react for at least 2 hrs at room temperature in the dark.

Cell labeling experiments

Experiments with live cells were carried out by our collaborators at UTMB (University of Texas Medical Branch), Galveston, TX.

To conduct some cell experiments, the prepared NPs conjugates were mixed with biotinylated antibodies anti-CD95 and anti-CD81. The product that formed via streptavidin-biotin linkage was used to target cell receptors CD95 or CD81.

For these experiments, different types of cell were used: T24 (human bladder carcinoma derived cells), BJAB and MOLT4 (the human cells derived from leukemia patients).

The particles were added to the media. The cells then took up the particles through many different methods including pinocytosis, receptor mediated endocytosis, etc.

TUNEL assay [Terminal deoxynucleotidyl transferase mediated

dUTP nick-end-labeling]

This assay has been designed to detect cells dying of apoptosis [Apoptosis (from a Greek word meaning the dropping of leaves from a tree) is a term referring to the cytologically observable changes associated with a process of cellular self-destruction observed in all eukaryotes]. This widely used and highly sensitive assay is based on the fact that nuclear DNA becomes fragmented by endogenous endonucleases during apoptosis and that characteristic, nonrandom DNA fragmentation is common to all cells undergoing this form of programmed cell death. Fragmented DNA is detected easily by agarose gel electrophoresis.

Results and discussion

Cadmium telluride (CdTe) bioconjugates

Experimenting with live cells, conjugates CdTe-BSA-Avidin were initially tested to determine their targeting capacity. The resulting conjugates have an emission peak maximum at 626 nm (Figure IV-2).

The CdTe-BSA-Adivin conjugates have high quantum efficiency that is shown on Figure IV-3.
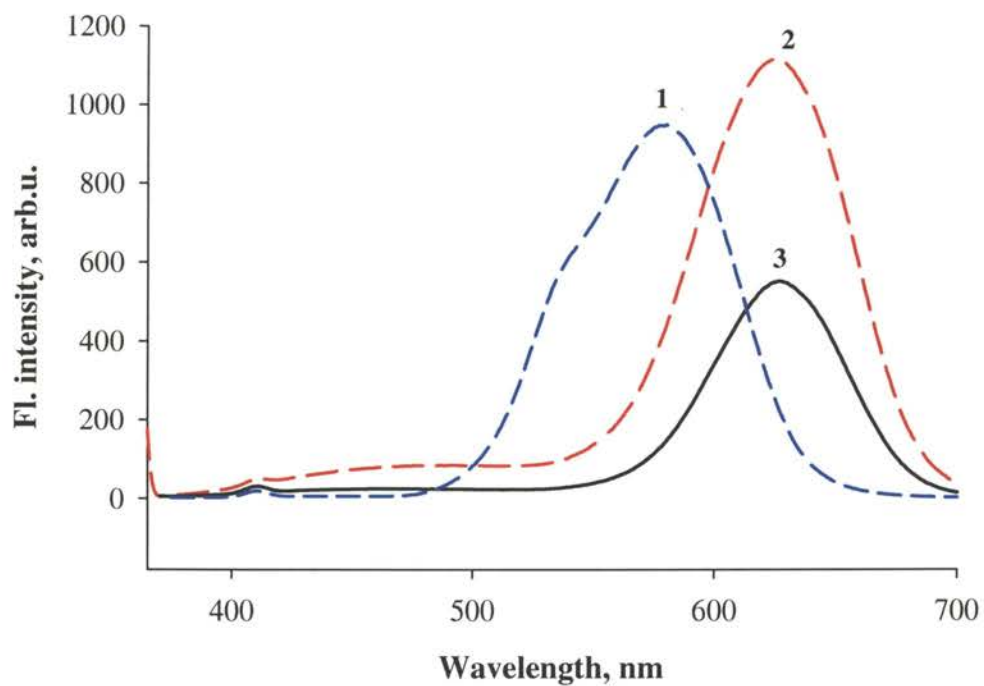
Figure IV-2. Photoluminescence emission spectra. 1 - CdTe, cysteine stabilized (PL=580 nm); 2 - CdTe-albumin (PL=625nm), and 3 - CdTe-albumin-avidin (PL=626nm). Excitation wavelength 360 nm.
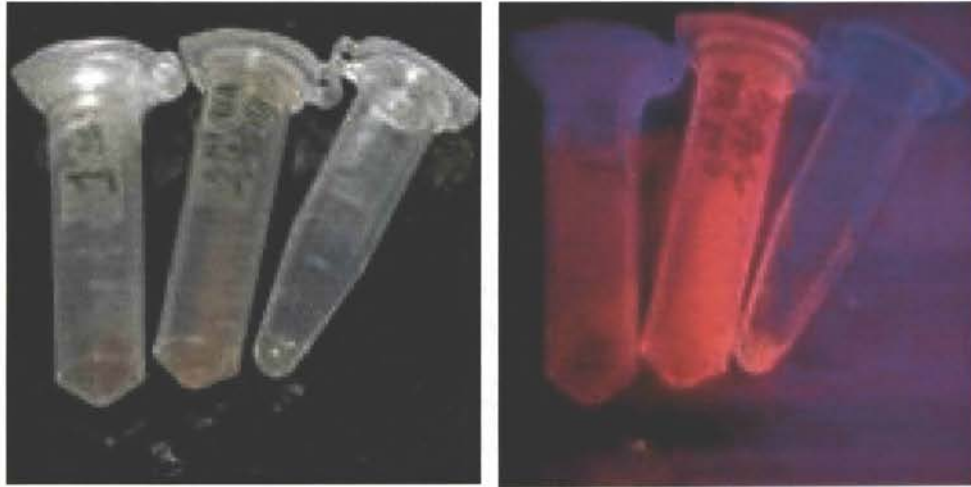
Figure IV-3. NP bioconjugates under UV light. Tube contents (from left to right): frozen-dry CdTe – BSA-Avidin; bioconjugate CdTe – BSA - Avidin in PBS buffer (pH=7.4); SAA but diluted 1:10 in PBS.

The prepared samples of bioconjugates CdTe-BSA-Adivin were further modified with anti-human CD95 or anti-human CD81 antibodies via adivin-biotin linkage. The obtained conjugates with CdTe core and anti-human CD95 or anti-human CD81 outer coatings were initially tested by incubation with cell lines known to express either CD81 or CD95. These experiments were repeated several times, but yielded only sub optimal results as assayed by fluorescence microscopy (data not shown). These CdTe NPs were most stable at pH>8, and after these experiments, considered to be incompatible with media designed for cell culture (pH=7.5).

Figure IV-4 shows that photoluminescence intensity of both CdTe NPs and conjugates CdTe-BSA decreases with decreasing of pH. But the conjugates have higher photoluminescence intensity compare to CdTe NPs at the same pH.

Microinjection of CdTe NPs- Avidin conjugates into live cells

In order to assess the possibility of using the NPs for intracellular targeting, CdTe based bioconjugates were microinjected into T24 cells. Once inside the cells, the NPs were assayed for their ability to fluoresce within the cellular compartment. The particles did retain their fluorescent properties within the cytoplasm of cells and were photographed shortly after injection (Figure IV-5).
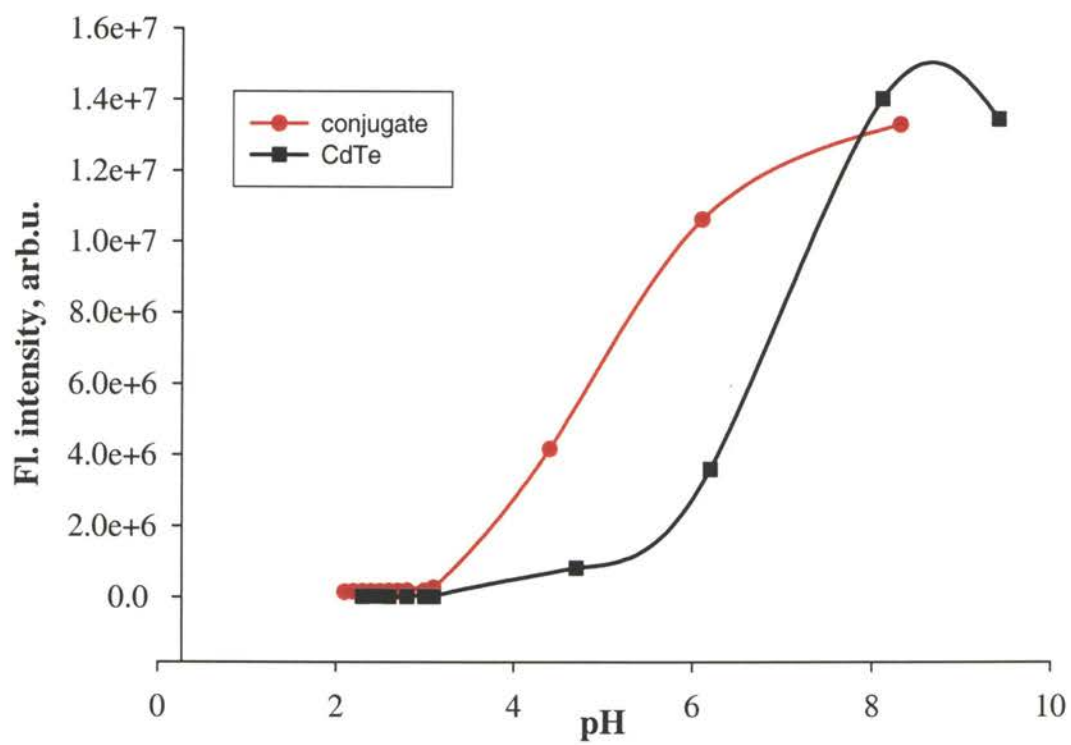
Figure IV-4. Luminescence intensity vs. pH for CdTe, cysteine capped, and for conjugate CdTe-BSA.
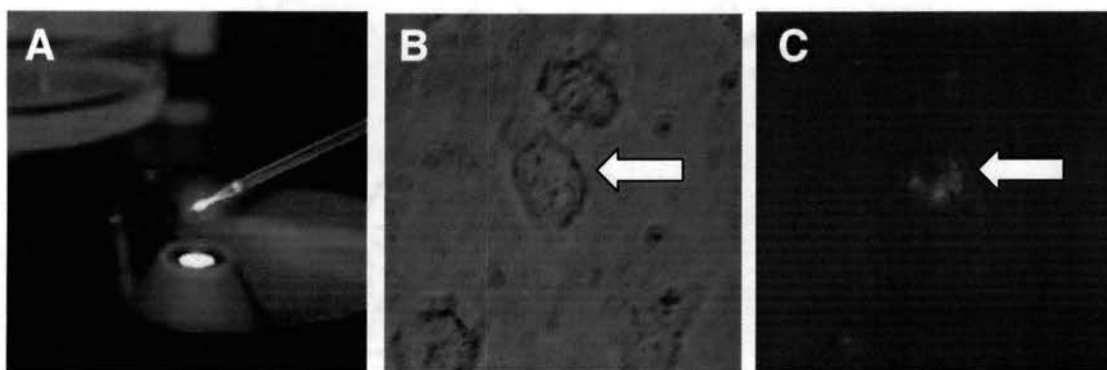
Figure IV-5. CdTe NPs coated with BSA/Avidin in PBS. Panel A shows CdTe NPs loaded into a pipette prior to microinjection. T-24 cells were microinjected with NPs and photographed under light field (Panel B) and fluorescence conditions (Panel C).

CdSe/CdS nanoparticles bioconjugates

In order to overcome disadvantages of the unstable nature of CdTe particles at physiological pH, a more stable particle was designed that had different outer layers. The particle of choice had, from the core out, a semiconductor CdSe core for fluorescence, a CdS coat for stability at physiological pH, and an outer shell of albumin/streptavidin. The final coat of streptavidin (STR) gives flexibility with respect to attaching targeting molecules to the surface of the particle. Initially, the plan was to use biotin labeled antibodies to target cells. Since antibodies are not cost effective for bulk preparation, other more cost effective biotin labeled moieties can be used in the future without changing the particle preparation.

The cadmium selenide nanoparticles were synthesized, coated with a layer of cadmium sulfide, photoactivated and conjugated first with albumin, and then with streptavidin (STR).

Characterization of CdSe/CdS bioconjugates

TEM of NP-BSA-STR conjugates

In order to verify the presence and determine the size of these nanoparticles, TEM (transmission electron microscopy) was performed (Figure IV-6). The size of the particles present was determined to be ~14nm and roughly spherical.
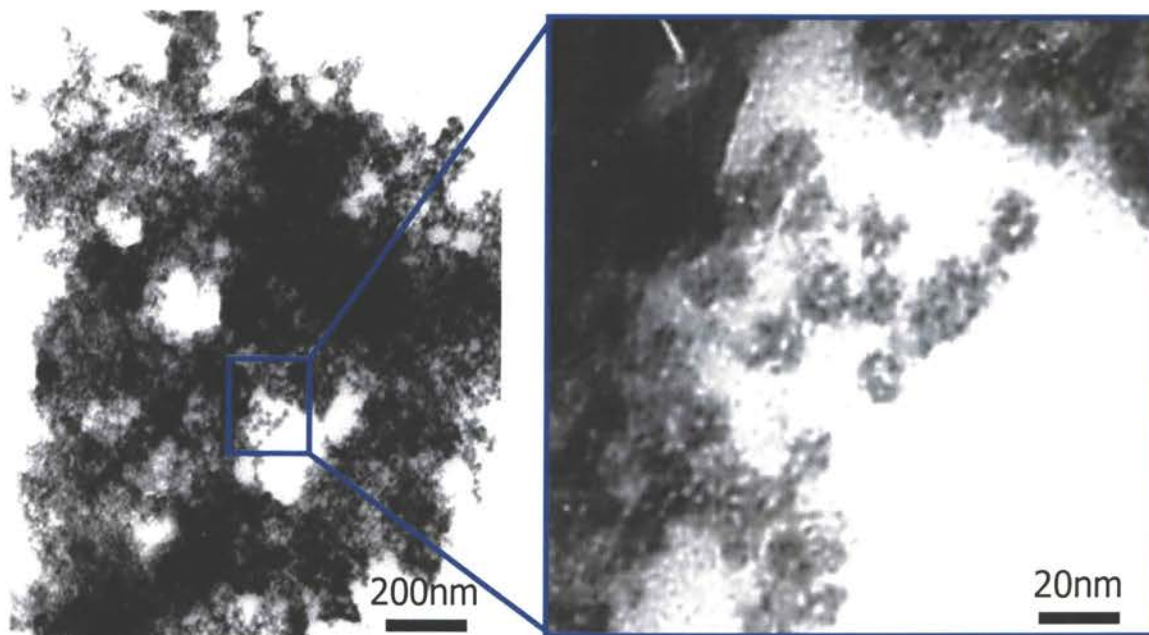
Figure IV-6. TEM data on CdSe NPs coated with CdS, BSA, and Streptavidin. Conjugates were evaluated for size and consistency. The particles appeared to be uniform and about 14 nm in diameter.

111

Native gel electrophoresis

Native Gel Electrophoresis results are shown in Figure IV-7. Since the STR band in the last well disappears, STR is consumed. NP-BSA-STR band broadens and slightly shifts to heavier molecular weight.

Photoactivation of CdSe/CdS nanoparticles

Exposure of freshly synthesized CdSe/CdS to ambient light for several days (intensity 0.12 mW) was noted to result in a drastic enhancement of the luminescence intensity with quantum yield (QY) reaching as high as 25-45%, while no obvious increase in photoluminescence was observed for the same NPs stored in the dark. (Figures IV-8 and IV-9).

Similar effects were also reported by several other groups with smaller changes in QY. It increased ca. 3 times for thioglycolic acid-capped CdTe NPs illuminated for 5 days to become 30% [10]. Exposure of CdSe/CdS/ZnS nanorods to laser light overnight resulted in a QY increase of luminescence yield from 1 to 16% [11]. A 10% QY was obtained after UV curing ZnS:Mn samples coated with polymers [12].

For citrate-stabilized CdSe/CdS colloids, the luminescence intensity of the excitonic peak typically increased 50-500 times (Figure IV-8 and IV-9).

Figures IV-8 and IV-9 demonstrate that by exposing the particles to ambient light for prolonged period of time (up to three weeks), it is possible to increase the fluorescence yield of these particles (Figure IV-9).
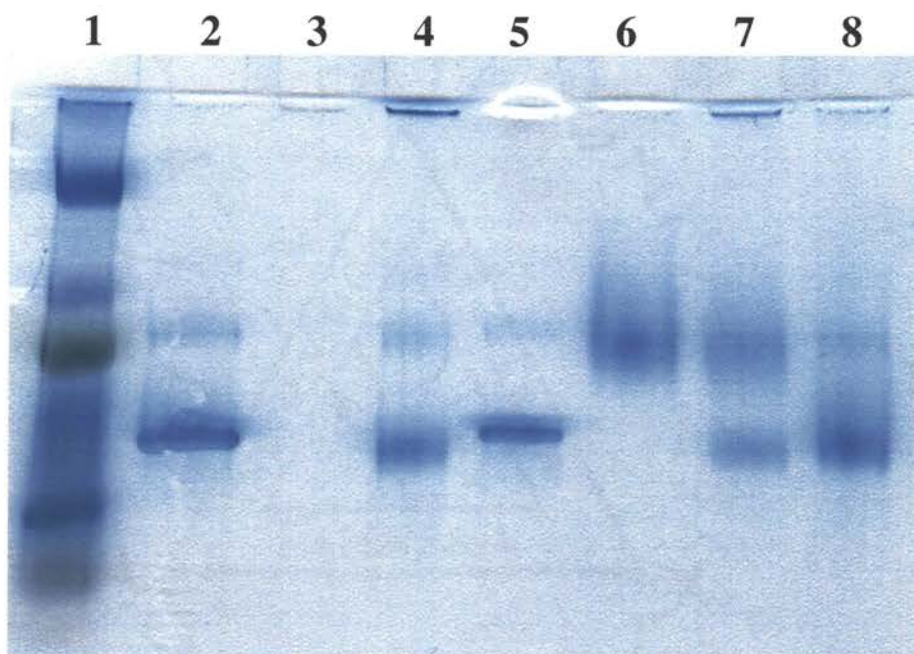
Figure IV-7. Native gel electrophoresis image. Wells: 1-Ladder; 2–BSA; 3–nanoparticles, cysteine stabilized; 4–conjugate NP-BSA; 5-mixture BSA-NP; 6-STR(streptavidin); 7- mixture conjugate NP-BSA and STR; 8- conjugate NP-BSA-STR. Gel =4-20% gradient Tris-HCl precast gel from Bio-Rad, Voltage=85 V, current = 21 mA, time =2 hours.
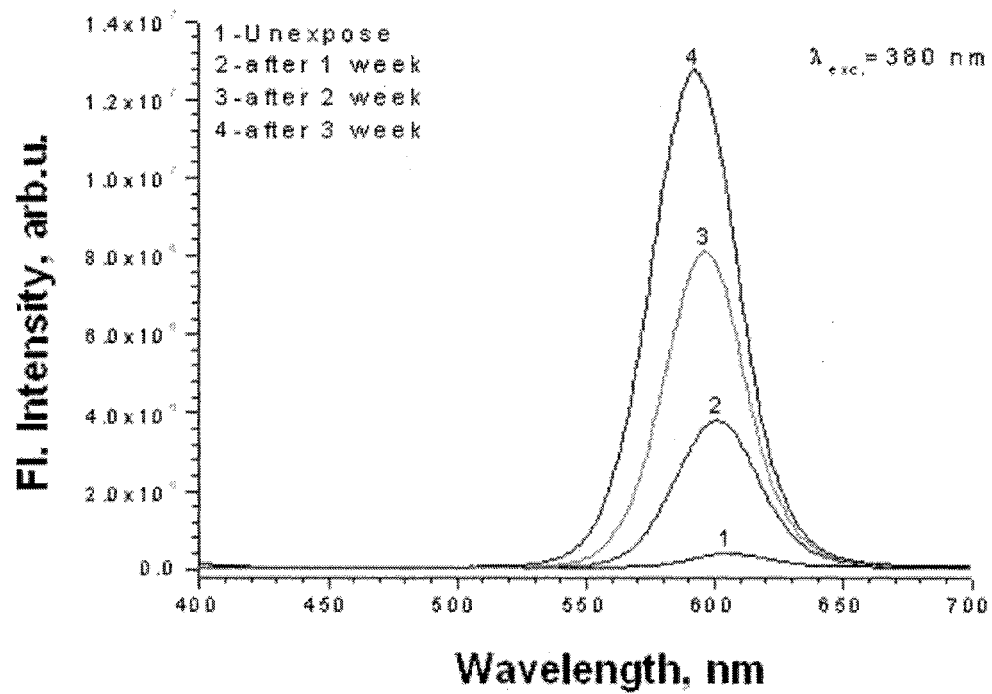
Figure IV-8. Fluorescent signal of CdSe/CdS-citrate measured after different irradiation times in air. λ_{exc} = 380 nm.
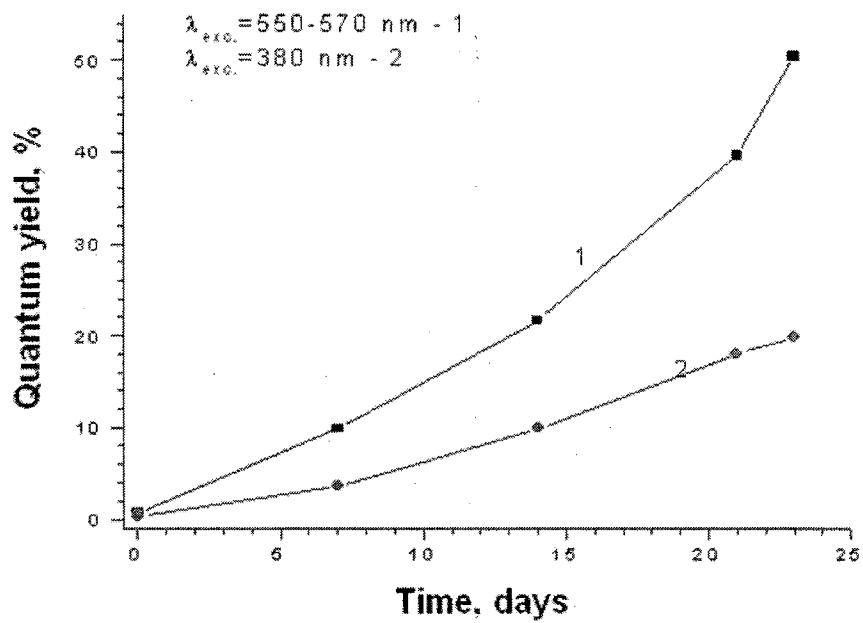
Figure IV-9. Quantum yield of CdSe/CdS-citrate measured after different irradiation times in air.

The transition from "dark state" to "bright state" for citrate-stabilized NPs involves reaction(s) of NPs with ambient oxygen; details are being investigated [13].

The well-known process of NP photoetching accompanies the photoactivation, observed as a gradual blue shift of the luminescence peak for long exposure time. This process can be used to control the emission wavelength of NPs in addition to the original synthetic conditions.

This effect has also been applied in Dr. Kotov's group for multicolor luminescence patterning by photoactivation of NPs films [14].

Here, the effect of photoactivation was applied to make high luminescent NPs with potential use for cell tagging. As an example, a photoactivatable variant of the *Aequorea victoria* green fluorescent protein (GFP) was offered to be used as a new tool for exploring intracellular protein dynamics by tracking photoactivated molecules in the cells [15]. Simplicity of the synthesis of citrate-stabilized CdSe/CdS NPs, tunability, and high intensity of their emission provide important advantages over the recombinant fluorescent proteins.

Photoluminescence spectra

Optical image of NP and conjugates and their emission spectra are shown in Figures IV-10 and IV-11 respectively

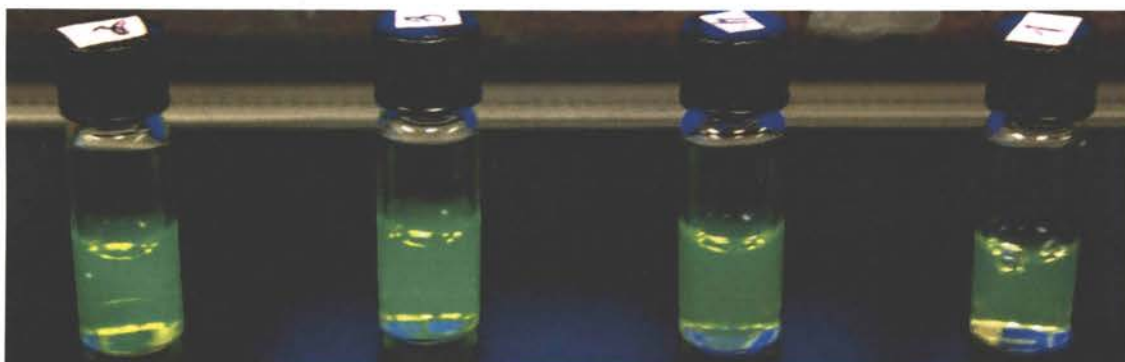The fluorescence intensities have been normalized to the CdSe/CdS bandgap

116

Figure IV-10. Optical image of core-shell CdSe/CdS NPs and their conjugates. From left to right: 1. CdSe/CdS, citrate stabilized; 2. CdSe/CdS, cysteine stabilized; 3. Conjugate NP-BSA; 4. Conjugate NP-BSA-STR(streptavidin).
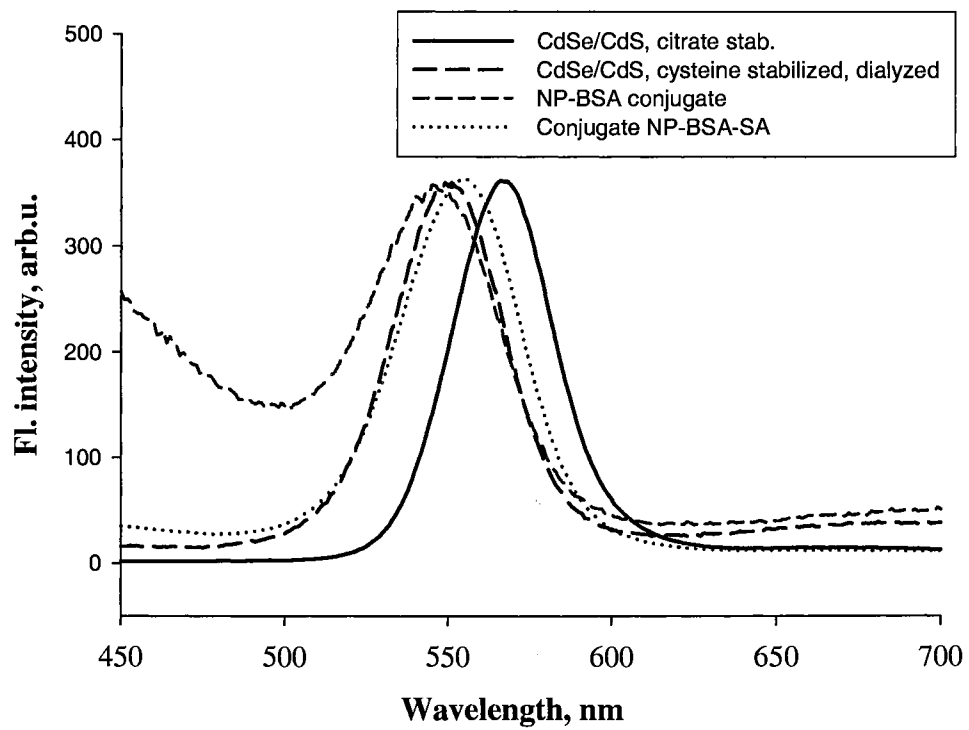
Figure IV-11. Emission spectra of different stages of conjugation (normalized intensity).

fluorescence intensity. The best results for the quantum yield at room temperature approximately 12% for citrate stabilized CdSe/CdS, 4% for L-cysteine stabilized CdSe/CdS nanoparticles, 20% for NP-BSA conjugates and 8% for conjugate NP-BSA-STR.

Initial CdSe/CdS NPs citrate stabilized show maximum luminescence emission intensity at 560 nm. Changing the stabilizing agent from labile citrate to L-cysteine leads to a decrease in luminescence intensity and blue shift. Such change can be attributed to hole-acceptor role of sulfur in L-cysteine during binding with a nanoparticle. Sulfur donates electrons into the valence zone, where they recombinate with holes decreasing the possibility of the recombination electron (from conduction band)-hole (valence band).

The conjugation with albumin results in recovery of luminescence and further blue shift of photoluminescence peak. The increase in emission intensity has been attributed to photo-induced healing of the surface states when the surrounding environment is equivalent to an insulator with a very high energy barrier, such as an organic matrix [16].

The final step, conjugation NP-BSA with streptavidin, leads to small red shift and shows the decrease in photoluminescence. This can possibly be explained by formation of a more complicated structure involving two proteins, such as revealed by confocal microscopy.

Confocal microscopy

Confocal microscopy images are shown on Figure IV-12. CdSe/CdS-BSA-STR conjugates tend to form long rod-like objects from 8 to 80 μm long during aging that can be easily observed by confocal microscopy. The similar shape aggregates have been reported to form from polymers through electrostatic interaction. However, in the present case, both proteins as well as NPs are negatively charged (isoelectric points pI~5 for BSA and STR). Moreover, the conjugates NP-BSA or NP-STR have not been noticed to aggregate with time. Thus the formation of the aggregates should be due to hydrophobic interactions or hydrogen bonding or some other type of specific interactions between two proteins that should be investigated elsewhere.

Cell labeling with CdSe/CdS bioconjugates

Nanoparticle cytotoxicity

Toxicity studies were performed for the conjugates CdSe/CdS-albumin-streptavidin. The endpoints examined in these studies were membrane integrity and apoptosis (Figures IV-13 and IV-14). MOLT4 cells were exposed to NPs for 24 hours and cells harvested at 1 and 24 hours for cytotoxicity assays. Harvested cells were assayed for membrane integrity at both 1 and 24 hours. Cells harvested at 24 hours were also assayed for late stage apoptosis by the TUNEL assay. No notable differences in membrane integrity occurred after 1 hour, with respect to the control samples. After 24 hours; however, there was a remarkable increase in cells with compromised membranes,
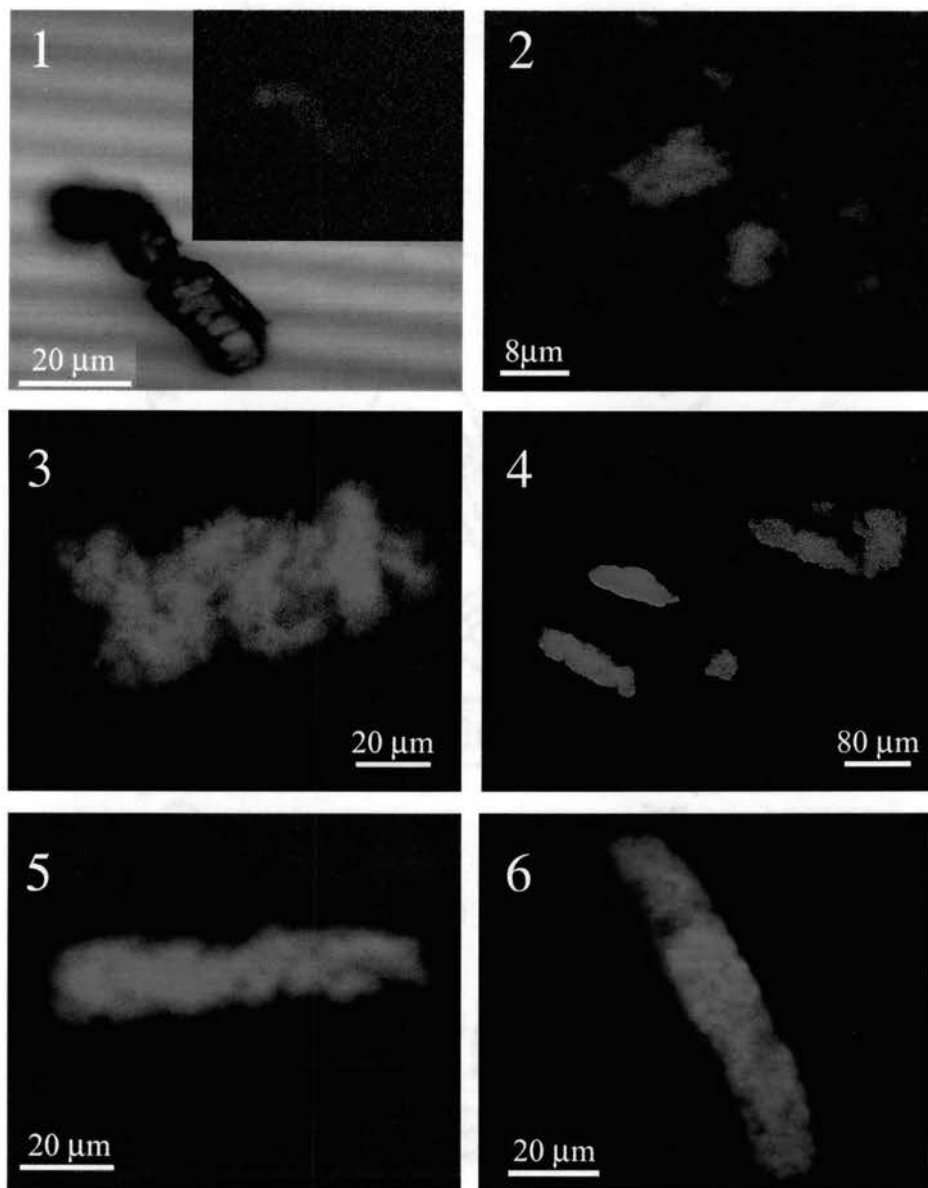
Figure IV-12. Confocal microscopy data for conjugate NP-BSA-STR. (1) BSA-Glutaraldehyde-STV(heat); (2) conjugate -4days; (3) conjugate – 11 days; (4) conjugate – 18 days, (5) conjugate – 33 days, (6) conjugate – 39 days.
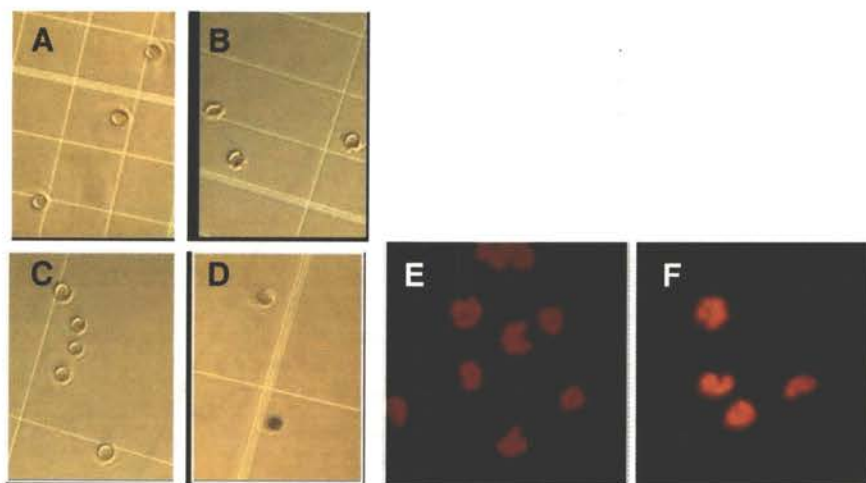
Figure IV-13. Cell viability and TUNEL assays in NP exposed cells. BJAB cells were incubated with NPs and cells harvested at 1 (Panels A and B) and 24 hours (Panels C, D, E, and F) for both trypan blue dye exclusion (Panels A, B, C, and D) and TUNEL assays (Panels E and F). In all time points examined, very few cells had compromised membrane integrity. After 24 hours, there appeared to be a modest increase in TUNEL positive (apoptotic) cells (Panel F) and a large increase in membrane compromised cells (Panel D).
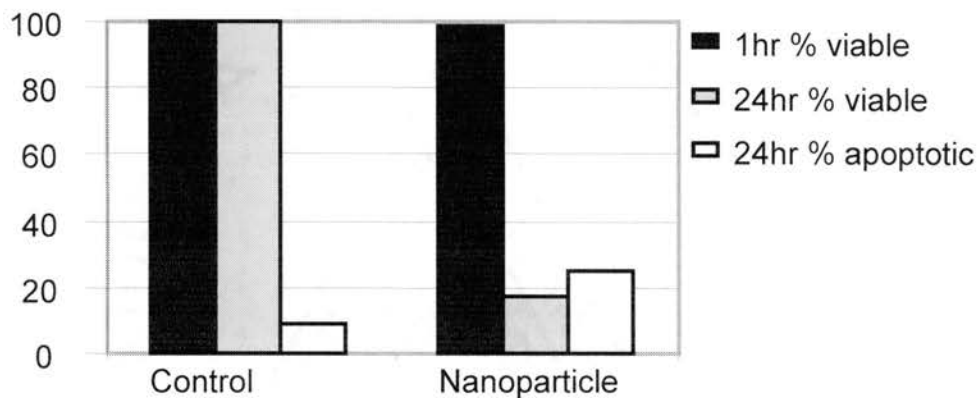
Figure IV-14. Membrane integrity and TUNEL positive cell counts. 10 fields of view at 40x were examined for membrane damage by trypan blue dye exclusion (black and gray bars) and TUNEL positive cells (lightest bars) after 1 and 24 hours of exposure to NPs. Membrane damage was represented by percent intact, where control cells were considered 100% (Control). TUNEL positive, or apoptotic, cells are shown as percent apoptotic, where the control cells are <10%. After 24 hours there was a marked loss in membrane integrity by the NP exposed cells, with only a modest increase in apoptotic cells.

shown as a decrease in percent viability when compared to control values. There was also a modest increase in late stage apoptotic cells, represented as an increase in percent apoptotic (Figure IV-14).

Coating nanoparticles for targeting and cell entry

The next step towards targeted delivery of NPs is the addition of targeting moieties to the streptavidin coated outer surface. Therefore, streptavidin coated NPs were assayed for their ability to bind biotin conjugated antibodies. Protein A coated non-fluorescent 5um beads were used to bind antibodies either bound or unbound to NPs. Protein A is a surface receptor expressed by *Staphylococcus aureus* and is capable of binding the Fc portion of immunoglobulins, especially IgGs, from a large number of species [17]. One protein A molecule can bind at least 2 molecules of IgG simultaneously [18,19]. Thus, if the streptavidin on the NPs can bind antibodies, incubation of this complex with protein A coated beads should yield fluorescent 5um beads with the same spectral characteristics as the NPs. In fact, this experiment did show fluorescent 5um beads, but as expected, NPs without antibody did not fluoresce (Figure IV-15). Confocal microscopy data from this application showed that the NPs were able to remain photostable after prolonged exposure to high intensity excitation wavelengths from a laser light source.
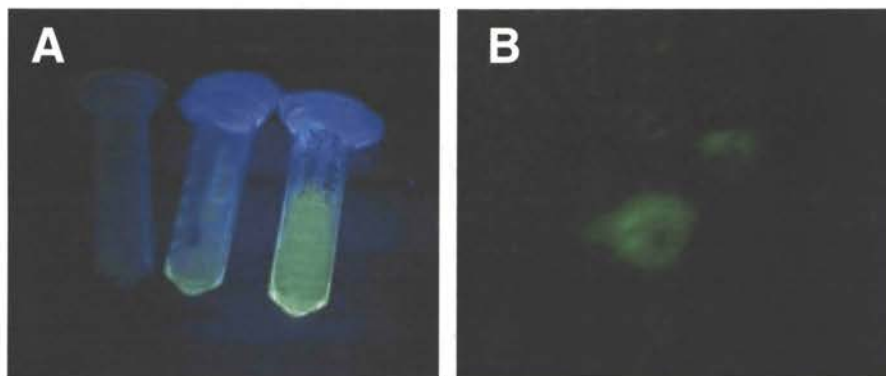
Figure IV-15. Verification of antibody conjugation to CdSe/CdS NPs. Particles made of: CdSe core, CdS, BSA, and streptavidin are illuminated with UV light (Panel A). Protein A binds the Fc portion of antibodies. CdSe/CdS NPs conjugated to anti-CD95 bound to non-fluorescent Protein A coated beads (5μm) (Panel B). NPs not bound to Abs did not result in fluorescent Protein A coated beads (data not shown).

Nanoparticles targeted to live human cells

Human cells, BJAB line, constitutively express CD95 on their surface. Since CD95 is an early indicator of radiation damage, we conjugated anti-human CD95 antibodies to the surface of CdSe/CdS NPs. This complex was then incubated with BJAB cells for 1 hour at 37°C. The resulting cell/NP mixture was washed three times prior to examination by confocal microscopy. NP clusters were found on the surface of the live human cells and were much brighter than background fluorescence (Figure IV-16). In most instances, the NPs appeared to cluster when bound to the cells. Thus, more experiments are needed to determine the optimal ratio of NPs to antibody.

Photostability of semiconductor nanoparticles attached to human cells

Prolonged exposure of semiconductor based NPs with high intensity UV laser light has been shown to increase fluorescence intensity over that of briefly pulsed NPs (Figure IV-17). This experiment was conducted with NPs bound to a living cell. In this system, the entire field of view was exposed to a high intensity UV laser beam and images taken in regular intervals for >630 seconds. Areas on the resulting images containing NPs or unlabeled cell or background were selected and intensity over time calculated. The background fluorescence (brown and black lines) quickly decreased, while the intensity of the NPs (red and blue) initially increased, then reached a plateau.
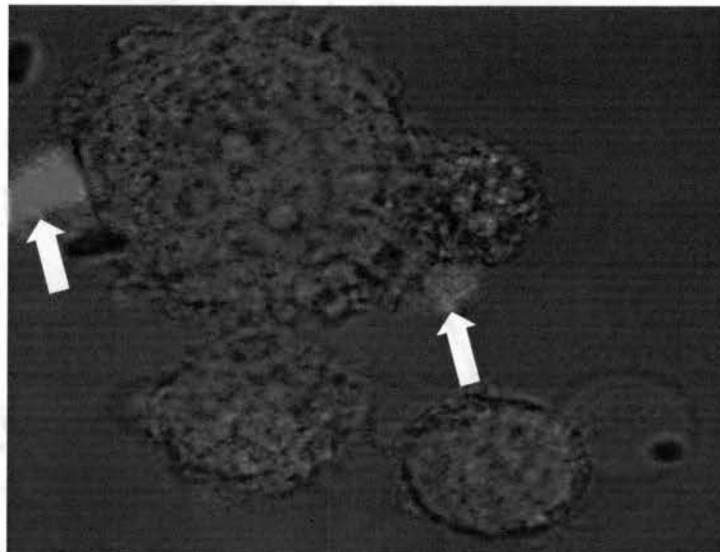
Figure IV-16. Anti-human CD95 coated CdSe NPs targeted to human cells. BJAB cells, which normally express CD95, were labeled with clusters of NPs previously coated with anti-human CD95. The cells were exposed to the NPs for 1 hour prior to viewing with a confocal microscope and appeared in good condition throughout the experiment.
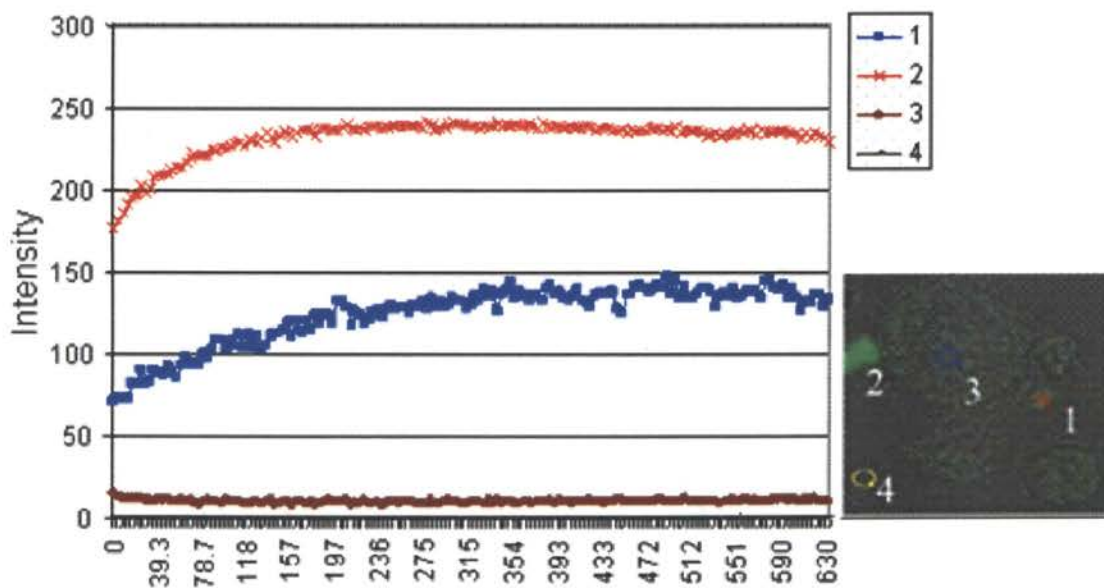
Figure IV-17. Effect of prolonged UV exposure on NP fluorescence intensity. The fluorescence intensity of NPs increased with prolonged UV laser beam exposure (Areas 1 and 2; Red and blue lines). Background and autofluorescence intensities (Areas 3 and 4, Brown and black lines) decreased initially and then reached a low intensity plateau. Overall, the NP clusters increased intensity initially and remained much brighter than the background fluorescence for over 630 seconds.

Optimization of nanoparticle conjugation protocol

The streptavidin coating is critical for these experiments; therefore, binding of streptavidin coated NPs to biotin coated 800 nm non-fluorescent polystyrene beads was tested. The success of these reactions was evaluated with confocal microscopy (Figure IV-18). In Figure IV-18 the black arrow indicates a bead. From these data, the emission spectra of the particles bound to the biotin coated beads were obtained (Figures IV-18 and IV-19). By using UTMB custom image analysis software, several critical measurements were determined (Figures IV-20 and IV-21). Firstly, the relative fluorescence intensity was determined of only those NPs bound to beads (Figure IV-20). Of those, Sample B, E, and F stood out as the brightest of the bound particles. Figure IV-21 was derived from a histogram that describes not only intensity, but also the relative binding ability of each NP sample. With this data in mind Samples B (cysteine stabilized BSA coated NPs coated with glutaraldehyde conjugated streptavidin) and E (cysteine stabilized NPs coated with NHS conjugated streptavidin in EDC) as the choice method for bioconjugation. Additionally, sample E appeared to stay in solution longer, with respect to sample B.
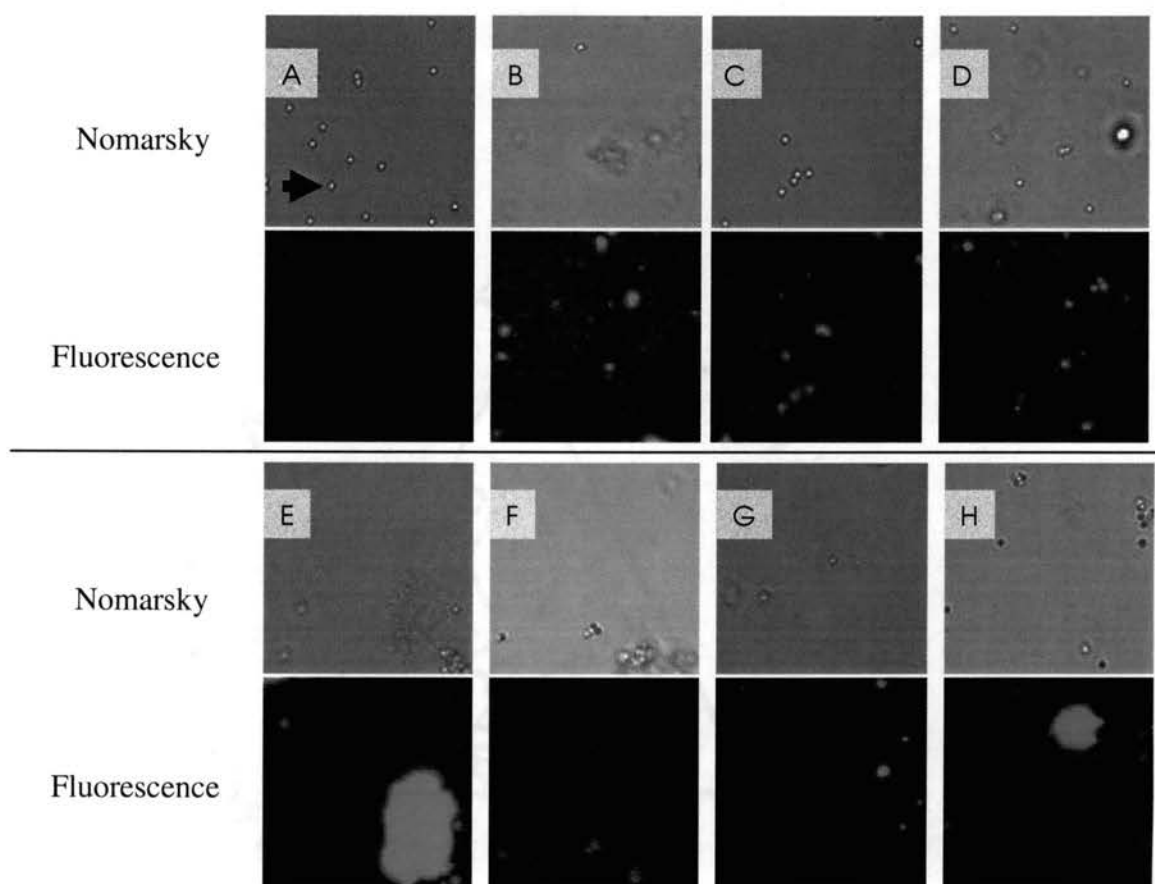
Figure IV-18. NP/streptavidin conjugation methods. Top Panel is Nomarsky scattering images, bottom Panel is fluorescence emission from 514 nm laser light. Panel A is beads alone, arrow indicated 1 μm biotin coated bead; Panel B is cysteine stabilized BSA coated NPs coated with glutaraldehyde conjugated streptavidin; Panel C is BSA coated NPs coated with glutaraldehyde conjugated streptavidin dialyzed; Panel D is NPs coated with glutaraldyhyde conjugated streptavidin; Panel E is cysteine stabilized NPs coated with NHS conjugated streptavidin in EDC; Panel F is cysteine stabilized BSA coated NPs coated with NHS conjugated streptavidin in EDC; Panel G is citrate stabilized NPs coated with NHS conjugated streptavidin in EDC; Panel H is citrate stabilized BSA coated NPs coated with NHS conjugated streptavidin in EDC.
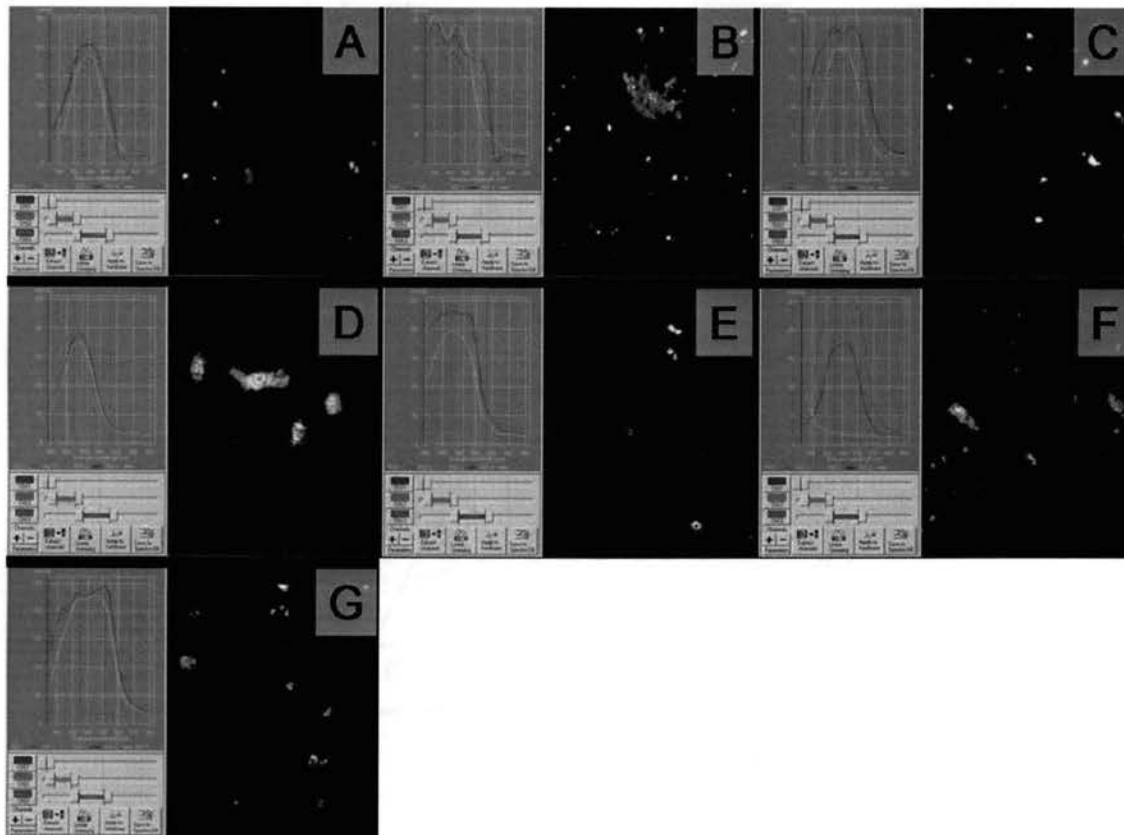
130

Figure IV-19. Emission spectra of conjugated NPs. Panel A is cysteine stabilized BSA coated NPs coated with glutaraldehyde conjugated streptavidin; Panel B is BSA coated NPs coated with glutaraldehyde conjugated streptavidin dialyzed; Panel C is NPs coated with glutaraldyhyde conjugated streptavidin; Panel D is cysteine stabilized NPs coated with NHS conjugated streptavidin in EDC; Panel E is cysteine stabilized BSA coated NPs coated with NHS conjugated streptavidin in EDC; Panel F is citrate stabilized NPs coated with NHS conjugated streptavidin in EDC; Panel G is citrate stabilized BSA coated NPs coated with NHS conjugated streptavidin in EDC.
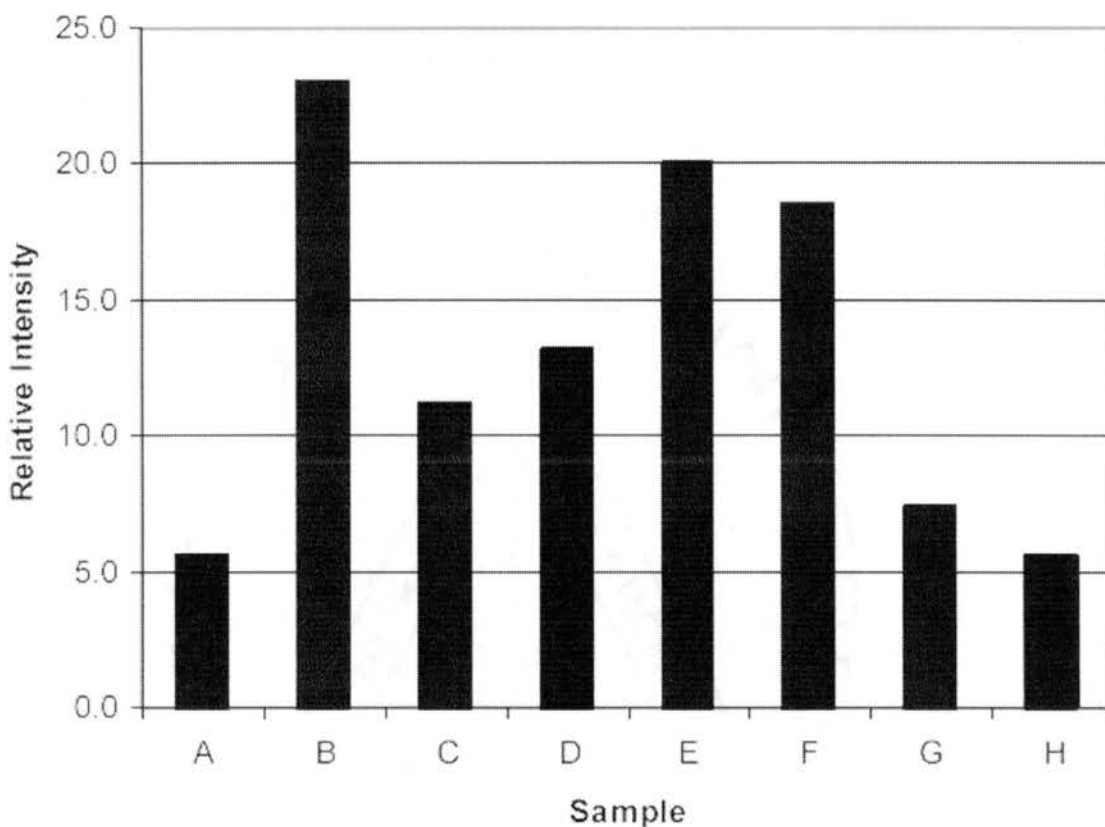
Figure IV-20. NP bound Biotin bead fluorescence. Average intensity of biotin coated beads exposed to streptavidin conjugated NPs. Sample A is beads alone; Sample B is cysteine stabilized BSA coated NPs coated with glutaraldehyde conjugated streptavidin; Sample C is BSA coated NPs coated with glutaraldehyde conjugated streptavidin dialyzed; Sample D is NPs coated with glutaraldyhyde conjugated streptavidin; Sample E is cysteine stabilized NPs coated with NHS conjugated streptavidin in EDC; Sample F is cysteine stabilized BSA coated NPs coated with NHS conjugated streptavidin in EDC; Sample G is citrate stabilized NPs coated with NHS conjugated streptavidin in EDC; Sample H is citrate stabilized BSA coated NPs coated with NHS conjugated streptavidin in EDC.
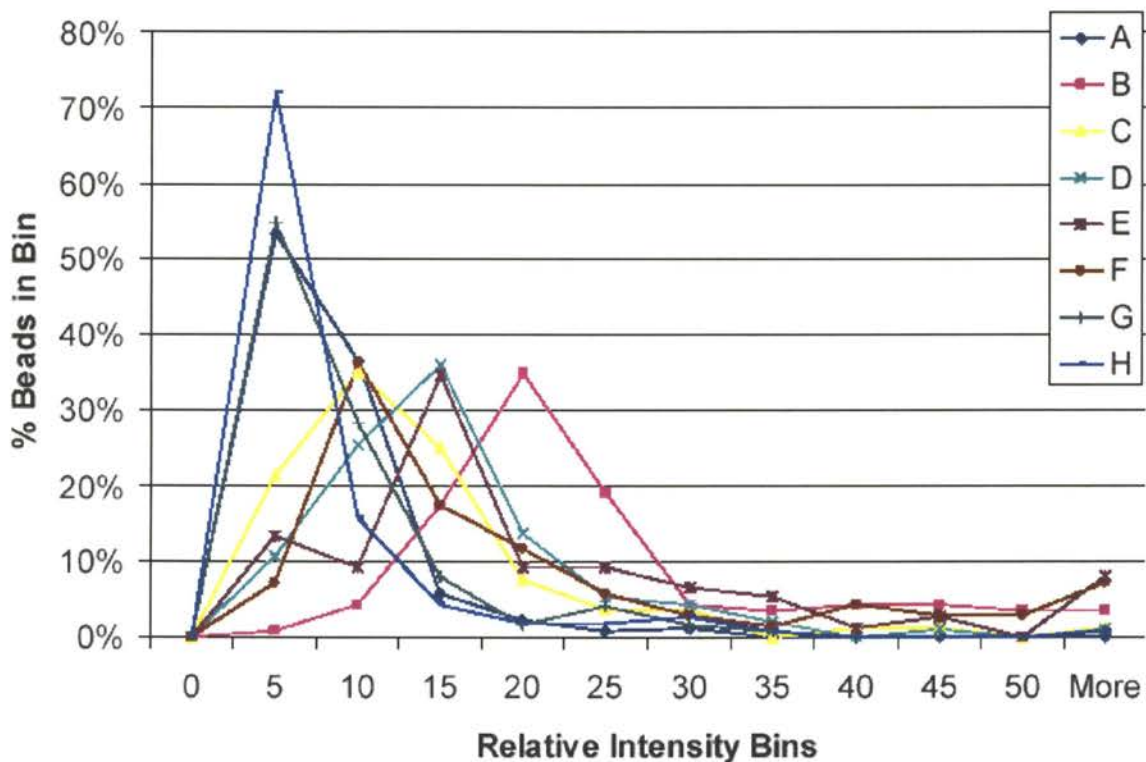
132

Figure IV-21. Intensity histogram of biotin coated beads exposed to streptavidin coated CdSe/CdS NPs. Line A is beads alone; Line B is cysteine stabilized BSA coated NPs coated with glutaraldehyde conjugated streptavidin; Line C is BSA coated NPs coated with glutaraldehyde conjugated streptavidin dialyzed; Line D is NPs coated with glutaraldyhyde conjugated streptavidin; Line E is cysteine stabilized NPs coated with NHS conjugated streptavidin in EDC; Line F is cysteine stabilized BSA coated NPs coated with NHS conjugated streptavidin in EDC; Line G is citrate stabilized NPs coated with NHS conjugated streptavidin in EDC; Line H is citrate stabilized BSA coated NPs coated with NHS conjugated streptavidin in EDC.

Recombinant peptide and antibody targeted nanoparticles

Several NP targeting strategies were tested in vitro (Figure IV-22) These data suggested that by using a biotinylated fragment of the HIV tat protein, the NPs could target to the nucleus of a living human white blood cell (BJAB cell line; Figure IV-22 panel C). To a lesser extent, a biotin labeled peptide containing only a six Arginine repeat could target NPs to the nucleus (Figure IV-22 panel B). Interestingly, the streptavidin coated particles alone were somewhat capable of entering the cell (Figure IV-22 panel D). Labeling the particles with an anti-CD95 antibody resulted in both outer membrane and strong nuclear staining (Figure IV-22 panel E).

Photostability of recombinant peptide targeted NP bioconjugates compared to a traditional Nuclear Dye, Hoechst 33342

To verify the presence and photostability of the NPs, a photobleaching experiment was carried out (Figure IV-23). During this experiment, lasting >400 seconds, the fluorescence of the NPs was far more resistant to photobleaching than the potent DNA dye Hoechst 33342.
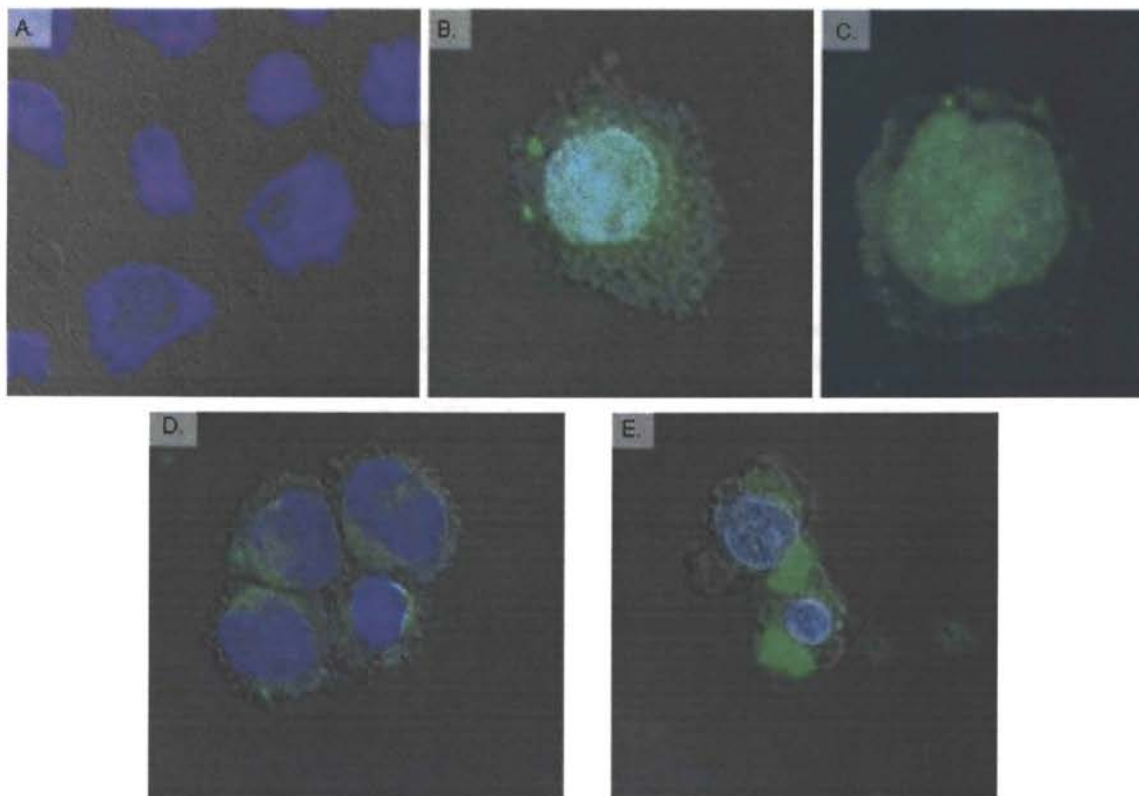
Figure IV-22. Nanoparticle targeting. BJAB cells exposed to: A – nothing, B – 6x Arg coated NPs; C – HIV Tat coated NPs; D – NPs alone; E – anti-CD95 coated NPs. All cells are counterstained with Hoechist 33342 (blue); NPs are green.
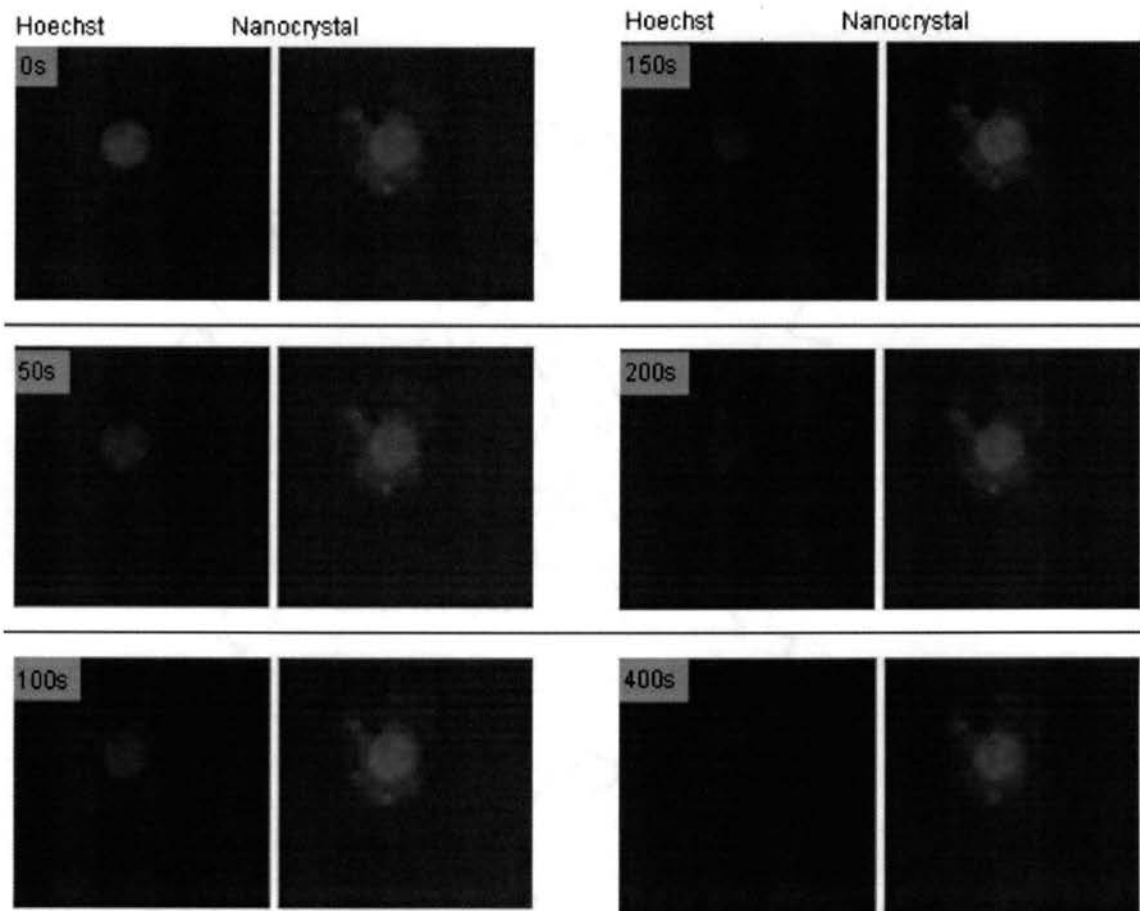
Figure IV-23. Photobleaching experiment data. Live BJAB cells were stained with tat tagged NPs (right panels, green) and counterstained with Hoechst 33342 (left panels, blue). Photobleaching from 0 to 400 seconds.

Conclusions

Semiconductor QDs are currently being developed for the field of biology in many different laboratories. These NPs have extraordinary spectral properties that have the potential to revolutionize fluorescent imaging. Although these particles hold promise, some substantial hurdles exist during their development for use under physiological conditions. First few batches of NPs, composed of CdTe were stable a pH>8. These NPs had excellent spectral characteristics and were easy to bioconjugate. Unfortunately, the pH requirement precluded their use in tissue culture. The next series of particles were composed of a CdSe core particle that was stable at physiological pH. These particles were optimized in collaboration with the Leary laboratory (UTMB) and used for the experiments with cells.

The small size of the NPs was probably the biggest factor contributing to their ability to enter transfection resistant cell lines, like the MOLT4. This cell line was repeatedly exposed to commercial lipid/DNA cocktails and could never be transfected, but NPs were able to enter these cells without any special coating. Interestingly, when these cells were exposed to NPs, regardless of coating, some of the cells contained large amounts of particles while other cells took up no detectable NPs. The original hypothesis was that most cells would take up NPs in a dose dependant manner. This hypothesis was rejected because in low dose cases only a few cells took up the NPs. These results point to a cell regulated uptake of NPs. This cellular characteristic could then be exploited to enhance the uptake of these small particles in cells that are notoriously difficult to transfect.

The next logical step would be to target these particles in vivo. The small size and excellent fluorescent properties would be very beneficial during these studies. Unfortunately, the CdSe based NPs fluoresce in the green wavelengths. Biological material absorbs this region of the spectrum, making green fluorescent probes very difficult, if not impossible to use in vivo.

Therefore, through collaboration with Dr. Kotov and Leary laboratories, a new NP, (CdHg/Te) has been developed for biological use. This NP has spectral properties similar to the clinical indocyanin dyes that were developed to fluoresce at wavelengths in the near infrared. Although these experiments with these particles will not be discussed in this dissertation, they are the next step in NP technology.

References

1. Dubertret, B.; Skourides, P.; Norris, D. J.; Noireaux, V.; Brivanlou, A. H.; Libchaber, A. *Science* **2002,** *298*(5599), 1759-1762.

2. Akerman, M. E.; Chan, W. C. W.; Laakkonen, P.; Bhatia, S. N.; Ruoslahti, E. *Proceedings of the National Academy of Sciences of the United States of America* **2002,** *99*(20), 12617-12621.

3. Wu, X.; Liu, H.; Liu, J.; Haley, K. N.; Treadway, J. A.; Larson, J. P.; Ge, N.; Peale, F.; Bruchez, M. P. *Nature Biotechnology* **2003,** *21*(1), 41-46.

4. Jaiswal, J. K.; Mattoussi, H.; Mauro, J. M.; Simon, S. M. *Nature Biotechnology* **2003,** *21*(1), 47-51.

5. Taton, T. A. *Nature Materials* **2003,** *2*(2), 73-74.

6. Rogach, A. L.; Nagesha, D.; Ostrander, J. W.; Giersig, M.; Kotov, N. A. *Chem.Mater.* **2000,** *12*(9), 2676-2685.

7. Dean, J. A. *Lange's Handbook of Chemistry, Fourteenth Edition;* 1992.

8. Hermanson, G. T. *Bioconjugate Techniques;* Academic Press: San Diego, CA, 1996.

9. Carraway, K. L.; Triplett, R. B. *Biochimica et Biophysica Acta* **1970,** *200*(3), 564-566.

10. Gaponik, N.; Talapin, D. V.; Rogach, A. L.; Hoppe, K.; Shevchenko, E. V.; Kornowski, A.; Eychmueller, A.; Weller, H. *J.Phys.Chem. B* **2002,** *106*(29), 7177-7185.

11. Manna, L.; Scher, E. C.; Li, L. S.; Alivisatos, A. P. *J.Am.Chem.Soc.* **2002,** *124*(24), 7136-7145.

12. Bol, A. A.; Meijerink, A. *J.Phys.Chem. B* **2001,** *105*(42), 10203-10209.

13. Wang, Y.; Pastoriza-Santos, I.; Tang, Z.; Correa-Duarte, M. A.; Kotov, N. A.; Liz-Marzan, L. M. *J.Am.Chem.Soc.* 2003. In Press

14. Wang, Y.; Tang, Z.; Correa-Duarte, M. A.; Liz-Marzan, L. M.; Kotov, N. A. *J.Am.Chem.Soc.* **2003,** *125*(10), 2830-2831.

15. Patterson, G. H.; Lippincott-Schwartz, J. *Science* **2002,** *297*(5588), 1873-1877.

16. Rodriguez-Viejo, J.; Mattoussi, H.; Heine, J. R.; Kuno, M. K.; Michel, J.; Bawendi, M. G.; Jensen, K. F. *J.Appl.Phys.* **2000,** *87*(12), 8526-8534.

17. Boyle, M. D. P.; Reis, K. J. *Bio/Technology* **1987,** *5*(7), 697-703.

18. Sjoquist, J.; Movitz, J.; Johansson, I. B.; Hjelm, H. *European Journal of Biochemistry* **1972,** *30*(1), 190-194.

19. Sjoquist, J.; Meloun, B.; Hjelm, H. *European Journal of Biochemistry* **1972,** *29*(3), 572-578.

VITA (2)

Nataliya N. Mamedova

Candidate for the Degree of

Doctor of Philosophy

Thesis: SEMICONDUCTOR QUANTUM DOTS BIOCONJUGATES

Major Field: Chemistry

Biographical:

Personal Data: Born in Minsk, Belarus, On September 23, 1973

Education: Graduated from Machulistchi Middle/High School, Minsk, Belarus in June 1990; received Diploma with Honors (equivalent of Master of Science) in Chemistry from Belarussian State University, Minsk, Belarus in June 1995; completed the requirements for the Doctor of Philosophy degree with a major in Chemistry at Oklahoma State University in December, 2003.

Experience: Employed as an undergraduate research assistant at Chemistry Department of Belarussian State University, Minsk, Belarus, 1993-1995; employed as secondary school teacher 1997-1998; employed as research assistant at the Institute of Inorganic Chemistry of National Academy of Science of Republic of Belarus, Minsk, Belarus, 1997-1998; employed by Oklahoma State University, Chemistry Department as a graduate teaching assistant and as a graduate research assistant; 1999-present.

Professional Memberships: American Chemical Society.